



Universitat Autònoma de Barcelona

ADVERTIMENT. L'accés als continguts d'aquesta tesi queda condicionat a l'acceptació de les condicions d'ús establertes per la següent llicència Creative Commons:  http://cat.creativecommons.org/?page_id=184

ADVERTENCIA. El acceso a los contenidos de esta tesis queda condicionado a la aceptación de las condiciones de uso establecidas por la siguiente licencia Creative Commons:  <http://es.creativecommons.org/blog/licencias/>

WARNING. The access to the contents of this doctoral thesis it is limited to the acceptance of the use conditions set by the following Creative Commons license:  <https://creativecommons.org/licenses/?lang=en>



Biodegradable batteries as sustainable power sources for portable devices

Perla Patricia Alday Lara

PhD dissertation
Materials Science Program

Directors: Dr. Juan Pablo Esquivel Bojórquez

Dr. Neus Sabaté Vizcarra

UAB Mentor: Dr. Iluminada Gallardo

Chemistry Department
Faculty of Sciences



2018



Dr. Juan Pablo Esquivel Bojórquez and Dr. Neus Sabaté Vizcarra at Microelectronic Institute of Barcelona IMB-CNM (CSIC), certify that the thesis entitled: "*Biodegradable batteries as sustainable power sources for portable devices*" were carried out under their supervision within IMB-CNM.

In witness whereof for the Department of Materials Science of University Autonomous of Barcelona, they herby sign this present certification.

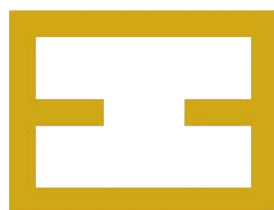
Bellaterra, July 2018

Dr. Juan Pablo Esquivel Bojórquez
(Director)

Dr. Neus Sabaté Vizcarra
(Director)

To download a copy of this thesis, go to:

<http://www.speedresearchgroup.com/research/thesis/>



**SELF
POWERED
ENGINEERED
DEVICES**



A la existencia y esencia.

Acknowledgements

First of all, I want to give a special thanks to my supervisors Dr. Juan Pablo Esquivel and Dr. Neus Sabaté for providing me the opportunity to realize a PhD at this Institute of Microelectronic of Barcelona and also for their excellent supervision, support, friendship and encouragement along the way. I wish to express my special and sincere appreciation for their advices, guidance and supervision during the research and for critically correcting this thesis through to its conclusion. They have been a constant source of ideas and suggestions from the initial planning stage until completion of this project.

Special thanks go to Dr. Erik Kjean and Omar Ibrahim from Simon Fraser University for the great collaboration we established during part of the development of this thesis.

I also thank Professor Manuela da Silva and Dr. Sandra Barros, from the University of Minho in Braga for assisting in some of the experiments, for their constant support and friendship during a special stage of this thesis.

I express my gratitude to CONACyT (Consejo Nacional de Ciencia y Tecnología) for providing financial support during my PhD study period.

My appreciation also goes to each and every one of colleagues at the Institute that in some way or another helped me to carry out this work. My dear SPEED group, Irene, Marina, Ana, Laura, Dimitri, thank you for your words of encouragement. Sole, it's been a total fun meeting you, thank you for your friendship. Sunil, you arrived at the end of my PhD and it was a fortuitous encounter. I will always have you in my memory.

Time and space may not permit me to mention the names of all the people who have contributed in one way or the other to my life. I will forever keep you in the golden book of my memory. It is not enough to say thank you but it is really a great privilege to have associated with you. You are all part of the history of my life. Roberto, my beloved friend, I could not have a greater reward in life than during this time in Barcelona have found you on my way and be brothers of the soul, with many stories lived. Inci, my dearest friend, beyond sharing names and personalities, we have shared beautiful moments and life-time experiences; you have been a guide and constant support. Cami, you've always been a pillar in my days, thanks for all your support, kindness and mate. Gicela, my funniest friend, thanks for all the adventures and laughs.

Finally, my special thanks and appreciation goes to my parents, Gustavo and Patricia, for their love, patience, support and understanding throughout my studies. I would like to thank my siblings, Saramarina and Gustavo for their support, friendship and memes. My love and gratitude go to my beautiful niece, Leilani, and nephews, Liam, Pável and Elí, for bringing lot of joy and light to my life. Most of all to God who made everything possible.

Index

Dedicatoria

Acknowledgements

1. Introduction	1
1.1. Objective	4
1.2. Methodology	5
1.2.1. Batteries working principle	6
1.2.2. Paper microfluidics	7
1.2.3. Organic redox chemistry	7
1.2.4. Natural electrochemically active polymers	8
1.3 Summary	11
References	13
2. Evaluation of chemical compounds for redox primary batteries	17
2.1. Introduction	18
2.2. Identification of redox compounds	18
2.3. Characterization of redox species	20
2.3.1. Quinone species	21
2.3.2. Innocuous redox alternatives	22
2.4. Characterization of storable electrolytes in powder	24
2.5. Conclusions	26
References	27
3. A biodegradable and all-organic redox flow battery for single-use applications	29
3.1. Introduction	30
3.2. Development of a paper-based redox flow cell	30
3.2.1. Design of a paper-based co-laminar flow cell	31
3.2.2. Validation of capillary flow cell with a suitable redox couple	32
3.2.3. Validation of capillary flow-through porous electrodes	35
3.2.4. Validation of dry storage of species and electrolytes	37
3.3. Biodegradable battery integration	38
3.3.1. Design and operating principle	39
3.3.2. Battery characterization	41
3.3.3. Battery voltage scalability	46
3.3.4. Practical application of the battery	48
3.3.5. Battery biodegradability	50
3.3.6. Discussion	52
3.4. Conclusions	53
References	54
4. Optimization of a paper-based capillary flow battery with flow-through electrodes	57
4.1. Introduction	58
4.2. Capillary-based flow cell design and working principle	59
4.3. Quasi-steady capillary flow characterization	61
4.4. Battery electrochemical characterization	63
4.4.1. Electrode configuration	63
4.4.2. Capillary flow rate	65
4.4.3. Electrode length modification	67
4.5. Conclusions	69
References	70

5. Bio-Polymer Electrolyte Membranes (BioPEMS) for primary redox batteries	73
5.1. Introduction	74
5.2. Polymer electrolyte preparation	75
5.2.1. Chitosan-based electrolytes	75
5.2.2. Starch-based electrolytes	76
5.3. BioPEMs ionic conductivity characterization	77
5.4. Performance of the BioPEMs in redox batteries	80
5.4.1. Experimental setup design	80
5.4.2. Characterization of redox species crossover	81
5.5. BioPEM-battery characterization	83
5.6. Conclusions	85
References	86
6. Biodegradable button cell battery based on redox biopolymers	89
6.1. Introduction	90
6.2. Preparation of hydrogels	92
6.2.1. Synthesis of the hydrogel backbones	92
6.2.2. Synthesis of the redox hydrogels	92
6.3. Preparation of redox hydrogel electrodes	93
6.4. Redox hydrogel electrochemical characterization	94
6.4.1. Effect of the hydrogel gelation in the open circuit voltage	94
6.4.2. Electrochemical performance in screen printed and porous carbon redox hydrogel electrodes	96
6.4.3. Increasing ionic conductivity of redox hydrogels	98
6.5. Redox hydrogel-based button battery	99
6.5.1. Battery design and fabrication	99
6.5.2. Button cell battery electrochemical characterization	101
6.5.3. In series connection of button-cell batteries	103
6.6. Conclusions	105
References	107
Conclusions	109
Scientific contributions	113
Appendix 1. Biodegradability assay	115
Appendix 2. Bill of materials for powerPAD batteries	119
Resumen en español	121
Nomenclature	123

1.

Introduction

At present it is difficult to find yourself in an environment free of electronic devices, in the last three decades the use of electronic devices has experienced a considerable increase, and logically, the increase in waste electrical and electronic equipment (WEEE) generated after their disposal is proportional.

The large quantities of WEEE and the wide variety of materials they often contain (ferrous metals, non-ferrous metals, glass and plastics) have raised a serious alarm on their potential adverse health and environmental consequences when incorrectly disposed. The WEEE dismantling produces persistent heavy metals in nature and is one of the biggest dangerous compounds that pollute soils and waters[1]. Moreover, this waste can be regarded as a resource of valuable materials (e.g., Au, Pt, Li) that if not recovered, has to be extracted again, resulting in natural resource depletion and environmental degradation. Recovering these metals and satisfying the demand for cheap second-hand equipment has become profitable business in emerging economies, which has turned Asia (in particular China and India) and Africa into recipients of 90% of globally exported WEEE.[2] However, dismantling procedures are often carried out in inappropriate infrastructures with discarded components being openly incinerated and disposed in unlined landfills that lack monitoring of leachate recovery systems of any kind. Due to their content of heavy metals, batteries are one of the most hazardous components of e-waste. For this reason, many OECD countries have established regulations on the

maximum permitted content of certain metals such as mercury or cadmium and the mandatory recycling of spent batteries[3].

Lithium-ion batteries are today the most predominant energy sources in portable applications because of their high energy density, low sensitivity to temperature variations and no memory-effect when recharging[4]. However, they are starting to arise important concerns related to the low relative abundance of lithium metal - which is likely to increase the environmental impact of its extraction methods- and the large amount of CO₂ generated during battery manufacturing. In fact, its life cycle assessment determines that the use of lithium is only justified in rechargeable applications beyond hundreds of cycles, which clearly excludes its use as primary batteries[4,5]. Despite all these worrying facts, effective battery recycling percentages are far from being met in regulated regions with more than 70% of batteries ending up in landfill sites and it is practically inexistent in low resource settings (Figure 1.1)[6]. The most alarming issue is that consumption of batteries is expected to rise significantly in the following years due to the growth of small-sized portable appliances in the ICT sector. Generally, these devices are powered by primary cells that are to be disposed after depletion. This means a future rise in the number of batteries that will be discarded in an uncontrolled way – and almost fully charged in case of applications with short duration such as single use point-of-care devices. In view of this perspective, tightened environmental laws and increased provisions for recycling infrastructure (primary battery collection and processing) are urgently needed. However, this approach is not embraceable in the short-term in developing economies due to the high cost and complexity of implementation. Indeed, this may not be environmentally sustainable even for developed economies either; building-up costly and energy-consuming recycling plants to take care of the batteries generated along the linear “take-make-dispose” path followed traditionally since the early days of industrialization entails a huge waste of natural resources, energy and labor.



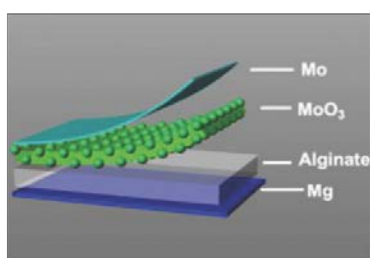
Figure 1.1. Overproduction of battery waste[7,8].



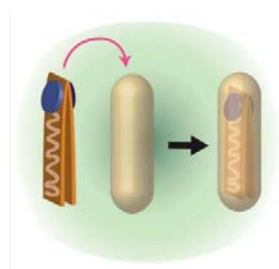
In this sense, the approach of the circular economy – which aims to minimize, track and eliminate the use of toxic chemicals and waste through careful device design and conception – appears to be a promising way to meet the technological needs of current society without compromising future generations.

In the same sense, the exploration of new materials those are not toxic, that are abundant in nature and are biodegradable, has been extended. Some materials such as cellulose, silk and a large number of synthetic and natural polymers have been explored as electronic substrates[9,10].

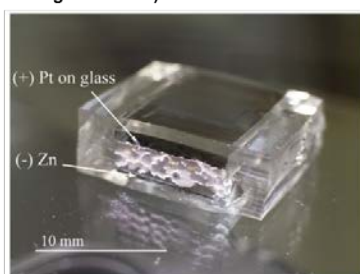
Thus far, efforts have been made to design and develop a new concept of batteries using natural, biocompatible materials for the electrodes and electrolytes, called transient primary batteries, which can minimize the incorporation of harmful compounds for the environment and the health of populations. A swallow able battery based on Zn and Pt electrodes and a ceramic separator have been reported, this battery exhibited a maximum potential of 0.42 V and current of 2.41 mA[11]. Kim et al. reported an edible water activated sodium battery based on melanin[12] and Yin et al. showed the abiotic degradation of a polymer encapsulated battery that uses metals like Mg, Fe, W and Mo as electrodes[13]. In the same sense, a battery for self-powered transient implants as an alternative approach for in vivo on-board power supply was reported [14]. These batteries are developed for implantable or edible applications and thus designed to be innocuous to the human body when decomposed in their primary elements in a short time after having been implanted or eaten. The rationale behind these devices is to make use of different non-toxic materials (both organic and inorganic) that once dissolved in the body, do not exceed the Recommended Dietary Allowance. Other transient battery approaches for ex-vivo applications have been explored, but to the author's knowledge, they all rely on lithium-based chemistries or toxic redox compounds,[15] and completely neglect what would be the impact of the battery after its degradation in water under unregulated conditions (i.e. rivers, lakes, landfills, etc.). Some of these transient batteries are shown in Figure 1.2.



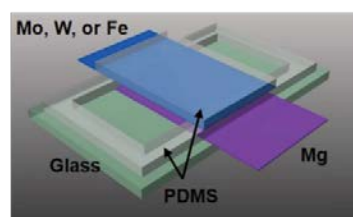
(Battery for self-powered transient implants. Huang et al. 2018)



(Edible battery. Kim et al. 2017)



(Swallowable battery. Jimbo et al. 2008)



(Abiotic degradable battery. Ying et al. 2014)

Figure 1.2. Examples of transient battery lately developed.

Recent works on paper fuel cells based on biocatalysts such as microbes and enzymes have opened a new alternative to sustainable power sources. However, there are still many challenges to overcome regarding their reproducibility, signal stability and power density to meet energy requirements of portable electronics. [16]

When it comes to fueling electrochemical power sources, various organic materials are used, such as direct methanol fuel cells or direct formic acid fuel cells. On the downside, precious metal catalysts such as platinum or palladium [17] which are highly expensive, are required for the electrochemical reactions involving these fuels. A more viable option would be the microbial fuel cell, where inexpensive biological microbes act as catalysts. However, their power output is generally much lower than the target application requirements and the biocatalysts often have limited stability [3].

1.1. OBJECTIVE

During the process of this research work, our objective was to develop batteries completely aligned with the circular economy principles (Figure 1.3) focusing in the utilization of raw materials that do not cause exhaustion of natural elements, do not require large amounts of energy to be produced, do not produce toxic by-products during their manufacture and feature biodegradability in mild degradation conditions at the end of their life cycle. Such components would thus bypass the need for complex recycling structures and associated investments. [18]

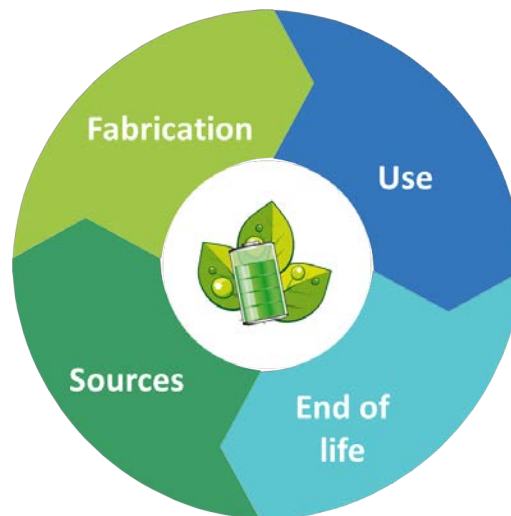


Figure 1.3. Proposed battery aligned with circular economy life cycle

In this regard, green electronics is an emerging area of research aimed at creating new methods and processes for the production of renewable and biodegradable materials with minimal amount of potentially toxic materials, environmentally friendly electronics.

Included in this category are all those devices or components where environmentally harmful materials are used, with eco-efficient manufacturing, presenting consume less power (in operation and stand-by modes) process and are fully recyclable with no hazardous waste.

Unlike conventional electronic devices that are designed to operate for extended periods of time, transient electronic devices are designed to operate under a short and defined period, as well as ideally, reach their self-destruction or degradation once their transiency is triggered[19]. These devices have a wide range of applications including in healthcare, biomedical devices, environmental sensing / monitoring, green electronics, military and homeland security. To power a real autonomous transient electronic device, a transient battery is essential.

1.2. METHODOLOGY

Therefore, the approach carried out for the effective realization of this research work has been the manufacture of batteries that empathize with the circular economy. For the following, an integration of knowledge of different disciplines was carried out. Batteries based on natural materials have been manufactured, including biopolymers such as cellulose and chitosan, carbon electrodes, beeswax, and redox species of low toxicity, including species of the quinone group. Based on principles such as capillary microfluidics and the diffusion of redox species in hydrogels. Next, the most relevant areas of knowledge used during this investigation are introduced.

1.2.1. Batteries working principle

Batteries are portable electrochemical devices that convert store chemical energy into electrical energy. There are two main types of batteries: primary and secondary battery. Primary batteries are those in which the electrochemical reaction is irreversible, that is, after the battery has been discharged it cannot be recharged, these are disposable batteries. In secondary batteries the electrochemical reaction is reversible, can be recharged by supplying direct current from an external source and reused multiple times. Basically, there are four main components in a battery: the anode, cathode, separator and electrolyte. The anode acts as the negative electrode which releases electrons during discharge and accepts electron on charge. The cathode acts as a positive electrode, which absorbs electron during discharge and release on charge. The electrodes do not touch each other; however, they are electrically connected by the electrolyte while the separator prevents them from mixing with each other, but it allows the movement of ions from one electrode to the other. The electrolyte of a battery consists of soluble salts, acids or other bases in liquid, gelled and dry formats. It can also be a polymer form, like in solid-state batteries, solid ceramic and molten salts, as in the sodium-sulfur battery. The electrolyte should be highly conductive, non-reactive with the electrode materials and stable with operating conditions such as temperature.

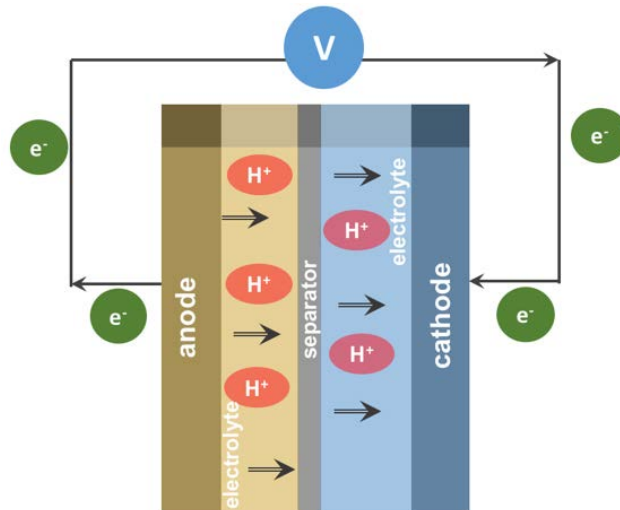


Figure 1.4. Scheme of a primary battery during discharge.

A flow battery or redox flow battery, is a type of electrochemical cell where the energy comes from two chemical compounds dissolved in containers and separated by a membrane, which facilitates the ion exchange through its matrix, while the two liquids are in your own compartment. A flow battery can be considered as a fuel cell, as long as the fuel that has been consumed is extracted and the system renewed with new fuel. As well as it can be used as a secondary battery, or rechargeable, where by adding electric power you can recharge the battery components.



Recently, a novel flow battery system for energy storage has been introduced by Aziz's group at Harvard University, where they coupled a Quinone redox species with a bromine anode. Their metal-free cell showed high power output during discharge and high cycling efficiency [4]. Another group at University of Southern California created the organic redox battery (ORBAT) [5], by substituting the toxic bromine anode with another, high-reduction potential Quinone, thus bringing forth an eco-friendly, water-based storage system.

1.2.2. Paper microfluidics

Paper-based microfluidics has been extensively investigated by researchers for various applications (such as disease diagnostics), in which transport may be sustained due to the capillary action of fluids through fibers and pores in the paper. [20][21] Paper is made with a porous network of hydrophilic fibers where the major flow driving is capillarity. The hydrophilic fiber surface favors the adhesion and spreading of liquids, while the surface tension of the liquid tends to decrease the liquid-gas interfacial area, resulting in the wicking action [22]. That can wick solution via the use of capillary action. This action allows the fluids in the system to flow through the capillary network without the use of an external power supply that would be normally required for traditional microfluidics.

The fluid in paper is transported primarily by wicking and evaporation. Wicking in cellulose paper is usually analyzed using two different models: the Lucas–Washburn equation, considering the pores in the medium as isotropic capillary tubes (1) [23].

$$L^2 = \frac{\gamma D t \cos(\phi)}{4\eta} \quad (1)$$

Where t is the time for a liquid of dynamic viscosity η and surface tension γ to penetrate a distance L into the capillary whose pore diameter is D . The contact angle between liquid and solid is ϕ .

Once the medium is fully wetted, subsequent flow is laminar and follows Darcy's Law. The use of paper for the manufacture of devices is based on the simplicity to design different patterns or geometries, their low cost and minimal use of reagents requirements, resulting in a disposable, simple to use platform. Flow control of the fluid in a capillary network and its rate manipulation can be managed by patterning hydrophobic barriers or controlling the geometry of the device and its paper components.

1.2.3. Organic redox chemistry

Quinones are products of oxidation of the phenols, found in living organisms and are responsible for the colors in many plants. Quinone compounds can be defined as a class of cyclic organic compounds that contain two carbonyl groups (C=O). This class includes benzoquinones, naphthoquinones or anthraquinones, among others. By the addition of more rings to the structure, the aqueous solubility is expected to decrease, and so is the

standard reduction potential.[24] Therefore, benzoquinones (BQ) will have the highest solubility and highest standard potential while anthraquinones (AQ) will have the least solubility and the lowest standard potential. Alternatively, naphthoquinones (NQ) are expected to have moderate solubility and standard reduction potential between BQ and AQ and may therefore be also suitable. These Quinone compounds can also be tuned for their standard reduction potentials together with their solubility by adding different functional groups to the structure.[25,26] When quinones are reduced reversibly to their respective hydroquinones, the two carbonyl groups change to two hydroxyl groups (C-OH).

Furthermore, quinones are highly prone to a fast biodegradation, as predicted by the biodegradation models (BIOWIN™) in the EPISuite™ and other works.[27] Hence the fact that the Quinone species are considered to satisfy the majority of the disposable battery criteria. Quinone redox compounds have proven to be the one of the most viable candidates for the investigation done in this thesis, due to the fact that they feature special characteristics: They have rapid kinetics on pure carbon electrodes and do not require any catalysts, with two electrons and two protons transferred in acidic media, have good solubility in water or some another aqueous electrolyte, to have the facility to flow by capillarity, not to be toxic, that its existence in nature be abundant. Moreover, they are inexpensive and can be extracted from natural organic compounds present in plants, which makes them eco-friendly and readily biodegradable.

1.2.4. Natural electrochemically active polymers

Naturally occurring materials employed as biocompatible and biodegradable substrates for various electronics applications include collagen, chitin, chitosan, alginate, dextran, shellac, hard gelatin and silk [28][29]

The discovery that some organic macromolecules were electrochemically active originated a great interest in this type of materials, generating numerous lines of research in different fields of science. This is because the oxidation and reduction reactions of these macromolecules have different associated processes (such as conformational changes in the chain or the bond of ions and molecules in it) that also occur in many macromolecules of biological interest.

The electrochemically active polymers can be divided into two groups according to the nature of the species responsible for the conductivity and the mechanism by which the cargo is transported within the macromolecule: redox polymers and electrically conductive polymers.



1.2.4.1. Redox polymers

Polymers with redox properties are those with the ability of changing their electrochemical properties with the oxidation state due to the loss of electrons (oxidation) or the gain of electrons (reduction). Redox hydrogels conduct electrons by self-exchange of electrons or holes between rapidly reduced and rapidly oxidized redox functions tethered to backbones of cross-linked polymer networks[30].

Redox polymers can incorporate redox active groups such as ferrocene into the polymer backbone or into pendant groups. The IUPAC definition for a redox polymer is a polymer containing groups that can be reversibly reduced or oxidized. Reversible redox reaction can take place in the polymer main-chain, as in the case of conducting polymers such as polyaniline, or in side-groups, as in the case of a polymer carrying ferrocene side-groups. [31] Thus, depending on their oxidation state (oxidized or reduced) polymers can present different electronic properties such as ionic and electrical conductivity, optical properties, mechanical or chemical properties. Therefore, electrochemical properties of these types of polymers (oxidation or reduction) will be directly related to the properties of the redox system incorporated into the polymer chain.

The development of redox polymers presenting organic chemical groups with redox properties such as nitroxyl, phenoxyl, carbazol, quinones, viologens, carbazol or hydrazyl is a very active research topic. In a pioneering work, Nishide et al. reported a variety of redox polymers developed over the years containing stable nitroxide radicals such as TEMPO moieties[32]. Moreover, an important chemical group with redox properties that it is actively being incorporated into polymer materials is the carbonyl group. [33] Different polymers including quinone, anthraquinone, quinine, anhydride or ascorbic acid and some other antioxidants have been investigated due to their redox ability. These polymers are suitable active materials for organic batteries and supercapacitors.

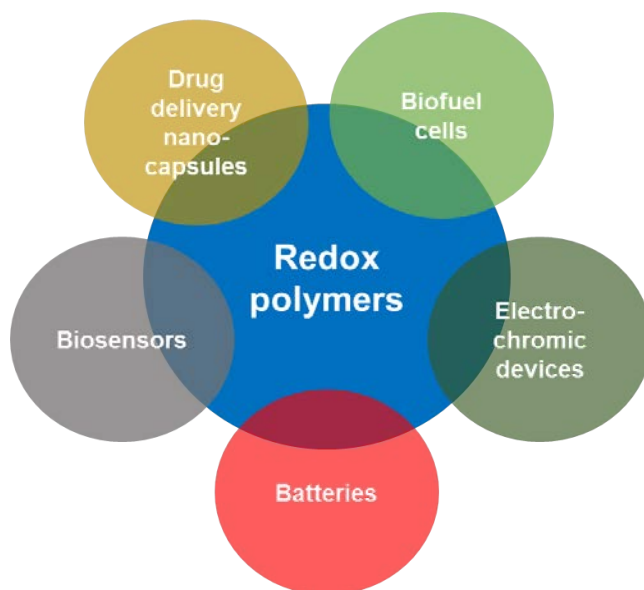


Figure 1.5. Redox polymer application fields.

During this thesis work we present a new concept of single use batteries specifically made to power small electronic devices that when disposed, breaks down into simple compounds as a result of the biotic degradative processes of microorganisms present in soils and natural water bodies. This means that unlike the previous examples of transient batteries where only some components were dissolvable in saline solutions or degraded due to self-corrosion phenomena, our batteries has the potential to undergo complete mineralization of its chemicals to CO_2 , CH_4 , H_2O and N_2 , which allows the battery to effortlessly close its cycle back to nature.



1.3. SUMMARY

This thesis presents the development of biodegradable batteries aligned with the sustainability principles of circular economy. These energy sources are focused on reducing the exorbitant quantity of electronic waste caused by the accelerated growth of electronic devices.

The present work has been developed at the Institute of Microelectronics of Barcelona, IMB-CNM (CSIC). The batteries presented in this thesis have been completely constructed from organic materials and can be manufactured by economic methods with low energy consumption. This thesis is composed of six chapters: the introductory chapter and five experimental chapters. A graphic representation of the thesis structure is shown in Figure 1.6.

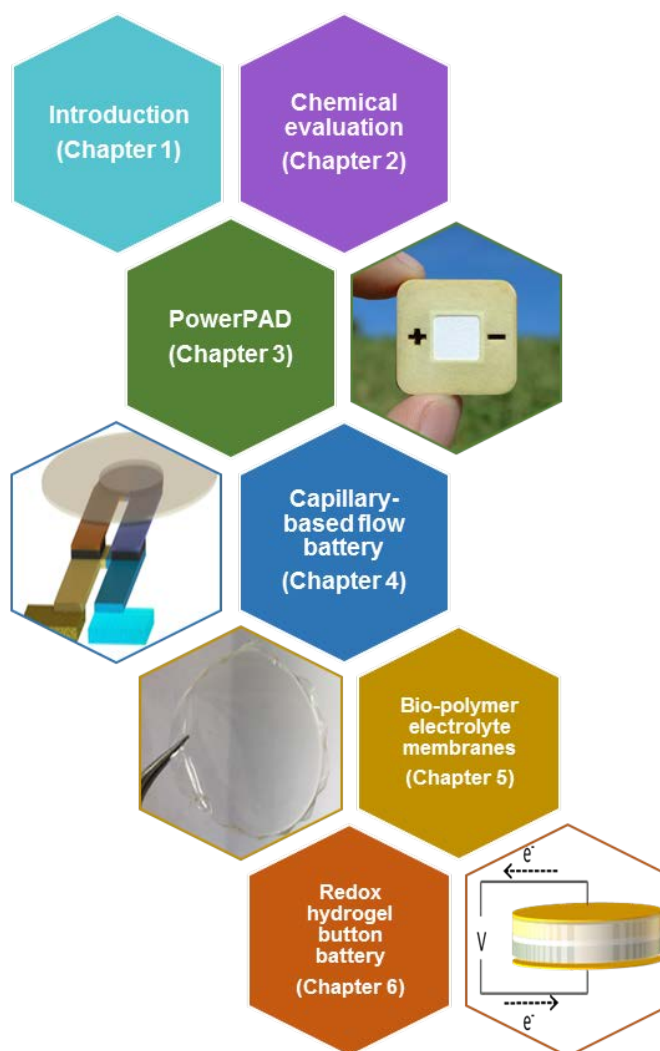


Figure 1.6. Schematic summary of the thesis content and chapter organization.

Chapter 2 of this work is dedicated to the exploration of different redox species appropriate for the development of ecological power sources. In this chapter, the electrochemical characterization of various redox and electrolyte species that met the requirements for the projected batteries was carried out. The selection of the redox species was based on their potential for oxidation, solubility, storage in the solid state and their low toxicity.

The third chapter presents the PowerPAD concept, the development of the first biodegradable battery made of paper, carbon electrodes, organic redox species and beeswax. The battery is biotically degradable, that is, the microorganisms present in soils and waters, can degrade the battery to basic compounds with minimal environmental impact. This new class of portable, biodegradable redox flow batteries is ideal for powering the upcoming generation of green electronics devices.

Chapter 4 of this thesis is devoted to the development of a capillary-based flow battery. This flow cell has been designed as an effort to optimize the PowerPAD device and has used the same natural materials. A cellulose absorbent pad has been incorporated at the end of the device to provide a quasi-steady flow of the redox species. The electrochemical evaluation of the cell was carried out at different capillary flow rates and electrode reaction areas. In this way, the device presents an optimized faradaic efficiency.

In the fifth chapter, a new approach to develop biodegradable batteries is presented. The synthesis and evaluation of biopolymer electrolyte membranes (BioPEMs). These BioPEMs have been manufactured based on natural polymers and organic compounds, such as chitosan, lyophilized cellulose and glycerol as a plasticizer. During this chapter it was possible to carry out the synthesis of two membranes with low toxicity and low manufacturing cost that presented adequate ionic conductivity and low migration of redox species, suitable characteristics for their use in primary flow batteries.

Chapter 6 of this thesis presents the development of a primary button cell battery based on lyophilized cellulose hydrogels, chitosan and redox species. This device has been manufactured using porous carbon electrodes, which have been impregnated by the redox hydrogel matrix and uses a BioPEM to separate anode and cathode. The result is a powerful button cell battery in harmony with the environment.

Finally, the general conclusions of this thesis are presented highlighting the most remarkable aspects of this work and some of the proposed future work in this research line.



References in Introduction

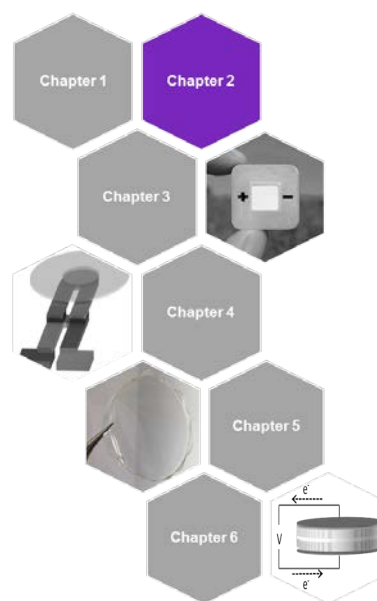
- [1] S. Damrongsiri, S. Vassanadumrongdee, P. Tanwattana, Heavy metal contamination characteristic of soil in WEEE (waste electrical and electronic equipment) dismantling community: a case study of Bangkok, Thailand, *Environ. Sci. Pollut. Res.* 23 (2016) 17026–17034. doi:10.1007/s11356-016-6897-5.
- [2] R. Widmer, H. Oswald-Krapf, D. Sinha-Khetriwal, M. Schnellmann, H. Böni, Global perspectives on e-waste, *Environ. Impact Assess. Rev.* 25 (2005) 436–458. doi:10.1016/j.eiar.2005.04.001.
- [3] L. Moreno-Merino, M.E. Jiménez-Hernández, A. de la Losa, V. Huerta-Muñoz, Comparative assessment of button cells using a normalized index for potential pollution by heavy metals, *Sci. Total Environ.* 526 (2015) 187–195. doi:10.1016/j.scitotenv.2015.04.068.
- [4] T.C. Wanger, The Lithium future-resources, recycling, and the environment, *Conserv. Lett.* 4 (2011) 202–206. doi:10.1111/j.1755-263X.2011.00166.x.
- [5] D. Larcher, J.M. Tarascon, Towards greener and more sustainable batteries for electrical energy storage, *Nat. Chem.* 7 (2015) 19–29. doi:10.1038/nchem.2085.
- [6] F.O. Ongondo, I.D. Williams, T.J. Cherrett, How are WEEE doing? A global review of the management of electrical and electronic wastes, *Waste Manag.* 31 (2011) 714–730. doi:10.1016/j.wasman.2010.10.023.
- [7] Fierge Jill, The beauty in batteries, (2017). <http://www.northamericanmissions.faith/blog/>.
- [8] Mavropoulos Antonis, Wasteless Future, (2016). <https://wastelessfuture.com/shaping-the-social-footprint-of-circular-economy/>.
- [9] D. Tobjörk, R. Österbacka, Paper electronics, *Adv. Mater.* 23 (2011) 1935–1961. doi:10.1002/adma.201004692.
- [10] T. Kaneko, T.H. Thi, D.J. Shi, M. Akashi, Environmentally degradable, high-performance thermoplastics from phenolic phytomonomers, *Nat. Mater.* 5 (2006) 966–970. doi:10.1038/nmat1778.
- [11] H. Jimbo, N. Miki, Gastric-fluid-utilizing micro battery for micro medical devices, *Sensors Actuators B Chem.* 134 (2008) 219–224. doi:10.1016/j.snb.2008.04.049.
- [12] Y.J. Kim, S.-E. Chun, J. Whitacre, C.J. Bettinger, Self-deployable current sources fabricated from edible materials, 1 (2013) 2050–750. <http://pubs.rsc.org/en/content/articlepdf/2013/tb/c3tb20183j> (accessed July 17, 2017).
- [13] L. Yin, X. Huang, H. Xu, Y. Zhang, J. Lam, J. Cheng, J.A. Rogers, Materials, designs, and operational characteristics for fully biodegradable primary batteries, *Adv. Mater.* 26 (2014) 3879–3884. doi:10.1002/adma.201306304.
- [14] X. Huang, D. Wang, Z. Yuan, W. Xie, Y. Wu, R. Li, Y. Zhao, D. Luo, L. Cen, B. Chen, H. Wu, H. Xu, X. Sheng, M. Zhang, L. Zhao, L. Yin, A Fully Biodegradable Battery for Self-Powered Transient Implants, *Small.* (2018) 1800994. doi:10.1002/sml.201800994.
- [15] Y. Ding, Y. Li, G. Yu, Exploring Bio-inspired Quinone-Based Organic Redox Flow Batteries: A Combined Experimental and Computational Study, *Chem.* 1 (2016) 790–801. doi:10.1016/j.chempr.2016.09.004.
- [16] Z. Zhu, T. Kin Tam, F. Sun, C. You, Y.H. Percival Zhang, A high-energy-density sugar biobattery based on a synthetic enzymatic pathway, *Nat. Commun.* 5 (2014) 1–8. doi:10.1038/ncomms4026.

- [17] J. Maya-Cornejo, E. Ortiz-Ortega, L. Álvarez-Contreras, N. Arjona, M. Guerra-Balcázar, J. Ledesma-García, L.G. Arriaga, Copper–palladium core–shell as an anode in a multi-fuel membraneless nanofluidic fuel cell: toward a new era of small energy conversion devices, *Chem. Commun.* 51 (2015) 2536–2539. doi:10.1039/C4CC08529A.
- [18] M. Irimia-Vladu, “Green” electronics: biodegradable and biocompatible materials and devices for sustainable future, *Chem. Soc. Rev.* 43 (2014) 588–610. doi:10.1039/C3CS60235D.
- [19] Y. Chen, R. Jamshidi, K. White, S. Cinar, E. Gallegos, N. Hashemi, R. Montazami, Physical-chemical hybrid transiency: A fully transient li-ion battery based on insoluble active materials, *J. Polym. Sci. Part B Polym. Phys.* 54 (2016) 2021–2027. doi:10.1002/polb.24113.
- [20] A.W. Martinez, S.T. Phillips, M.J. Butte, G.M. Whitesides, Patterned Paper as a Platform for Inexpensive , Low-Volume , Portable, (2010) 1318–1320. doi:10.1002/anie.200603817.
- [21] E. Fu, S.A. Ramsey, P. Kauffman, B. Lutz, P. Yager, Transport in two-dimensional paper networks, (2011) 29–35. doi:10.1007/s10404-010-0643-y.
- [22] S. Ahmed, M.-P.N. Bui, A. Abbas, Paper-based chemical and biological sensors: Engineering aspects, *Biosens. Bioelectron.* 77 (2016) 249–263. doi:10.1016/J.BIOS.2015.09.038.
- [23] R. Masoodi, K.M. Pillai, *Wicking in Porous Materials Traditional and Modern Modeling Approaches.*, CRC Pr I Llc, 2017.
- [24] J.B. Conant, H.M. Kahn, L.F. Fieser, S.S. Kurtz, AN ELECTROCHEMICAL STUDY OF THE REVERSIBLE REDUCTION OF ORGANIC COMPOUNDS¹, *J. Am. Chem. Soc.* 44 (1922) 1382–1396. doi:10.1021/ja01427a020.
- [25] K. Wedege, E. Dražević, D. Konya, A. Bentien, G. Sandstede, Organic Redox Species in Aqueous Flow Batteries: Redox Potentials, Chemical Stability and Solubility, *Sci. Rep.* 6 (2016) 39101. doi:10.1038/srep39101.
- [26] U. Er, C. Suh, M.P. Marshak, A. Aspuru-Guzik, Computational design of molecules for an all-quinone redox flow battery, *Chem. Sci.* 6 (2015) 845–1592. doi:10.1039/c4sc03030c.
- [27] F.J. Enguita, A.L. Leitão, Hydroquinone: Environmental pollution, toxicity, and microbial answers, *Biomed Res. Int.* 2013 (2013). doi:10.1155/2013/542168.
- [28] Y. Onuki, U. Bhardwaj, F. Papadimitrakopoulos, D.J. Burgess, A review of the biocompatibility of implantable devices: current challenges to overcome foreign body response., *J. Diabetes Sci. Technol.* 2 (2008) 1003–15. doi:10.1177/193229680800200610.
- [29] W. Suginta, P. Khunkaewla, A. Schulte, Electrochemical Biosensor Applications of Polysaccharides Chitin and Chitosan, *Chem. Rev.* 113 (2013) 5458–5479. doi:10.1021/cr300325r.
- [30] A. Heller, Electron-conducting redox hydrogels: design, characteristics and synthesis, *Curr. Opin. Chem. Biol.* 10 (2006) 664–672. doi:10.1016/J.CBPA.2006.09.018.
- [31] R. Gracia, D. Mecerreyes, Polymers with redox properties: materials for batteries, biosensors and more, *Polym. Chem.* 4 (2013) 2206. doi:10.1039/c3py21118e.
- [32] T. Suga, S. Sugita, H. Ohshiro, K. Oyaizu, H. Nishide, p- and n-Type Bipolar Redox-Active Radical Polymer: Toward Totally Organic Polymer-Based Rechargeable Devices with Variable Configuration, *Adv. Mater.* 23 (2011) 751–754. doi:10.1002/adma.201003525.
- [33] K. Oyaizu, A. Hatemata, W. Choi, H. Nishide, Redox-active polyimide/carbon



nanocomposite electrodes for reversible charge storage at negative potentials: expanding the functional horizon of polyimides, *J. Mater. Chem.* 20 (2010) 5404.

2.



Evaluation of chemical compounds for redox primary batteries

Overview

The aim of the current chapter of the thesis is to present all the efforts and results regarding to the establishment of the parameters involved to identify the redox compounds and electrolytes which are completely safe and non-toxic, yet inexpensive for the transient batteries taking place during this thesis work.

This work focuses on the half-cell evaluation of the redox compounds and electrolytes concerning their redox potential, and cell characterization measuring their discharge performance. The evaluation of catholytes in different acidic media electrolyte is presented in order to identify the most adequate candidates for the aims of this thesis.

2.1. INTRODUCTION

At present, the evaluation and exploration of several organic and inorganic redox species as candidates for a prospective use as fuel in a disposable capillary flow cell are presented in this chapter. For this purpose, the compounds studied must meet certain requirements for their suitable incorporation into paper-based devices. The requirements of the chemical species involved in this type of batteries were studied based on their solubility in water, storability, biodegradability and primarily their electrochemical characteristics.

First, a characterization of the redox potentials of the species involved in the electrolyte that favored its reaction was carried out. Subsequently, the search for neutral medium was carried out in two ways: the use of mixed medium and the test in neutral medium. For this test, the alternate redox couple was used for the quinone pairs, since the latter is the same species in a different oxidation state, so there would not be a voltage window when tested in a neutral medium. And finally, the search for storable electrolytes in solid state and their electrochemical characterization was carried out.

2.2. IDENTIFICATION OF REDOX COMPOUNDS

In order to select the most suitable redox species, the study was ideally centered on organic species, due to the firm idea of developing biodegradable devices with minimal environmental footprint. Although the evaluation of inorganic species that could close the redox reaction was also considered. A subset of redox species was analyzed, identifying the chemicals that met the requirements regarding to solubility, storability in solid state, biodegradability and redox state, optimal standard redox potential to obtain an adequate open circuit and a good kinetic reaction response.

A quinone is a type of organic compound that is formally derived from aromatic compounds (such as benzene or naphthalene) by change of groups $-CH =$ by groups $-C(=O)-$, without rearranging double links, resulting in a fully conjugated cyclic dione structure. This type includes derivatives of heterocyclic aromatic compounds. Quinones are very abundant compounds in nature, found in higher plants in fungi and bacteria, found in the leaves, pods, roots and seeds of various plants.

Organic quinone redox species have recently captured the attention of the flow battery research community, owing to their eco-friendly, nature-inspired redox reactions with fast kinetics and low cost[1]. These quinone compounds match the majority of the requirements for the proposed battery.

For the reduced hydroquinones to be used at the negative electrode, hydroquinone sulfonic acid (H_2BQS , Table 2.1a), is an example identified as a potential benzoquinone available in the reduced form. Other quinones that are known to have relatively low standard potential are anthraquinones, so they have been considered suitable for the use in the negative electrode of the current approach, as they provide a sufficiently negative electrode potential when they are used in alkaline media.



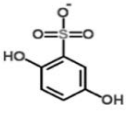
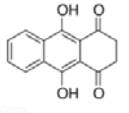
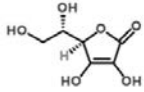
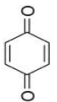
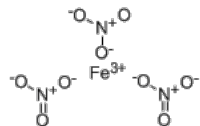
However, the reduced forms of anthraquinones available commercially are limited, so the most suitable option for the negative half-cell is deemed to be 1,4,9,10-Tetrahydroanthracene or leucoquinizarin (LQ, Table 2.1b). Other biodegradable options for the negative half-cell that could be considered are organic acids with anti-oxidant characteristics, such as ascorbic acid (AA, Table 2.1c), also known as vitamin C. Such acid is deemed to be a theoretically viable candidate for the negative half-cell due to the fact that it is a soluble phytochemical and commonly used antioxidant with a suitable negative standard potential for oxidation.

In table 2.1. It is possible to observe the structure of the candidate redox species for this chemical evaluation, as well as the reaction that takes place in the process of reduction (catholytes) and oxidation (anolytes).

On the other hand, p-benzoquinone (pBQ, Table 2.1d) was identified and selected for the oxidized quinone to be used in the positive electrode. Being the simplest form of quinone compound, pBQ is soluble in aqueous media and readily biodegradable. Besides, pBQ is commercially available in solid form in its oxidized state, and this enables direct use for electrochemical reduction in the positive half-cell of the battery. The reason for such choice is that other oxidized quinones such as naphthoquinones (NQ) and anthraquinones (AQ) have lower solubility and a lower standard reduction potential, which renders them inadequate for the current application. Ortho-benzoquinone (o-BQ) was also considered due to fact that it has a higher reduction potential than pBQ, but it is not commercially available in the oxidized form, and the only form available is its reduced form (Catechol).

Various inorganic salts, which may enable high solubility as well as other environmental benefits, could also be used for this concept. Iron nitrate (Fe^{3+}) (Table 2.1e) is abundant and has a standard potential slightly higher than the pBQ used in this work (0.77 V vs. SHE), which would enable a much higher aqueous solubility limit and therefore higher energy densities. Hence, ferric salts of nitrates, sulfates or phosphates, which are known to enrich soils, may lead to a battery that could even add value to the soil or water in which it is disposed of.

Table 2.1. Structures and redox reaction of quinones, ascorbic acid and iron nitrate used in this work.

Anolyte	Structure	Reaction
a) Hydroquinone sulfonic acid (H ₂ BQS)		$\text{H}_2\text{BQS} \leftrightarrow \text{BQS} + 2\text{e}^- + 2\text{H}^+$
b) Leucoquinizarin (LQ)		$\text{H}_2\text{LQ} \leftrightarrow \text{LQ} + 2\text{e}^- + 2\text{H}^+$
c) Ascorbic acid		$\text{AA} \leftrightarrow \text{AQS} + 2\text{e}^- + 2\text{H}^+$
Catholyte	Structure	Reaction
d) Para-benzoquinone (pBQ)		$\text{pBQ} + 2\text{e}^- + 2\text{H}^+ \leftrightarrow \text{HBQ}$
e) Iron nitrate (Fe ³⁺)		$\text{Fe}^{3+} + \text{e}^- \leftrightarrow \text{Fe}^{2+}$

2.3. CHARACTERIZATION OF REDOX SPECIES

By using cyclic voltammetry (CV) and linear sweep voltammetry (LSV) techniques, the redox species were evaluated measuring their half-cell open circuit potentials (OCPs) and electrochemical kinetics. The measurements were performed in a conventional three-electrode electrochemical cell bubbled with nitrogen to minimize solution oxidation due to dissolved oxygen or ambient air. Glassy carbon electrode (0.07 cm²), platinum wire electrode and Silver-silver chloride electrode (Ag/AgCl) (CH instruments Inc, TX, USA) are used as working electrode, counter electrode and reference electrode, respectively, and the cell is operated by a frequency response analysis compatible potentiostat (DropSens μ Stat400 Bipotentiostat/Galvanostat and DropView 8400 Software (DropSens S.L., Asturias, Spain) Prior to scanning, the OCP of each half-cell is measured at zero applied current. Cyclic voltammetry is then recorded at a scan rate (ω) of 50mV/s followed by linear sweep voltammetry measurements in the voltage sweep direction of the respective discharge reaction of interest.



2.3.1. Quinone species

One of the objectives of this work was to identify redox species whose use results in the least toxic environmental damage, so that having waste at neutral pH became crucial. Given that the Quinone species used are the same species in different oxidation state, the evaluation in a neutral medium would result in a significantly small OCP. Another option of having a neutral electrolyte media was the use of mixed electrolytic-media. Mixed-media operation offers an opportunity for the acidic and alkaline electrolytes to neutralize downstream by means of diffusive mixing to form neutral or near neutral pH conditions that allow safe disposal, which is an essential requirement for the disposable cell. Moreover, the use of mixed electrolytic-media allows the obtaining of higher electrochemical voltages during the discharge operation. Therefore, the dependence of pH to modify the redox potential of the chemical species and leading a neutral final pH used in this section, such as quinones, was exploited in this application. Therefore, reduced quinones (-OH) can be used in the alkaline conditions in the anolyte and combined with an acidic positive half-cell. The mixed electrolyte system is enabled by membrane-less devices such as co-laminar flow cells[2] where by means of an external force you keep the flows flowing through the microfluidic channels without getting into contact or mixing.

As already mentioned, para-Benzoquinone (pBQ) was selected for the positive half-cell, this specie undergoes a two electron, two proton transfer in acidic media, with a standard reduction potential of 0.69 V vs. SHE.[3] Here, pBQ was found to have an aqueous solubility limit of 0.1 M at room temperature and is thus dissolved to this saturation concentration in 1 M sulfuric acid (H₂SO₄) as a standard acidic supporting electrolyte. The solubility in aqueous media was evaluated and was found that H₂BQS is soluble up to 0.7 M in water. However, LQ is found to be hardly soluble in water and to have a hydrophobic behavior, resulting in the formation of agglomerates, which is limiting for the desired application. The solubility limit for the three compounds is expected to be particularly high in KOH solution due to the deprotonation that provides solubility and higher electron donation capabilities.[4]

For the negative half-cell, the two anolyte quinone compounds selected were evaluated at a concentration of only 0.1 M in order to match the concentration of the limiting reactant, pBQ, and therefore balance the final reaction in the cell. The electrochemical reaction for the quinones (H₂BQS and LQ) was assessed in 1 M potassium hydroxide (KOH) to establish the desired alkaline conditions for this electrode involves transfer of two electrons after deprotonation in alkaline conditions.[4]

The cyclic voltammograms for the redox species is shown in Figure 2.2 at a scan rate of 50 mV/s. Before the potential sweep, the anolyte half-cell OCPs are measured to be -0.34 V, and -0.80 V vs. Ag/AgCl for the H₂BQS and LQ, respectively, which suggests a prospective full cell potential window of > 1 V when paired with pBQ. Nevertheless, the LQ is found to be rather unstable and its oxidized form has limited solubility in KOH causing visually observed precipitation which challenges its

prospective use in capillary flow cells due to possible clogging of the porous media excluded from operation of the final device. Despite the more positive half-cell OCP of H₂BQS compared to LQ which results in a lower cell voltage, the CV results also show that H₂BQS has a higher peak current density than LQ which may reflect higher species diffusivity and faster kinetics.

The measured p-BQ half-cell OCP equals 0.565 V vs. Ag/AgCl, which is in reasonable agreement with the standard potential given the more acidic condition and fully oxidized form used here. pBQ presents good kinetics on the carbon electrode, as shown in the figure, and is deemed an adequate reactant species for the positive half-cell of the present application.

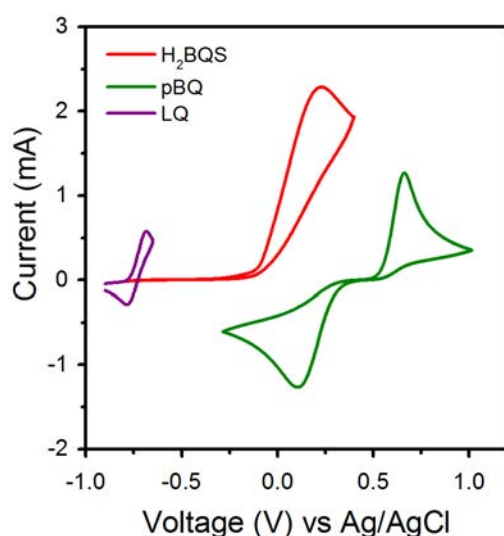


Figure 2.2. Cyclic voltammograms at a scan rate of 50 mV/s for reduction of 0.1 M pBQ in 1 M H₂SO₄ and oxidation of 0.1 M H₂BQS and LQ in 1 M KOH.

2.3.2. Innocuous redox alternatives

As a result of the evaluation of other alternative species to the group of quinones, in the negative electrode, ascorbic acid AA; a commonly used antioxidant compound present in nature was selected as promising alternative anolyte. The electrochemical reaction in highly alkaline media also involves a two electron oxidation of ascorbate[5,6], since deprotonation of the acid occurs by reaction with KOH. The solubility of AA was up to 1.9 M in water. As another catholyte possibility, iron nitrate was also evaluated, as it has water solubility above 4 M.



To continue working with concentrations previously established for the quinone species, AA was used at 0.1M and in the case of iron nitrate, 0.2 M was used to obtain a stoichiometric balance of charges involved, since for every two electrons donated during the oxidation of the anolyte, iron nitrate can gain one by requiring twice as many species to balance the redox reaction. In this sense, solutions of AA 0.1M were evaluated in KOH 1M and PBS, and solutions of 0.2 M of iron nitrate in 1 M sulfuric acid (H_2SO_4) and in PBS were evaluated in a half-cell. The cyclic voltammograms of these solutions are shown in Figure 2.3. The half-cell potential for AA was measured to be -0.39 V and 0.15 V vs. Ag/AgCl for the H_2SO_4 and PBS electrolyte solution, respectively. In the cathode side, iron nitrate expressed a reduction potential of around 0.53 V vs Ag/AgCl, in both electrolyte media which is in fact very similar to the previous one presented for the p-BQ compound.

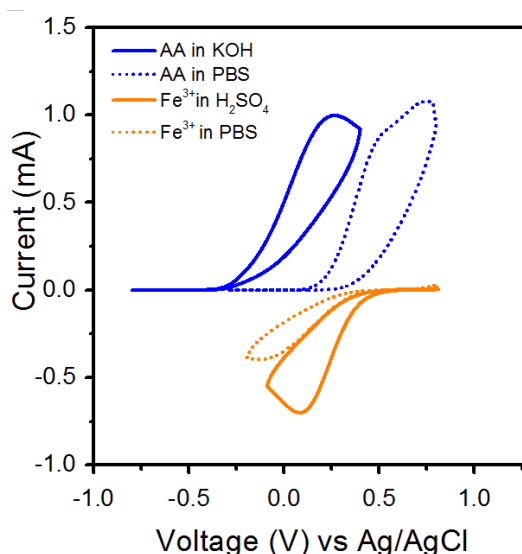


Figure 2.3. Cyclic voltammograms at a scan rate of 50 mV/s for reduction of 0.1 M Fe^{3+} in 1 M H_2SO_4 , and in PBS; and oxidation of 0.1 M, AA in 1 M KOH and in PBS.

As a general discussion, the absence of the reverse peak in both anolyte cases of AA and H_2BQS is likely attributed to the instability of the electro-oxidation produced species in alkaline conditions, as also observed in other works.[7–10]. Despite these indications that both H_2BQS and AA may not be reversible under alkaline conditions and hence unsuitable for a conventional flow battery application in alkaline conditions, both are adequate for the primary battery approach presented in this work, since only the electro-oxidation portion of the cycle is of interest.

It is thus concluded that both AA and H_2BQS are suitable as anolytes for the final device application, with AA having a more negative half-cell OCP advantage and H_2BQS having a higher diffusion rate and faster kinetics, while pBQ and iron nitrate are identified, both, as candidates for the positive electrode. Moreover, it was reassured that the use of mixed media not only allows increasing the cell voltage, but also increases the spectrum of candidates for electrolytes that can be used.

2.4. CHARACTERIZATION OF STORABLE ELECTROLYTES IN POWDER

Then, since one of the requirements to be met by the redox species and the electrolytes required for this and subsequent tests in this section, the compounds should be able to be stored in the solid state and be soluble in water, in what refers to the electrolyte of the anode, KOH, perfectly fulfills this requirement. However, while H₂SO₄ cannot be dried or stored in the solid phase on the final device the evaluation of other more suitable acidic electrolytes was carried out.

At the line of investigation of this work was based on the identification of innocuous redox species and electrolytes. Various organic or inorganic acids could be considered for this purpose; however, the resulting supporting electrolyte must be stable with inert chemical and electrochemical activity, acidic at low pH in order to maintain the mixed-media benefits and have high ionic conductivity in order to retain the good discharge performance.

An organic acid is an organic compound with acidic properties. Common organic acids are the carboxylic acids, whose acidity is associated with their carboxyl group –COOH. Within this kind of acids and based on the logarithmic measure of the acid dissociation constant (pK_a), that categorizes the strength of an acid, two main organic acids with lower pK_a were oxalic acid (OA) and citric acid (CA). were identified. Both of them are compounds founds in solid state and fulfilling the main requirement of the electrolytes.

Therefore, oxalic acid (OA) is identified as a strong organic acid with low measured pH and aqueous solubility up to 1 M. Moreover, citric acid (CA) is also identified as another organic acid with a much higher solubility limit. Both OA and CA are phytochemicals that are present in nature and are both predicted to have fast biodegradation probability by EPISuite™ from the US Environmental Protection Agency.[11]

2.4.1. Characterization of redox species in organic acids

The cyclic voltammeteries performed for both redox species used as catholytes were 0.1 M p-BQ and 0.3 M Fe³⁺, in three different electrolytes, 0.5 M, 1M CA and 1 M H₂SO₄ are shown in Figure 2.3. The pH of the electrolytes at a concentration of 1M of the species was measured, obtaining values between a range of 0.5-1 and 1.5-2 for OA and CA, (914 pH / Conductmeter, Metrohm AG, Switzerland).

The OCP of 0.1 M pBQ in 1 M OA and in 1 M CA was measured to equal 0.39 and 0.36 vs. Ag/AgCl, respectively (Figure 2.4a). The relatively low (less positive) half-cell OCP in case of CA supporting electrolyte is likely attributed to the higher pH which results in lower Nernstian potential due to the pH dependence of pBQ standard potential.

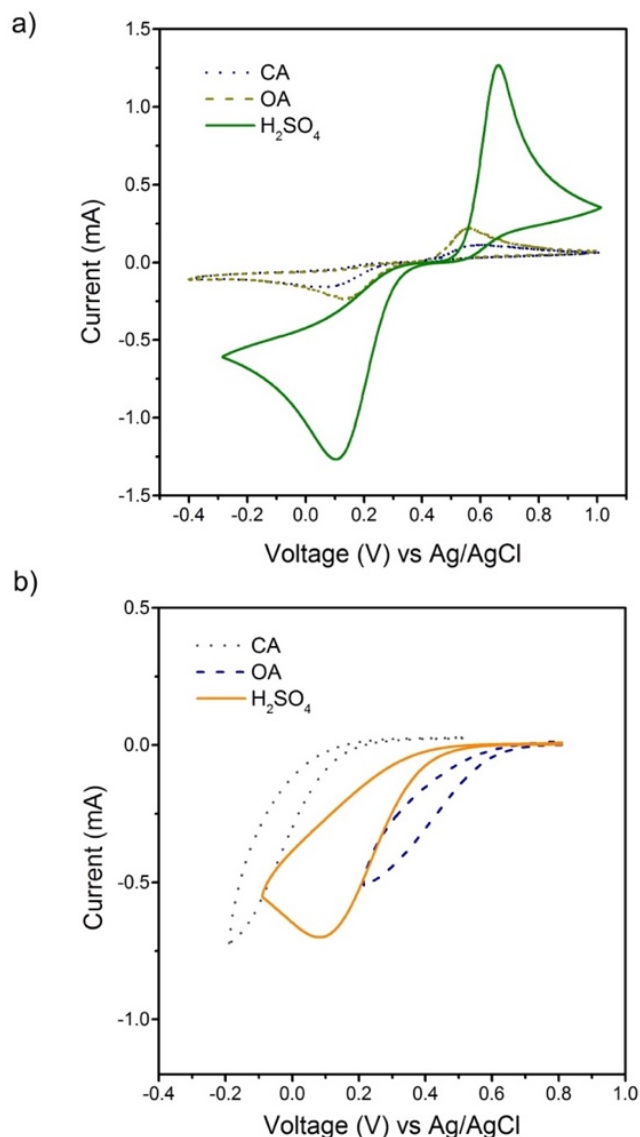


Figure 2.4. Cyclic voltammograms of catholytes pBQ (a) and iron nitrate (b) in different acidic media compounds: citric acid (CA), oxalic acid (OA) and sulfuric acid (H₂SO₄).

The data show a lower cathodic peak current (i_{pc}) for pBQ reduction in CA supporting electrolyte compared to the corresponding result for OA, which is consistent with the previous results and likely due to the lower availability of protons for the pBQ reduction.[7] In the case of the iron nitrate, the more positive reduction potential in the presence of OA is clearly observed in comparison to the CA performance and the H₂SO₄ (Figure 2.4b).

Nevertheless, despite the much higher solubility of the CA supporting electrolyte than OA, the latter option is likely preferred due to the more positive potential, faster kinetics and higher ionic conductivity, which are likely to positively impact the cell performance. Regarding to the requirements for the device in mind, OA is considered the more suitable electrolyte for the cathode half-cell in this work.

2.5. CONCLUSIONS

This study reviewed the general requirements regarding solubility, biodegradability, storability in correct redox state, redox potential of the reactant chemistries for biodegradable batteries for single-use disposable applications. Mixed-media operation suitable for membrane-less cells was leveraged to allow direct use of commercially available organic compounds such as quinones by using an alkaline negative half-cell and an acidic positive half-cell with the added benefit of downstream neutralization for safe disposal. Prospective redox chemistries for each half-cell were systematically assessed by ex-situ measurements of solubility, redox potential and in-situ discharge performance. The overall most effective chemistry identified for disposable cells was based on either ascorbic acid or H₂BQS in KOH and pBQ and Fe³⁺ in oxalic acid at the negative and positive electrodes, respectively.

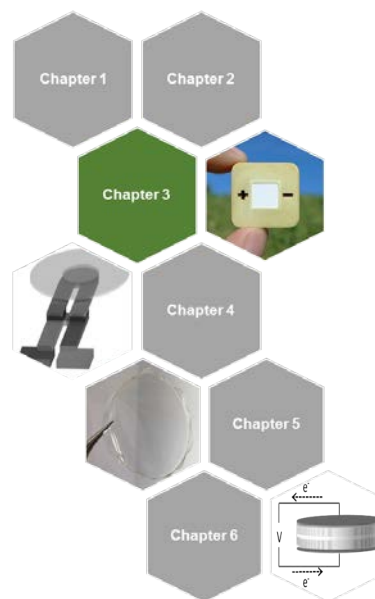
The redox chemistry screening carried out during this section identified suitable redox species and supporting electrolytes that are commercially available, according to the literature, and fit for use in the following chapters of this work. The devices in mind for this investigation required redox biodegradable components for the negative and positive half-cell with high performance and stability. For the future work in this thesis, the active redox species use as reactants need to exist in the solid phase at ambient conditions, for instance in powder form, for the suitable storage of the chemistries in the cell. Such storage must be done in the correct redox state required for discharge operation with net current generation at an adequate cell voltage, soluble in water or other desired electrolyte, owning a catalyst-free carbon electrode with fast kinetics behavior. Therefore, the results provide the departing redox compounds for a new generation of biodegradable and sustainable primary batteries that minimize waste from conception and design.



References in Chapter 2.

- [1] G.L. Soloveichik, *Electrochemistry: Metal-free energy storage*, (2015) 3–5. doi:10.1038/505163a.
- [2] J.P. Esquivel, F.J. Del Campo, J.L. Gómez de la Fuente, S. Rojas, N. Sabaté, Microfluidic fuel cells on paper: meeting the power needs of next generation lateral flow devices, *Energy Environ. Sci.* 7 (2014) 1744. doi:10.1039/c3ee44044c.
- [3] W. M. Haynes, *CRC Handbook of Chemistry and Physics*, 94th Edition, 2013–2014, 2013. doi:10.1136/oem.53.7.504.
- [4] K. Lin, Q. Chen, M.R. Gerhardt, L. Tong, S.B. Kim, L. Eisenach, A.W. Valle, D. Hardee, R.G. Gordon, M. Aziz, M.P. Marshak, Alkaline quinone flow battery, *Science* (80-.). 349 (2015) 1529–1532. doi:10.1126/science.aab3033.
- [5] J. Du, J.J. Cullen, G.R. Buettner, Ascorbic acid: Chemistry, biology and the treatment of cancer, *Biochim. Biophys. Acta - Rev. Cancer.* 1826 (2012) 443–457. doi:10.1016/j.bbcan.2012.06.003.
- [6] N. Fujiwara, S. Yamazaki, Z. Siroma, T. Ioroi, K. Yasuda, l-Ascorbic acid as an alternative fuel for direct oxidation fuel cells, *J. Power Sources.* 167 (2007) 32–38. doi:10.1016/j.jpowsour.2007.02.023.
- [7] C. Giacomelli, K. Ckless, D. Galato, F.S. Miranda, A. Spinelli, Electrochemistry of Caffeic Acid Aqueous Solutions with pH 2.0 to 8.5, *J. Braz. Chem. Soc.* 13 (2002) 332–338. doi:10.1590/S0103-50532002000300007.
- [8] M. Rafiee, D. Nematollahi, Voltammetry of electroinactive species using quinone/hydroquinone redox: A known redox system viewed in a new perspective, *Electroanalysis.* 19 (2007) 1382–1386. doi:10.1002/elan.200703864.
- [9] S.I. Bailey, I.M. Ritchie, A cyclic voltammetric study of the aqueous electrochemistry of some quinones, *Electrochim. Acta.* 30 (1985) 3–12. doi:10.1016/0013-4686(85)80051-7.
- [10] R. Gulaboski, I. Bogeski, V. Mirčeski, S. Saul, B. Pasiëka, H.H. Haeri, M. Stefova, J.P. Stanoeva, S. Mitrev, M. Hoth, R. Kappl, Hydroxylated derivatives of dimethoxy-1,4-benzoquinone as redox switchable earth-alkaline metal ligands and radical scavengers, *Sci. Rep.* 3 (2013) 2841–2888. doi:10.1038/srep01865.
- [11] US EPA, Estimation Programs Interface Suite for Microsoft® Windows (EPISuite), v 4.11, Estim. Programs Interface Suite Microsoft® Wind. (EPISuite), v 4.11. (2016).

3.



A biodegradable and all-organic redox flow battery for single-use applications

Overview

This chapter presents a new approach for environmentally benign, low-cost batteries intended for single use applications. We present a new concept of single use battery specifically made to power small electronic devices that when disposed, breaks down into simple compounds as a result of the biotic degradative processes of microorganisms present in soils and natural water bodies. This means that unlike the previous examples of transient batteries where only some components were dissolvable in saline solutions or degraded due to self-corrosion phenomena, our battery has the potential to undergo complete mineralization of its chemicals to CO_2 , CH_4 , H_2O and N_2 , which allows the battery to effortlessly close its cycle back to nature.

3.1. INTRODUCTION

The battery presented below was completely built upon organic materials made of cellulose, carbon paper, beeswax and integrated quinone-based redox chemistry to generate electricity within a compact form factor. Fabricated by affordable methods with low energy consumption. Once activated, the flow redox battery can be disposed in an organic waste container or even discarded in the field, where it will biotically degrade by bacteria with a minimal environmental impact.

In a redox flow battery the chemical energy is provided by two water soluble redox compounds dissolved in liquid electrolytes contained within the system and separated by a membrane. Hence an electrolyte in which one redox species is solved flows through one half cell of the flow battery. During charge or discharge the reacting species is reduced or oxidized in the flow battery[1]. In the present redox battery, the flow is established by capillarity of the paper. The redox species flow through the paper-based cell until they reach a final absorber, without the existence of recirculation of the redox species, which is why it behaves like a primary battery, only the discharge of the battery being carried out. Another point to consider for the choice of chemical compounds was their innocuousness, with particular interest in developing an all organic battery, so that organic redox species from the group of quinones were used.

In order to reach the final objective of having a paper-based battery, the previous steps for its fabrications are also shown in this present chapter. First of all, the fluidic validation was carried out developing a proper paper-based flow battery. This design allowed establishing a co-laminar flow of the species without the addition of a membrane to avoid the species mixing. The establishment of flow-through porous carbon electrodes was developed, allowing continuing the co-laminar redox species flow in the whole cell. Moreover, the validation of the storability in solid form of the redox species and their dissolution and flow through the paper capillary was performed. The assembly of all of these concepts in order to get the powerPAD device is presenting in this work. To show the outstanding capabilities of this final device, five different research challenges pertaining to battery development are addressed in this chapter: device design, battery operation, voltage scalability, practical application and effective biotic degradation. Proposed solutions to each of these six challenges are outlined in the following sections

3.2. DEVELOPMENT OF A PAPER-BASED REDOX FLOW CELL

The work on this chapter starts assessing the development of the capillary-based microfluidic platform for the redox flow cell. Firstly, we focused on the design and fabrication of a paper-based flow cell, which meant finding redox species compatible with paper-based devices. This setup was used to evaluate the fluidic operation on a paper-based device before incorporating the organic redox species into a vertical configuration in the final device.



3.2.1. Design of a paper-based co-laminar flow cell

Recently, the intrinsic properties of paper, such as capillarity, porosity, surface area or patternability have been rediscovered, as well as its capabilities. It is thus now being used to develop complex microfluidic functions, which has proved to be of special interest in the field of clinical diagnostics. In order to develop a paper-based microfluidic fuel cell in which the fluids are driven by capillary action, so no external pumps are needed, these features have been used[2]. Based upon those previous works, the co-laminar flow cell developed follows a similar approach. Different laminated materials have been used in the fabrication of this first prototype.

The mass transport of liquid phase species is based on capillary flow through a paper channel that is placed over carbon electrodes, as can be observed in Figure 3.1. Oxidation and reduction electrodes are placed on opposite sides of the paper channel, separated by a few millimeters. A larger carbon electrode has also been included, which will be used as counter electrode in the half-cell characterization.

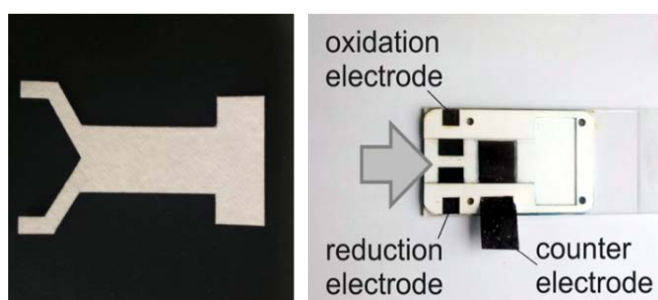


Figure 3.1. Pictures of the paper channel (left) and redox cell prototype indicating its electrodes (right).

Firstly, the co-laminar flow of two parallel laminar flow streams jointly driven by capillary forces were evaluated. In a paper channel the relevant length scale is the membrane pore diameter (typically from 1 to 10 μm) resulting in Reynolds numbers on the order of 10^{-3} at the typical flow rates. This low Reynolds number allows the laminar flow of anolyte and catholyte to co-exist in a common paper channel without presenting a turbulent mixture of streams. Under this regime, mixing of the two streams occurs only by diffusion and is restricted to an interfacial width at the center of the channel. Thus, if the anode and cathode electrodes are far enough from the inter-diffusion zone, electrode reactions can take place independently. In order to evaluate the correct laminar flow in the prototype, two color dyes were flown through the paper channel. The paper selected as substrate for the paper-based microfluidic flow cell was Whatman® paper, grade Fusion 5 (370 μm thick), due to its high wicking rate, the pieces were cut using a CO₂ laser cutter (Mini 24, Epilog Laser, Golden, CO, USA). Figure 3.2 shows a sequence of pictures of the capillary flow during this experiment.

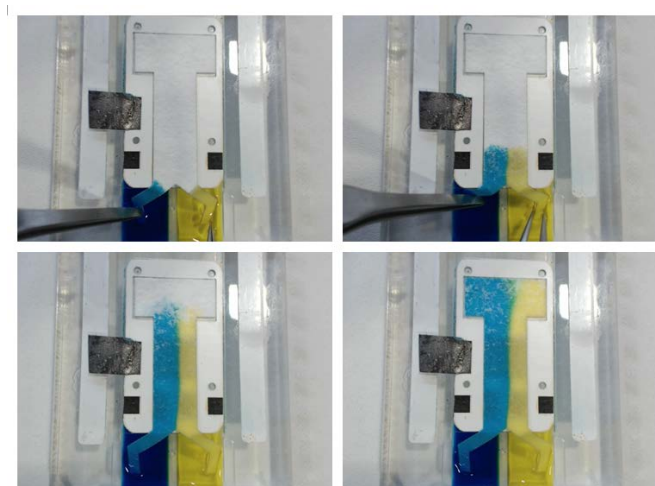


Figure 3.2. Pictures showing the progression of the co-laminar capillary flow along the paper cell and how the two flows can be kept effectively separated until they reach the absorbent pad.

It is observed the establishment of a capillary co-laminar flow of two different fluids inside the paper channel in a pumpless system. These dyes replace the redox reactants that will be used later to carry out the paper-based flow cell.

3.2.2. Validation of capillary flow cell with a suitable redox couple

After demonstrating that a co-laminar flow is presented in a paper channel, the same paper configuration was used as the platform for the paper-based flow cell.

It is important to mention that the voltage generated by an electrochemical cell, in this case a co-laminar redox flow cell, can be expressed as follows:

$$V_{cell} = V_{reduction} - V_{oxidation}$$

So as to obtain a positive cell voltage the catholyte (reduction), aided by the electrolyte, must express a higher reduction potential than the oxidation potential shown by the anolyte (oxidation). Moreover it was necessary to take into consideration properties like solubility or toxicity. In fact, in nature it is difficult to find species that are in a suitable oxidation state for "ready-to-use" power generation, which was one of the main requirements in this work.

In order to validate the paper-based flow cell, a suitable and well-known redox couple was chosen. On the one hand, as a potential anolyte, $K_4[Fe(CN)_6]$ was selected because despite its potential toxicity, it is a well-established, highly stable compound with a low redox potential. On the other hand, iron nitrate was chosen as a potential catholyte, as it showed good performance and although its reduction potential is relatively low, it can be combined with the $K_4[Fe(CN)_6]$ to yield a redox cell for the purpose of paper-based flow cell development. In order to evaluate the reduction and oxidation potentials of the redox species, their performance were characterized in a separate electrochemical cell in a three electrode system[3] , the cyclic



voltammograms can be observed in Figure 3.3. The redox pair consequently was used to conduct half-cell measurements of both anolyte and catholyte in the paper platform.

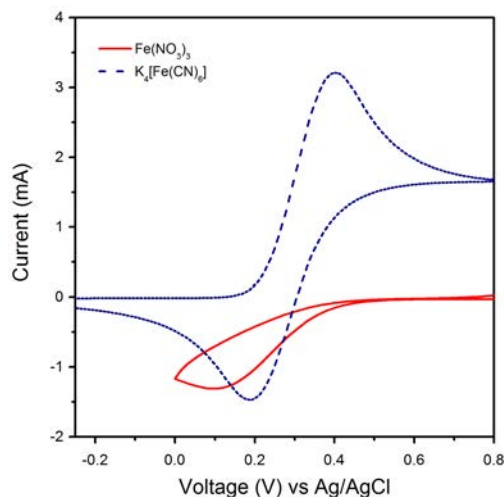
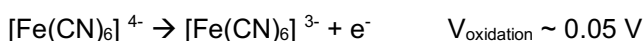


Figure 3.3. Cyclic voltammeter responses of $K_4[Fe(CN)_6]$ and $Fe(NO_3)_3$ redox couple.

The redox potential of the chemistry compounds previously tested in beaker, were now evaluated in the paper a paper channel. The setup used for the paper-based half-cell characterization is presented in Figure 3.4a. A support piece made of poly(methyl methacrylate) - PMMA - was designed and fabricated using a CO_2 laser cutter (Mini 24, Epilog Laser, Golden, CO, USA). The PMMA piece consisted of two fuel reservoirs, one for the anolyte and one for the catholyte, and provided the support for the paper channel piece. An absorbent pad made of a folded wipe from Kimtech Science was set at the end of the paper channel in order to ensure a continuous and quasi-steady flow of the fluids.

Working and counter electrodes were placed under the paper channel. The working electrode was a Toray porous carbon paper electrode (TGPH-120; E-TEK) with thickness $370\ \mu m$ cut in a size of $2 \times 5\ mm$, whereas the counter electrode was made of a $5 \times 10\ mm$ adhesive graphite sheet from Farnell. The reference electrode was a Ag/AgCl electrode from Metrohm. In order to contact it with the flowing solution, the electrode is placed in the electrolyte reservoir.

The anolyte consisted of a solution of $0.25\ M\ K_4[Fe(CN)_6]$ in $0.1\ M\ KCl$ whereas the catholyte was a solution of $0.25\ M\ Fe(NO_3)_3$ in $0.1\ M\ HNO_3$. Figure 3.4b shows that the oxidation reaction taking place in the anode starts at $0.05\ V$ approximately:



whereas the reduction reaction at the cathode starts at about $0.65\ V$:



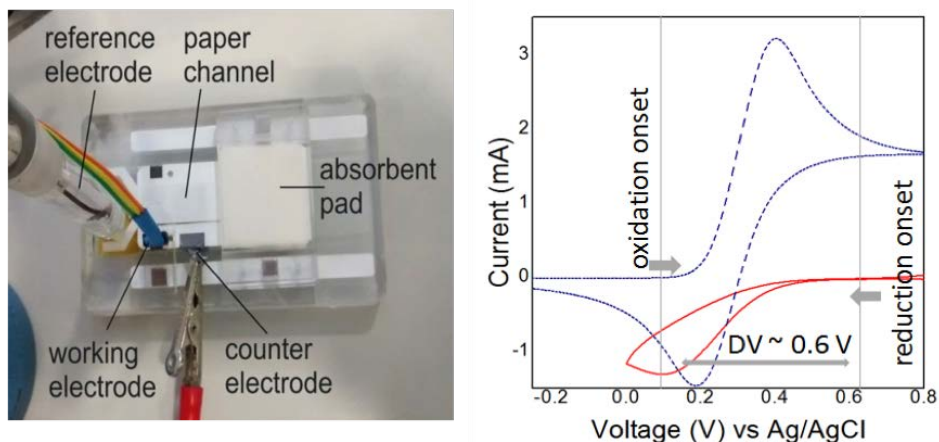


Figure 3.4. a) Picture of the device used for half-cell characterization. b) Cyclic voltammetry of anolyte (0.25 M $\text{K}_4[\text{Fe}(\text{CN})_6]$ in 0.1 M KCl) and catholyte (0.25 M $\text{Fe}(\text{NO}_3)_3$ in 0.1 M HNO_3) (right)

Following a separate characterization of the redox species, they were tested simultaneously in a cell level system. The measuring setup can be seen in Figure 3.5. The anolyte consisted of a solution of 0.25 M $\text{K}_4[\text{Fe}(\text{CN})_6]$ in 0.1 M KCl whereas the catholyte consisted of 0.25 M $\text{Fe}(\text{NO}_3)_3$ in 0.1 M HNO_3 . The activation of the device was done by inserting both legs of the paper channel into the solution reservoirs. Fig. 2.5b shows the polarization curves measured in this device. It is observed that when an absorbent pad is placed at the end of the paper channel, the power delivered by the device increased from 7 μW to 30 μW . Such increase corroborates the influence of the flow rate on the device performance. These preliminary results demonstrate the feasibility of this prototype as a microfluidic platform for paper-based electrochemical evaluation of further redox couples.

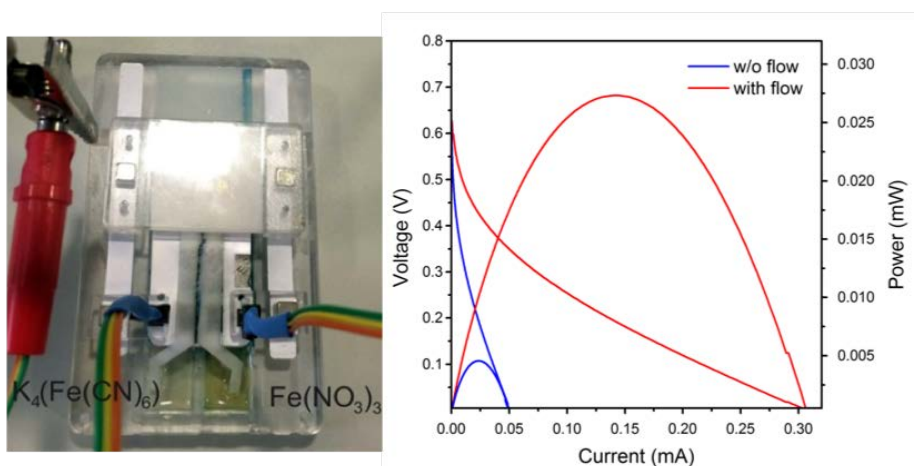


Figure 3.5. Picture of paper-based redox flow cell prototype (left) and polarization curves of the device with and without flow of reactants (right).



3.2.3. Validation of a capillary flow flow-through porous electrodes

Toray carbon paper (TGP-120) was tested for its potential use as a flow-through electrode. The porous carbon electrodes were annealed in a butane flame to confer the hydrophilic behavior needed for the flow-through capillary flow system. The carbon porous electrodes were initially tested for the using a blue ink as shown in Figure 3.6. Both horizontal and vertical (against gravity) orientations were tested and the ink was seen to successfully reach the absorbent pad. Moreover, a setup was customized to confirm the capillary lateral flow. The setup was made of two strips of paper material, which are similar to the ones used in this present work. Between the liquid source and the absorbent pad on the other end electrode strips were placed. The ink flowed by capillary action.

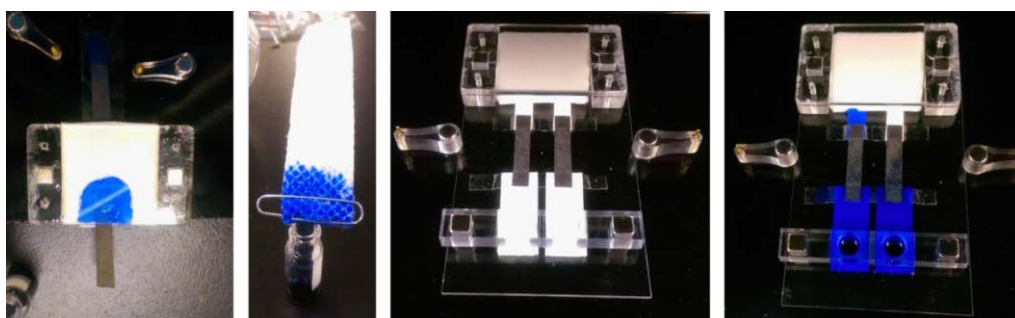


Figure 3.6. Testing of carbon paper for capillary flow-through electrodes (From left to right): Horizontal flow, Vertical flow against gravity, designed setup with hanging electrodes and Ink reaching the absorbent pad after flowing through the porous electrode.

Images in Scanning Electron Microscopy (SEM) of the carbon electrode before and after the heat treatment are observed in Figure 3.7. A cleaner, lack of hydrophobic coating porosity electrode is clearly observed after treatment by removing a good amount of Teflon with a butane flame.

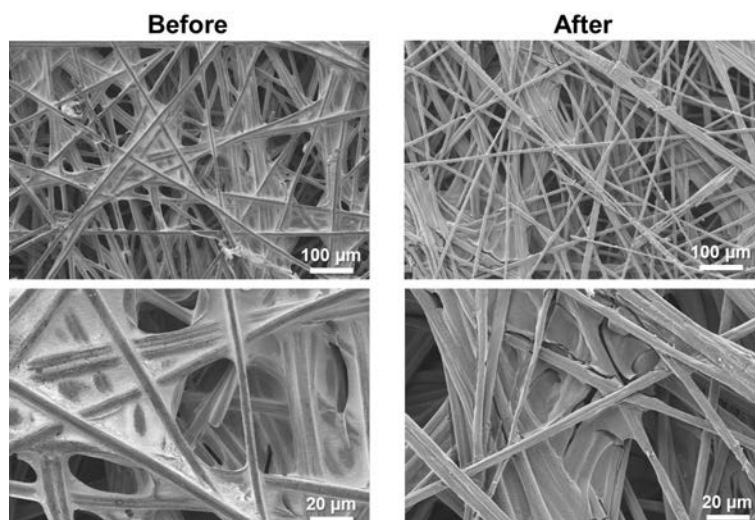


Figure 3.7. Scanning Electron Microscopy (SEM) images of the carbon electrode appearance before and after the heat treatment.

Two custom setups were built in order to assess the performance enhancement by utilizing flow-through electrodes. The two setups are shown in Figure 3.8. The setup design ensured the same geometrical area of the electrode for comparison purposes. The all-Quinone chemistry given in the previous chapter was selected for the experiment. Liquid solutions of 0.1M H₂BQS in 1M KOH and 0.1 pBQ in 1M Oxalic acid were used in the anodes and cathodes, respectively.

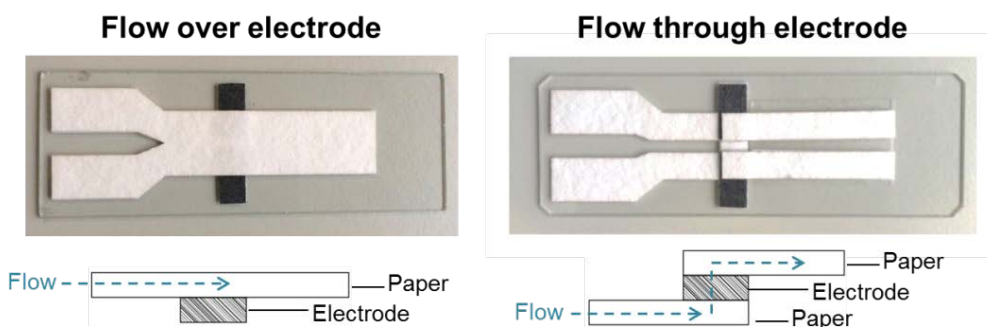


Figure 3.8. Setups for both flow over electrodes (left) and flow-through electrodes (right).

The preliminary screening of redox chemistries described in chapter 2, identified a suitable pair of commercially available quinone species, comprising of p-Benzoquinone (pBQ) at the positive side and hydroquinonesulfonic acid potassium salt (H₂BQS) at the negative side, using as electrolytes oxalic acid dihydrate (OA, O0376), potassium hydroxide (KOH, P1767), respectively. These species were selected for the proof-of-concept as they are the most convenient off-the-shelf forms of quinones/hydroquinones with two ketone/phenol groups[4]. The simplicity of the compounds enables good solubility, which is desired for PowerPAD operation. In addition, benzoquinones were predicted to have ready biodegradability according to EPISuite™ and other works[5]. For the experiments using pre-dissolved reagents, redox electrolytes were prepared at concentrations of 0.2 M H₂BQS in 2.0 M KOH and 0.2 M pBQ in 1.0 M OA. During the storage of redox species in solid form within the device, an amount equivalent to the maximum solubility concentrations of the redox species was added to the compartments: H₂BQS (0.023 g), pBQ (0.011 g), KOH (0.056 g) and C₂H₂O₄ (0.063 g). Each species was dissolved in 500 μL of water.

The performance of the two cells was measured and the polarization and power curves are given in Figure 3.9a. From the figure, it is shown that the performance of the flow-through electrodes was forty times higher than the flow-over electrodes. The chrono-amperograms, when the cells were running at a fixed potential of 0.25 V, are also shown in Figure 3.9b. The result shows roughly an order of magnitude higher current output for the flow-through electrodes.

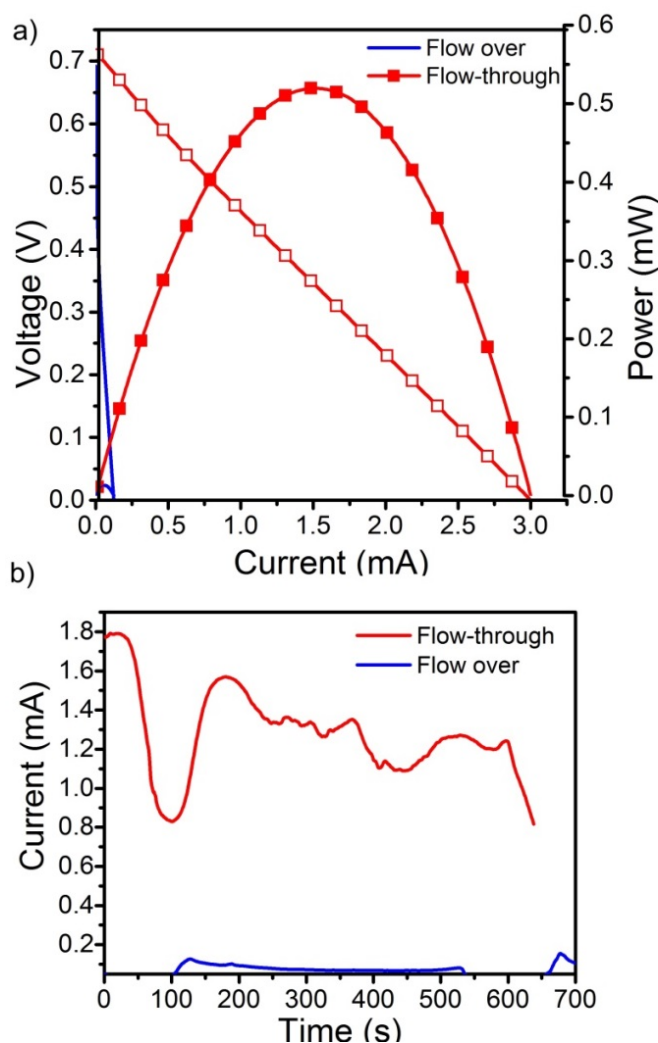


Figure 3.9. Performance results of All-Quinone chemistry on flow over and flow-through electrodes: a) Polarization and power curves, and b) Chronoamperograms at 0.25 V.

3.2.4. Validation of dry storage of species and electrolytes

The next step was to evaluate and validate the possibility of storing the solid species in the paper strips and regenerating them when activated by water. For this purpose, a cell with flow through porous electrodes was designed and tested using both prepared solutions and stored solid species. The setup is shown in Figure 3.10. The device had two paper strips for the anode and the cathode species, respectively, and they are both connected at the end by the absorbent pad. Again, the all-quinone chemistry was chosen for this experiment. The solid species and supporting electrolytes were stored in the storage pads as shown in the figure, for both the anode (H_2BQS in KOH) and the cathode (pBQ in Oxalic acid). It was ensured for the two experiments that the concentrations of the solutions match those of the solid stored ones.

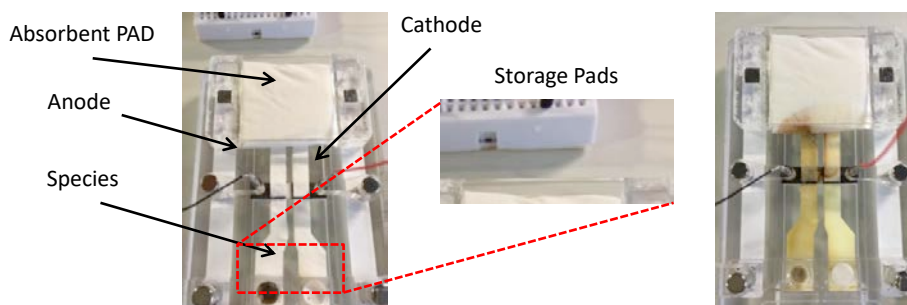


Figure 3.10. Experimental setup used for evaluating the storage of solid species.

During this experiment, the electrodes were connected to a 500Ω resistor as a load and the potential was recorded over time as shown in Figure 3.11. The figure shows comparable performance for the both cases, which confirms the regeneration of the stored solid species.

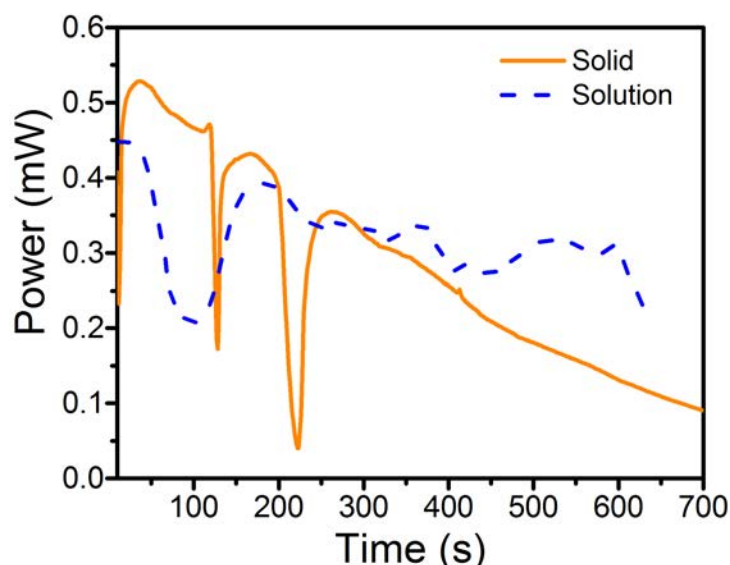


Figure 3.11. Power output over a 500Ω load in a lateral flow device for both liquid solutions and stored solid species regenerated by water.

3.3. BIODEGRADABLE BATTERY INTEGRATION

The effective integration of previously evaluated concepts, capillary flow on paper, flow-through electrodes, solid storability of redox compounds, resulted in the obtaining of a fully organic and completely biodegradable battery concept inspired by the sustainability principles of green electronics, PowerPAD (Power: Portable And Disposable) is introduced. As illustrated schematically in Figure 3.12, the PowerPAD concept[6] represents a new class of batteries designed to operate for relatively short periods of time (from minutes to 1-2 hours) to fulfill the power needs of portable applications while not requiring any specific recycling facility for its disposal.



3.3.1. Design and operating principle

The PowerPAD design, as well as its acronym, was inspired from a traditional notepad made from a stack of paper sheets, i.e., layered organic materials. The battery was thus designed using organic materials such as cellulose, carbon paper and beeswax that can be fabricated by affordable methods with low energy consumption and layered to form an integrated device.

The device components were designed in a CAD program (CorelDRAW, Corel, Ottawa, ON, Canada). Cellulose membranes were cut using a CO₂ laser cutter (Mini 24, Epilog Laser, Golden, CO, USA). Most of the device assembly was done layer by layer using alignment jigs. The structural cellulose components (238, 320, 601, CFSP223000, from Ahlstrom, Helsinki, Finland) were impregnated with melted natural beeswax (Iberceras, Madrid, Spain), which provided an impermeable coating and was also used to bond the layers. An inlet cellulose pad (238, Ahlstrom) was used to receive the liquid sample into the device. Different absorbent pad configurations were tested. A single layer of cellulose membrane 222 (Ahlstrom) with a thickness of 0.83 mm was taken as baseline material, labeled h . The absorbent pads $2h$ and $4h$ consisted of two or four layers of cellulose 222 to obtain pad thicknesses of 1.66 mm and 3.32 mm, respectively. In order to test a thinner pad configuration, the pad labeled as $h/2$ consisted of one layer of cellulose 238 (0.34 mm thick). The electrodes consisted of porous carbon paper (TGP-120, Toray, Japan) that was thermally pre-treated to ensure capillary flow.

Energy is stored in the form of water-soluble organic redox species inside the pad, representing two dormant electrochemical half-cells. The battery was activated by the addition of a liquid sample that dissolves the reactants and carries them to the electrodes by capillary flow. After electrochemical discharge of power, the device can be disposed together with organic waste or even discarded on the ground for natural decomposition, as it comprises of exclusively biodegradable materials and does not contain any metals, plastics or harmful substances. In summary, the proposed battery function comprises of three simple steps: 1) add water; 2) extract power; and 3) dispose.

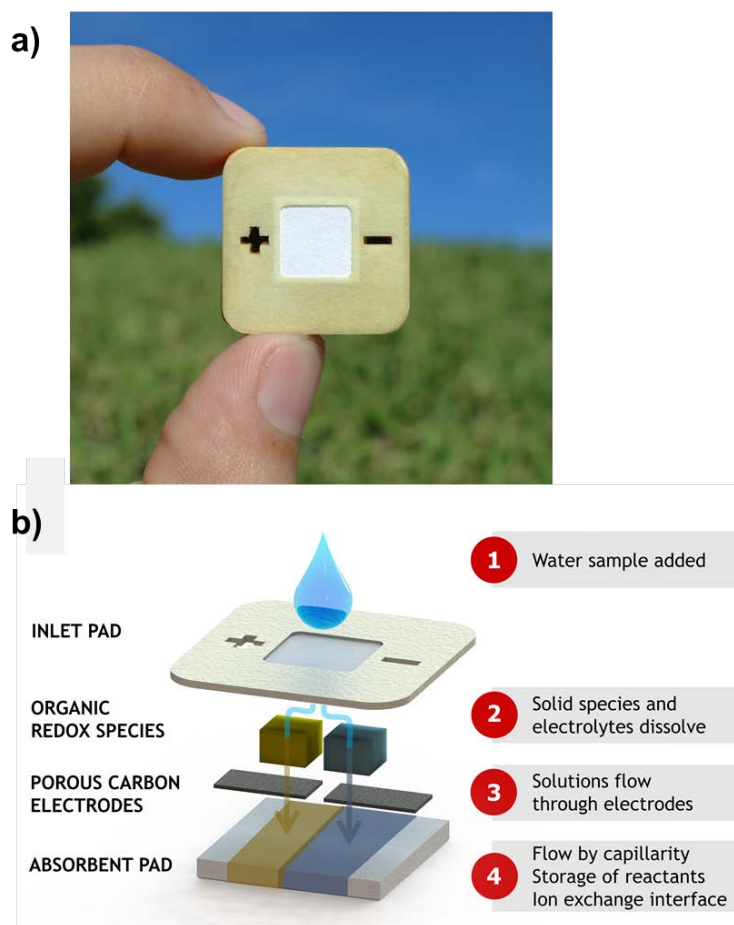


Figure 3.12. PowerPAD: (a) actual photograph and (b) conceptual schematic of the proposed biodegradable redox flow battery composed of cellulose, carbon electrodes, organic redox species, benign electrolytes and beeswax.

More specifically, the proposed biodegradable battery was designed as a vertical redox flow cell, centering its operation on a diffusive flow. As shown in Figure 3.12b, the device structure was composed of several patterned cellulose layers that when stacked together define the microfluidic paths of the cell and the compartments that house the electrodes and reactant compounds. In order to render the structural parts rigid and impermeable, the cellulose was impregnated with natural beeswax, which allows creating hydrophobic areas in a strategically designed pattern. The top structural cellulose layer hosts a central inlet pad able to receive an external liquid sample.

Underneath this pad, two separated small reservoirs contain the positive and negative redox species and the supporting electrolytes originally stored in the solid state. The two electrodes made of hydrophilic porous carbon paper were placed below the respective reactant reservoirs and sandwiched between two thin layers of cellulose in order to ensure reliable capillary flow of reactants through the electrodes and into the large cellulose absorbent pad at the bottom.



The outward facing surfaces of the device were sealed with a beeswax-covered cellulose layer in order to prevent liquid leakages. The electrodes were accessed via the positive and negative terminals on the top surface of the device in order to connect a load. The proposed battery was conceived as a single use power source that is activated by the addition of a small sample of liquid, such as water, urine or saliva, on the inlet cellulose pad. When the inlet pad is saturated, water flows by capillarity to each of the reservoirs and dissolves the stored redox species and electrolytes. Once dissolved, the reactant species flow through the porous carbon electrodes towards the absorbent pad. The battery starts generating power when the two electrolytes get in contact at the absorbent pad. This pad has an important role in the device function as it establishes the capillary flow that makes the species flow through the electrodes while also providing electrolytic contact between the two electrochemical half-cells. Due to the co-laminar flow established by capillarity in the paper sheets, the two reactant streams were effectively separated after activation of the battery and start mixing only by diffusion at their contact interface[7]. Taking into account the diffusion coefficient of the redox species in aqueous media ($\sim 10^{-6} \text{ cm}^2 \text{ s}^{-1}$) and the distance between the electrodes (2 mm), no significant crossover of reactants is expected during the battery operation time, which ranges from minutes to a few hours. Consequently, the proposed redox flow battery can operate effectively without an ion-conducting membrane otherwise used to separate the electrodes, which was particularly critical in the present case considering that most membranes are made from specialized polymer films that are not readily biodegradable. Furthermore, the capillary flow enables convenient integration of flow-through porous electrodes, which have been shown to deliver drastic performance improvements compared to flow-over and planar electrodes by means of high active surface area and internal mass transport rates[8]. The provision of flow in the form of a redox flow battery thus contributes three critical services that together enable the unique function of the PowerPAD: 1) activation; 2) membrane elimination; and 3) high-performing electrodes. Finally, it was noteworthy that the passive capillary flow facilitated by the device eliminates the need for an external pump otherwise required to drive the flow of electrolyte, and hence does not add any overhead or parasitic power consumption.

3.3.2. Battery characterization

The cell voltage/current was recorded using a DropSens μ Stat400 Bipotentiostat/Galvanostat and DropView 8400 Software (DropSens S.L., Asturias, Spain). The polarization and power curves for the single cell and battery stacks were generated using linear sweep voltammetry, sweeping from the open circuit voltage (OCV) to 0 V at a scan rate of 50 mV s^{-1} . The discharging curves were recorded under different external loads of 0.5, 1.0 or 2.0 k Ω . All tests were performed at room temperature.

As per the previously described PowerPAD design (Figure 3.12), the proposed biodegradable redox flow battery activates upon the addition of a liquid that dissolves the reactants stored within the device in solid form. The dissolved reactants were carried by capillary flow through the electrodes, where the electrochemical reactions take place, and into an absorbent pad at the bottom of the device. The battery

operation was thus a transient process that starts upon reactant dissolution and continues for a period of time until the reactants were consumed or mixed internally, thereby causing the output voltage to drop below a certain cut-off value. Provided the passive nature of the device operation once liquid is added, the flow characteristics were fundamentally controlled by the geometrical features and surface properties of the internal materials, while the reactant concentrations were controlled by the relative dissolution rates. In order to decouple these effects, the device was first characterized with reactants in pre-mixed solutions at the defined target concentrations based on their solubility. This approach was used to demonstrate the overall flow battery operation and to evaluate the impact of the absorbent pad dimensions on the battery performance. This pad plays an important role, as it drives the capillary flow, defines the ion-exchange interface and serves as storage of dissolved reactants. Four different absorbent pads with varying thickness (h) are tested (Figure 3.13).

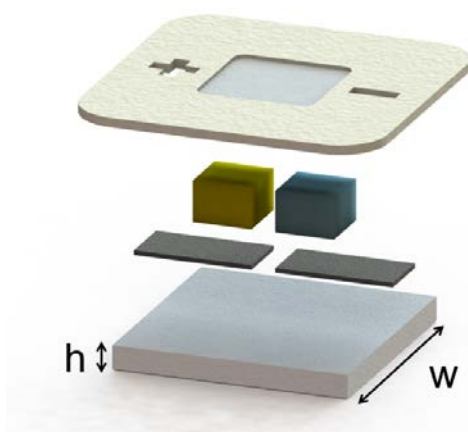


Figure 3.13. PowerPAD conceptual schematic of the proposed biodegradable battery showing the geometrical parameters evaluated for the characterization of the battery performance: absorbent pad width (w) and thickness (h).

The total volumes of solutions added to the batteries for each measurement were 170 μL , 390 μL , 740 μL and 1440 μL for absorbent pad thicknesses of $h/2$, h , $2h$ and $4h$, respectively, in order to reach saturation of the internal components. The open circuit voltage (OCV) of the batteries was continuously measured after adding the solutions, reaching a pseudo-steady state value of 0.75 ± 0.05 V in all cases. Polarization curves for battery discharge were measured once the solutions were completely absorbed in the absorbent pad, with results shown in Figure 3.14. It is observed that the maximum power delivered by the battery increased with the absorbent pad thickness, reaching a maximum value of 1.7 ± 0.2 mW with the thickest pad ($4h$).

Based on the geometrical electrode area of 0.25 cm^2 , the battery yields a maximum power density of 6.8 ± 0.5 mW cm^{-2} at a current density of 18.9 mA cm^{-2} , which is comparable to the power densities of large-scale redox flow batteries with all-quinone chemistry[9] and at least an order of magnitude higher than any biodegradable battery reported so far[10,11].



The significant rise in power output obtained by increasing the absorbent pad thickness was primarily attributed to the reduced internal cell resistance associated with the increased cross-sectional area for ion conduction in the pad. This can be qualitatively observed by the changes in the linear slope of the polarization curves as the pad thickness is increased.

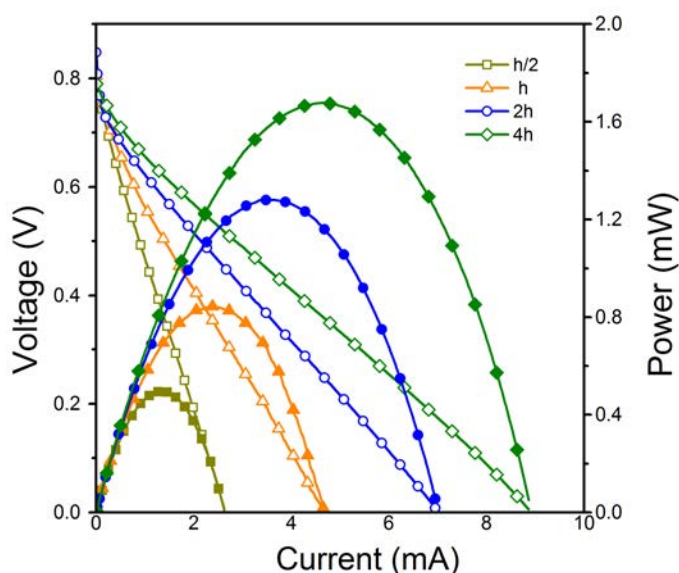


Figure 3.14. Discharge polarization curves of biodegradable redox flow battery prototypes with four different absorbent pad thicknesses (as indicated; $n \geq 3$) supplied with pre-mixed solutions of 0.2 M H_2BQS in 2 M KOH and 0.2 M pBQ in 1 M $\text{C}_2\text{H}_2\text{O}_4$ at the negative and positive electrodes, respectively, at room temperature.

Next, continuous battery operation was characterized by measuring discharging curves for different external loads (0.5, 1 and 2 k Ω). The battery cut-off voltage was set to 0.5 V, representing two-thirds of the original OCV. Figure 3.15 shows the discharging curves obtained with the four different absorbent pad thicknesses. As expected, batteries operated at the lowest load (500 Ω) delivered higher power values (0.50 – 0.85 mW) but for shorter service times (2 – 13 min), while batteries working under the highest load (2 k Ω) delivered lower power outputs (0.12 – 0.25 mW) for longer operation times (15 – 85 min). For any given load, the batteries with thicker absorbent pad show better performance not only in terms of delivered power but also in operation times. The latter result is attributed to the larger amount of electroactive species stored in the pad, which enlarges the capacity of the device. The output capacity achieved with the batteries with absorbent pad thickness of 4h operated under 2 k Ω load reached 0.42 mAh (Figure 3.15), which considerably exceeds the measured capacities of the other battery designs.

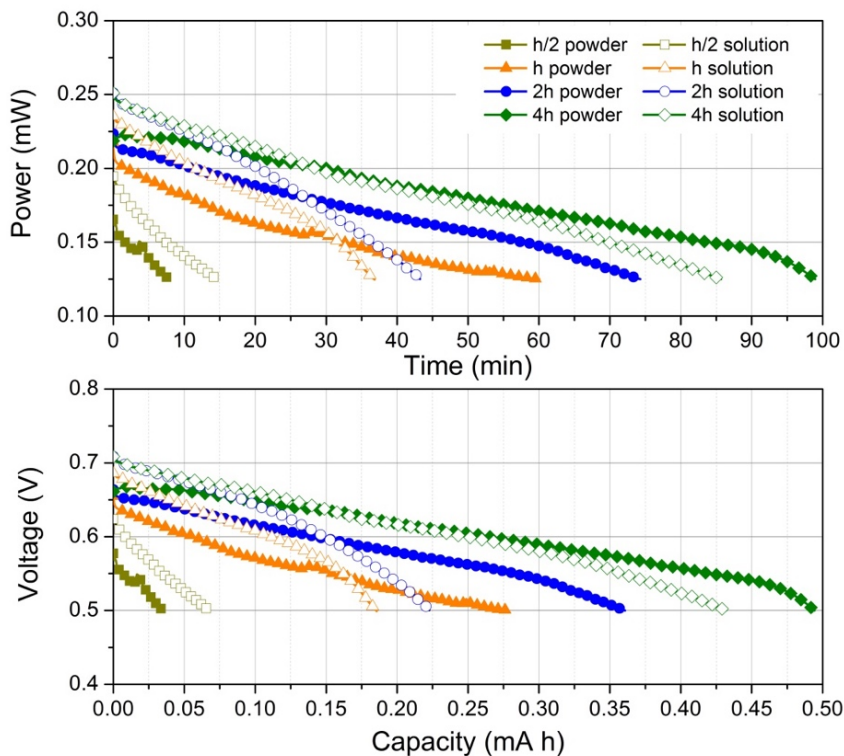


Figure 3.15. Continuously measured discharging curves of the biodegradable redox flow battery prototypes with four different absorbent pad thicknesses subjected to fixed external loads (as indicated; $n = 3$) and a cut-off voltage of 0.5 V, using pre-mixed solutions of 0.2 M H_2BQS in 2 M KOH and 0.2 M pBQ in 1 M $\text{C}_2\text{H}_2\text{O}_4$ at the negative and positive electrodes, respectively, at room temperature.

The complete, integrated battery device was then tested with redox species and electrolytes stored internally in solid form and dissolved dynamically during operation upon the addition of water on the inlet pad. For comparative purposes, the amounts of liquid (volume) and stored reactants (moles) used in these experiments were identical to those used previously in the pre-mixed solutions for each of the four different absorbent pad thicknesses. Given that the operational nature of the device is inherently transient, its performance was evaluated solely during continuous operation in the form of complete discharge runs until the cut-off voltage was reached.

The obtained discharging curves under a fixed external load of 2 k Ω are provided in Figure 3.16.

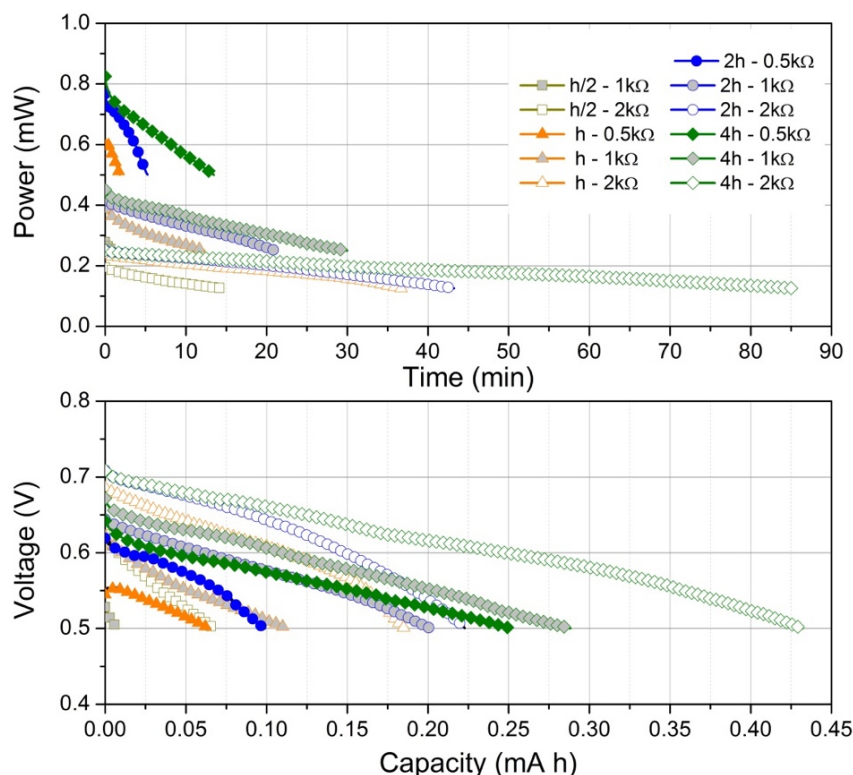


Figure 3.16. Discharging curves of integrated biodegradable redox batteries activated with water measured at room temperature for various absorbent pad thicknesses and external loads with a cut-off voltage of 0.5 V (as indicated; $n = 3$). The battery prototypes contained internal storage of redox species and electrolytes in the solid state that dissolved and flowed by capillarity upon the addition of water at the inlet pad.

Overall, the results indicate that the batteries with internally stored reactants have a similar response to those operated with pre-mixed solutions. In most cases, the batteries with internal storage initially deliver lower voltages but sustain the power output for longer times (up to 100 min). This is reasonable considering the dynamic dissolution of reactants, which is not instantaneous and rather leads to a gradual ramp in concentration of reactants flowing through the porous electrodes as a function of time. The close proximity of storage and reaction sites allowed a gradual release that counteracted the diffusive mass transport limitations during battery discharge and improved the performance at high run-times.

The high-capacity pad configuration combined with internal reactant storage provides a particularly effective solution with performance and capacity that exceed those of the pre-mixed reactant experiment. The operational energy density of the prototype device, based on the electrical energy generated from the discharge data in Figure 3.16 normalized by the mass of the stored reactants, was estimated to be 32 Wh kg^{-1} . This value compares favorably to other recently reported biodegradable batteries[11,12], albeit further improvements are needed to reach the level of conventional primary batteries such as Li-ion batteries. An important advantage of the

present device configuration, in terms of energy density, is that the reactants were stored in the dry, solid state. Compared to an equivalent redox flow battery with the same reactants stored in liquid electrolytes, the operational energy density is approximately 7x higher. This feature is particularly important for the portable applications intended for the battery.

The coulombic electroactive material utilization calculated from the discharging curves of the battery prototypes in Figure 3.14 is shown in Figure 3.17, as the fraction of active species converted by the battery during discharge until the cut-off voltage (in this case 0.5 V) is reached. The batteries with an intermediate absorbent pad thickness operated under a high load show the highest active material utilization among the tested conditions. Interestingly, under these conditions, the device with internally stored reactants achieves a higher utilization (13.3%) than the corresponding device supplied with pre-mixed reactant solutions (8.9%). This indicates yet another advantage of the proposed PowerPAD flow battery configuration with onboard reactant storage in terms of reactant utilization, although further optimization is required to fully exploit its potential in this regard.

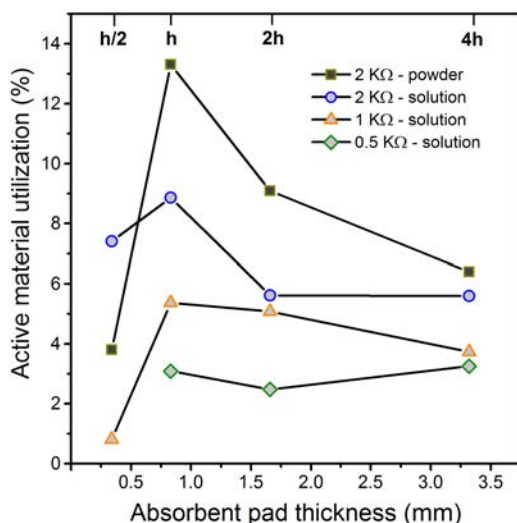


Figure 3.17. Electroactive material utilization of the biodegradable redox battery prototypes calculated from the discharging curves.

3.3.3. Battery voltage scalability

Most commonly used electronic applications require power delivery at higher voltage ($\sim 2.0 - 3.0$ V) than that produced by a single-cell battery such as the PowerPAD cell reported above. One of the strategies to obtain a higher output voltage from a battery was to stack several cells in series, which was the strategy selected here in order to demonstrate scalability. For the present PowerPAD device configuration, it was necessary to reduce the width of the absorbent pad (w) in order to increase the number of cells within the same device footprint. In addition, by splitting the absorbent pads, the cells within the stack were isolated electrolytically, which is practical in order



to minimize internal shunt currents and losses occurring in serial stacks with electrolytic connection[13]. Single cells with different absorbent pad widths were hence analyzed as a first step in order to explore the scalability of the PowerPAD concept. For comparative purposes, the absorbent pad volume was kept constant by increasing the thickness of the pad proportionally to the reduction in width. Figure 3.18 shows the average polarization curves obtained for single cell batteries with $1h-1w$, $2h-w/2$ and $4h-w/4$ absorbent pad dimensions of fixed volume supplied with pre-mixed reactant solutions. All devices showed good performance with similar overall characteristics. Interestingly, however, the devices with the lowest absorbent pad width achieved the highest performance (1.2 ± 0.1 mW peak power), which is attributed to the greater absorbent pad thickness.

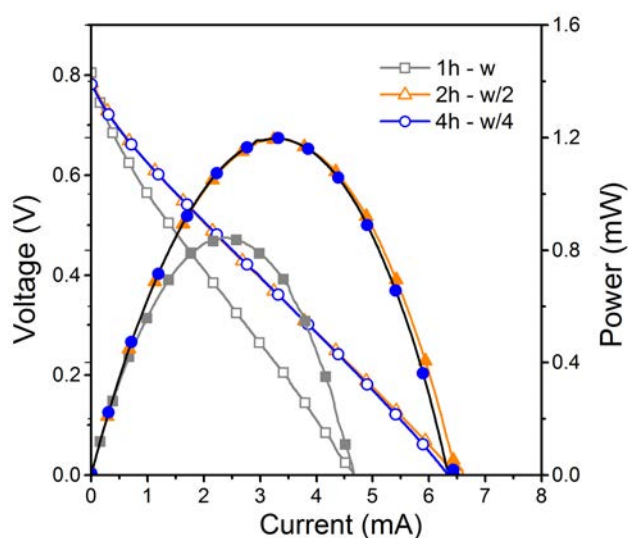


Figure 3.18. Polarization curves of biodegradable redox flow batteries with three different absorbent pad widths. Shown are the average polarization curves ($n \geq 3$) of batteries supplied with pre-mixed solutions of 0.2 M H_2BQS in 2 M KOH and 0.2 M pBQ in 1 M $C_2H_2O_4$.

Next, batteries with absorbent pad dimensions of $2h-w/2$ were used to assemble a 2-cell stack with a nominal output voltage of 1.5 V. In addition, a 4-cell stack with absorbent pad dimensions of $4h-w/4$ was developed to provide a nominal output voltage of 3.0 V. The multi-cell stacks used the same footprint as the single cell device (26 mm x 26 mm). Each stack features two or four pairs of reactant compartments placed above the corresponding electrodes. The individual cells were connected internally in series and shared a single inlet pad such that they can be simultaneously activated by a single shot of water, but used separate absorbent pads for voltage scalability. The assembled battery stack prototypes are shown in Figure 3.19a along with measured polarization curves in Figure 3.19b. The 2-cell and 4-cell stacks were observed to reach 1.5 ± 0.2 V and 3.0 ± 0.2 V open circuit voltage, respectively, as intended by design. Similarly, the two stacks produced a maximum power output of 1.5 ± 0.1 mW and 2.8 ± 0.1 mW, respectively, close to the optimal doubling and quadrupling of the single cell performance.

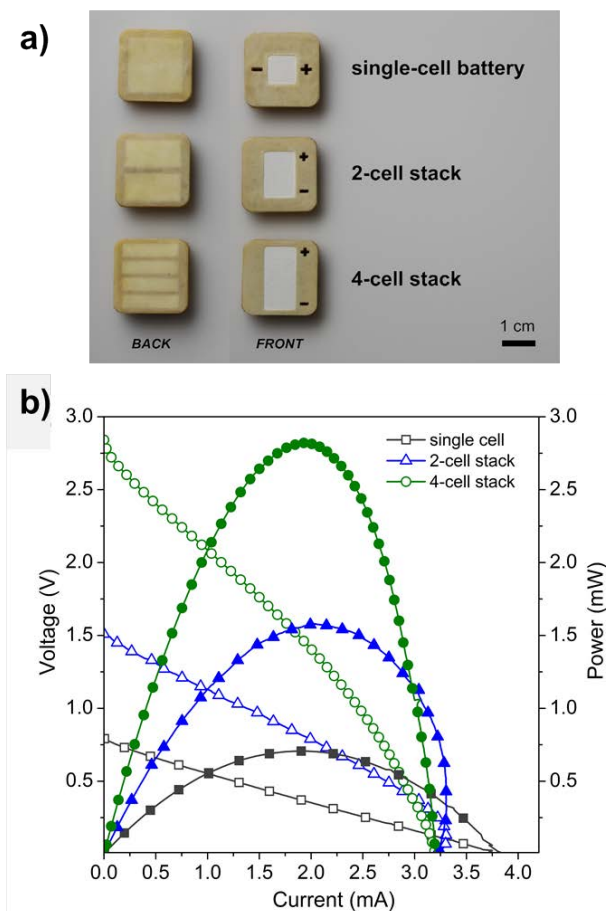


Figure 3.19. Scalability of the biodegradable redox flow battery demonstrated by integration of one, two and four cells within the same device footprint. (a) Image of the assembled single cell, 2-cell stack and 4-cell stack prototypes. (b) Average polarization curves ($n \geq 3$) measured with pre-mixed reactant solutions of 0.2 M H_2BQS in 2 M KOH and 0.2 M pBQ in 1 M $\text{C}_2\text{H}_2\text{O}_4$.

3.3.4. Practical application of the battery

As a proof-of-concept of the utility of the PowerPAD for practical, real-world applications, the 4-cell stack was demonstrated as the power source for a portable water-monitoring instrument that usually runs with a 3V Li-ion coin cell battery, which was removed. The instrument measures temperature, conductivity and total dissolved solids in a water sample, which are typically relevant parameters in water sensing. For this experiment, two different samples were used: a sample of laboratory grade deionized water and a sample of natural water collected from a local river in Barcelona, Spain. The water analyzer was connected to the PowerPAD device and the detector is inserted into a beaker containing the water sample. A small volume of the same water sample to be analyzed is then added to the battery inlet pad for activation. An image of the water analyzer powered directly by the 4-cell PowerPAD stack, without any ancillary power conversion systems or components, is shown in Figure 3.20a. The current drawn by the water analyzer and the battery output voltage obtained for the two different water samples during the experiment are depicted in



Figure 3.20b. It can be seen that the battery activated with the river sample yielded a fairly similar open circuit than the one activated with deionized water. The measurement was successfully engaged after 30 seconds of battery activation. The analyzer required an average current of ~ 0.2 mA to continuously measure the sample and display the result on its LCD display. Once the measurement was taken (results yielding 6 ppm TDS and $12 \mu\text{S cm}^{-1}$ for the deionized water and 424 ppm TDS and $958 \mu\text{S cm}^{-1}$ for the river water), the reading was stored by pushing a button of the instrument, which halts the sensing function and freezes the information in the display. During this phase, the current required by the analyzer decreased to $\sim 20 \mu\text{A}$. After activation, the battery voltage decreased up to 300 mV during the high current demand phase when the analyzer measures and displays the results, after which the voltage increased again to a value close to its open circuit during the secondary phase when the result was stored and displayed. Throughout this experiment, the PowerPAD unit is shown to reliably deliver the required levels of voltage and current for both operational phases of the measurement in the complete absence of supplementary electronics.

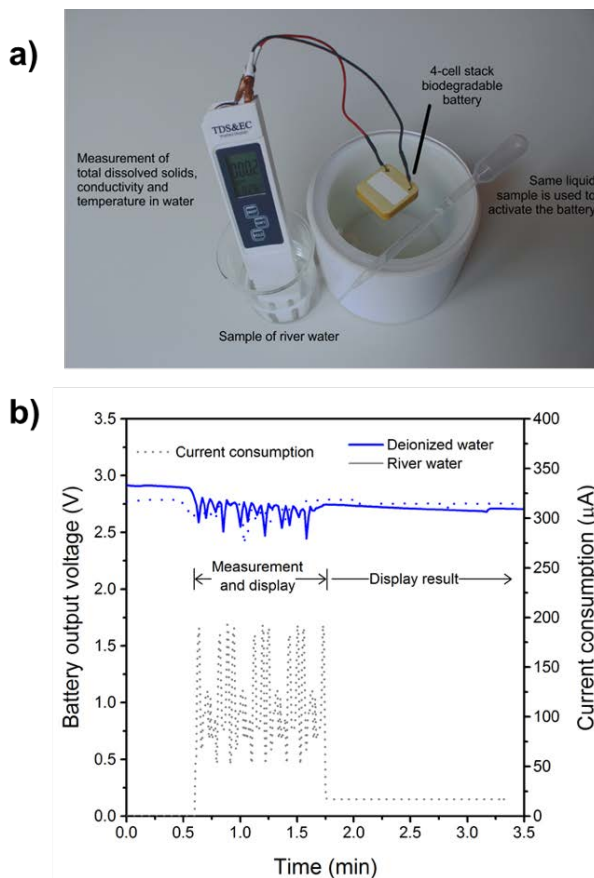


Figure 3.20. Practical utility of the biodegradable redox flow battery demonstrated by powering a portable water monitoring instrument. (a) Image of a portable water monitoring device powered directly by a biodegradable redox flow battery. The device analyzes a river water sample that is also used to activate the battery. (b) Electric current drawn by the water monitoring device and output voltage of the battery during the measurement process.

3.3.5. Battery biodegradability

The biodegradability of the PowerPAD battery, expressed as primary degradation (D_p), was determined following the guideline of the Organization of Economic Cooperation and Development (OECD) Test 311[14] that comprises recommendations of other normalized tests (ISO,[15] ASTM,[16] US-EPA[17]), and is widely used as standard test. Biodegradation is defined as a process where a material breaks down into simple compounds, such as CO_2 , CH_4 , H_2O and N_2 , as a result of the action of microorganisms.

The test was carried out on the same type of single-cell batteries used for the electrochemical characterization, which contained H_2BQS (0.023 g), pBQ (0.011 g), KOH (0.056 g) and OA (0.063 g) as stored reactants. For comparison, batteries without reactants were also tested, labeled as blank battery. A reference material consisting of cellulose acetate powder (CAS number 9004-35-7) was also included in the study. Prior to physico-chemical characterization, four specimens of each device were shredded to a particle size of <0.5 mm in a cryogenic grinder (Freezer/Mill 6850, SPEX, Metuchen, NJ, USA). The minced devices were used for the biodegradability test in order to avoid abiotic degradation or disintegration. The materials were evaluated after being characterized by their total solids (TS), total chemical oxygen demand (TCOD) and total carbon (TC) content as shown in Appendix 1.

The assay was prepared in duplicate, using glass vessels that contained 50 mL of liquid media and 70 mL of headspace. A greater headspace volume than in the OECD-Test 311 was fixed in order to avoid excess overpressure inside the vessels.

The initial concentration of device per vessel is given in Appendix 1. An anaerobic digested sludge from an urban wastewater treatment plant was used as inoculum, which was filtered to eliminate coarse materials and was kept for 7 days at 35 °C to diminish residual organic matter. The inoculum to material ratio was selected based on the OECD-Test 311 recommendations ($10 \text{ g}_{\text{TS-inoculum}} \text{ g}_{\text{TC-material}}^{-1}$), but a higher inoculum concentration per vessel was fixed ($14.5 \text{ g}_{\text{TS}} \text{ L}^{-1}$) that allowed shortening the start-up time and duration of the test. Once filled, all vessels were bubbled with nitrogen to remove oxygen and closed with gastight seals (crimp cap and septum). The assay was performed at 35 ± 2 °C for 94 days. The biodegradation was monitored through the evolution of CO_2 and CH_4 content in the gas space of the vessels as determined by gas chromatography (Varian GC 3800, Agilent Technologies, Santa Clara, CA, USA), instead of using a pressure-measuring device and signal transducer as described in OECD-Test 311. The biodegradation extent was calculated as primary degradation (D_p) after 60 days and was expressed as the percentage of the initial carbon mass of the material that was transformed into C- CO_2 and C- CH_4 .

The assay simulates the biodegradation process under biotic anaerobic conditions of disposable devices taking into account a specific WEEE management practice. Furthermore, the low concentration of the evaluated materials in the performed test



ensures that the biodegradation kinetics reflect those expected in the environment being simulated. The selection of an anaerobic test represents the worst-case scenario for the biodegradation of the batteries, as the biodegradation of cellulose-based materials is slower than in aerobic conditions[18]. Only 5-10% of cellulose degrades in natural environment anaerobic conditions because in the case of landfills, water-logged soils or aquatic sediments where anaerobic or anoxic environments are expected, lower rates and longer times for biodegradation are expected due to the lower quantity of anaerobic microorganisms[19]. The test monitors the inherent biodegradability in anaerobic conditions, expressed as the percentage of the initial total carbon mass of the material that is transformed into C-CO₂ and C-CH₄ after a minimum period of 60 days. The initial total carbon content (TC) that is biodegraded was calculated from periodic measurements of gas products and its evolution was plotted in a curve. Figure 3.21 shows the evolution of the obtained biodegradation curves of the complete and blank batteries (with and without internally stored chemical reactants), as well as the reference material (cellulose acetate).

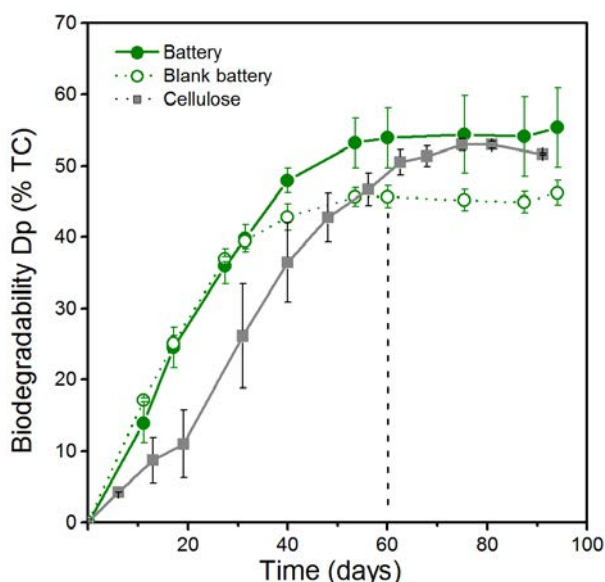


Figure 3.21. Battery biodegradability. Primary degradation (Dp) or biodegradability of complete batteries, blank batteries (without internally stored reactants) and reference material (cellulose acetate) in terms of initial total carbon content (%TC) that is biodegraded.

A clear plateau, indicating maximal degradation, was attained from day 40 for the batteries and from day 63 for the cellulose reference. It is noteworthy that the degradation rate of the batteries was even greater than that of pure cellulose, despite their larger particle size. All tested materials reached similar levels of biodegradation after 60 days, with values of $54 \pm 4\%$, $46 \pm 2\%$ and $52 \pm 2\%$ for the complete battery, blank battery and cellulose, respectively, indicating that primary biodegradation of the studied materials occurred. These values were coherent with those reached in cellulose acetate based materials biodegradation tests, with values between 40 – 60% TC under anaerobic conditions. Based on these results, the batteries can be considered biodegradable, and no toxic effects may be expected from the use of the

present quinone-based redox chemistry. Therefore, according to the norm, these devices can be considered non-persistent and assumed to degrade by microorganisms present in soils or water bodies in the medium to long term or in simple waste treatment plants or other environmental compartments in the short term.

3.3.6. Discussion

The biodegradable battery prototypes presented here can operate for up to 100 minutes with an output voltage that can be scaled to match the voltage needs of portable electronic devices (1.5 - 3.0 V). Despite its working principle is based on the well-known redox flow batteries, it is the first time this principle has been explored to develop a single-use portable format with clear environmental advantages. Moreover, the technology allows further increases of both operation time and output power. It is noteworthy that even at the present laboratory stage, the prototypes have proven to readily substitute a coin cell battery in a real application; with a cost of materials in the range of tens of euro/dollar cents (see Bill of Materials in Appendix 2).

This new class of biodegradable, portable redox flow batteries is ideally suited to provide power for a new generation of green electronic devices, and could further be explored in terms of operative design, structural materials and chemistry. For instance, the battery absorbent pad can be engineered to sustain a capillary flow of species for a longer duration. Moreover, the present battery is designed to work for a single time and its operation is intrinsically transient. Several relevant parameters affecting its performance are time-dependent and start changing after the liquid is added; for example, the rate of dissolution of species/electrolytes, the concentration of species/electrolytes and the flow rate of reactants. These aspects offer a rich set of parameters to further optimize in future studies.

For this proof-of-concept, beeswax was used as structural material because it is abundant, organic, inexpensive, moldable, impermeable and mechanically robust. Furthermore, its properties can be customized for hardness and melting temperature. However, other materials such as biopolymers (PLA or PHA)[20] are potential alternatives to substitute beeswax. These materials, already used in the industry as biodegradable paper coatings, would confer the device a compostable characteristic and an industrially scalable fabrication process.

The redox chemistry proved for this first development was based on suitable quinone species available off-the-shelf with good kinetics on carbon. However, the device is not restricted to these species, and other commercially available candidates could be considered. Caffeic acid, a hydroquinone and antioxidant found in coffee, and water-soluble vitamin K₃, a naphthoquinone, are examples of other commercially available quinone species that are available in the desired redox state for discharge. Moreover, other research groups are working on modeling the effect of functional groups on quinones[21] For example, hydroxyl functional groups were shown to enhance solubility and reduce standard potential, which would benefit the battery anode, while sulfonic acid functional groups were shown to enhance solubility and increase standard potential, which would be beneficial for the cathode. By in-house synthesis



of quinone species with custom functional groups, the number of candidates meeting the requirements of our approach could be increased and the performance of the device may be further enhanced. This would enable tailored solubility, rate of dissolution and standard potential difference as well as reducing the cost of chemical compounds. Furthermore, besides using quinone species, inorganic redox couples can also be suitable for this approach, while maintaining a similar or even higher cell voltage. Some of these inorganic salts may form hydroxide precipitates in alkaline media, yet are compatible for the cathode by utilizing mixed-media operation. For example, nitrates, sulfates or phosphates are known to benefit the soils, which if combined with cheap and abundant metal redox ions, may lead to a battery that could even be compostable, adding value to the soil or water in which it is disposed.

The biodegradability study of the PowerPAD batteries was carried out at biotic anaerobic conditions which proved their primary biodegradation. Upcoming work will include long-term biodegradability tests at aerobic conditions that could even meet the certification of home compostability[22]. Additional biodegradation tests without previous conditioning steps would be of interest such as simulation tests of regulated disposal in landfill conditions as well as unregulated disposal in soils or aquatic systems.

3.4. CONCLUSION

This work introduced the PowerPAD concept, a fully biodegradable battery for portable and disposable single-use applications that follows the sustainability guidelines of the circular economy. The battery was prepared using exclusively organic materials and low-energy consuming fabrication techniques. According to the results obtained in the biodegradability test, it can be disposed in soils and waters and thus eliminate the need for recycling and the associated cost and energy consumption. Ultimately, this disposable power source concept holds great promise to radically change the portable battery paradigm; from considering it a harmful waste to a source of materials that nurture the environment, enrich soil or remove toxins from water, far beyond the traditional life cycle of a battery.

However, with regard to the fuel utilization, the diffusive flow system showed an efficiency of 3%, which can be clearly improved, not having a constant flow of reactants in the reaction area causes the consumption of the redox compounds, so implement a steady flow rate system to avoid this situation was becoming emergent. During the next chapter of this thesis, the improvement of the fuel utilization is described.

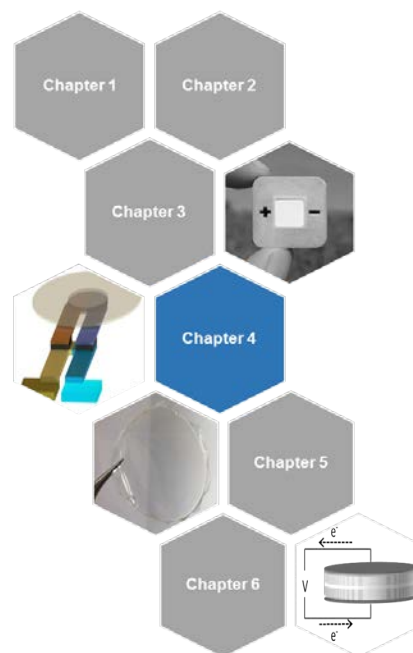
References in Chapter 3.

- [1] D. Rosenberg, S. Böttger, M. Busker, W. Jansen, *Organic Redox Flow Batteries : An Innovation in the Field of Education for Sustainable Development for Educational Curricula*, (n.d.) 1–5.
- [2] V.A. Online, J.P. Esquivel, F.J. Del Campo, S. Rojas, *Environmental Science Microfluidic fuel cells on paper : meeting the power needs of next generation lateral flow devices †*, (2014) 1744–1749. doi:10.1039/c3ee44044c.
- [3] C.P. Andrieux, J.M. Dumas-Bouchiat, J.M. Saveant, *Homogeneous redox catalysis of electrochemical reactions: Part I. Introduction*, *J. Electroanal. Chem. Interfacial Electrochem.* 87 (1978) 39–53. doi:10.1016/S0022-0728(78)80378-7.
- [4] F.J. Enguita, A.L. Leitão, *Hydroquinone: Environmental pollution, toxicity, and microbial answers*, *Biomed Res. Int.* 2013 (2013). doi:10.1155/2013/542168.
- [5] US EPA, *Estimation Programs Interface Suite for Microsoft® Windows (EPISuite)*, v 4.11, *Estim. Programs Interface Suite Microsoft® Wind. (EPISuite)*, v 4.11. (2016).
- [6] J.P. Esquivel, P. Alday, O.A. Ibrahim, B. Fernández, E. Kjeang, *A Metal-Free and Biotically Degradable Battery for Portable Single-Use Applications*, 1700275 (2017). doi:10.1002/aenm.201700275.
- [7] J.L. Osborn, B. Lutz, E. Fu, P. Kauffman, D.Y. Stevens, P. Yager, *Microfluidics without pumps : reinventing the T-sensor and H-filter in paper networks †*, *Lab Chip.* 10 (2010) 2659–2665. doi:10.1039/c004821f.
- [8] E. Kjeang, R. Michel, D.A. Harrington, N. Djilali, D. Sinton*, *A Microfluidic Fuel Cell with Flow-Through Porous Electrodes*, (2008) 4000–4006. doi:10.1021/JA078248C.
- [9] B. Yang, L. Hooper-Burkhardt, F. Wang, G.K. Surya Prakash, S.R. Narayanan, *An Inexpensive Aqueous Flow Battery for Large-Scale Electrical Energy Storage Based on Water-Soluble Organic Redox Couples*, *J. Electrochem. Soc.* 161 (2014) A1371–A1380. doi:10.1149/2.1001409jes.
- [10] Y.J. Kim, S.-E. Chun, J. Whitacre, C.J. Bettinger, *Self-deployable current sources fabricated from edible materials*, 1 (2013) 2050–750. <http://pubs.rsc.org/en/content/articlepdf/2013/tb/c3tb20183j> (accessed July 17, 2017).
- [11] C. Chen, Y. Zhang, Y. Li, J. Dai, J. Song, Y. Yao, Y. Gong, I. Kierzewski, J. Xie, L. Hu, *All-wood, Low Tortuosity, Aqueous, Biodegradable Supercapacitors with Ultra-High Capacitance*, *Energy Environ. Sci.* 10 (2017) 538–545. doi:10.1039/C6EE03716J.
- [12] Y.J. Kim, S.-E. Chun, J. Whitacre, C.J. Bettinger, *Self-deployable current sources fabricated from edible materials*, *J. Mater. Chem. B.* 1 (2013) 3781–3788. doi:10.1039/C3TB20183J.
- [13] O.A. Ibrahim, M.-A. Goulet, E. Kjeang, *Microfluidic Electrochemical Cell Array in Series: Effect of Shunt Current*, *J. Electrochem. Soc.* 162 (2015) F639–F644. doi:10.1149/2.0211507jes.
- [14] O. 311 Organization of Economic Cooperation and Development, *Test No. 311: Anaerobic Biodegradability of Organic Compounds in Digested Sludge: by Measurement of Gas Production*, OECD, 2006. doi:10.1787/9789264016842-en.
- [15] I. 11734 International Organization for Standardization, *Water Quality: Evaluation of the ultimate anaerobic biodegradation of organic compounds in digested sludge*, *Norme Int. ISO.* (1995).
- [16] American Society of the International Association for Testing and Materials, *ASTM E2170 - 01(2008) Standard Test Method for Determining Anaerobic*



- Biodegradation Potential of Organic Chemicals Under Methanogenic Conditions (Withdrawn 2013), (n.d.). <https://www.astm.org/Standards/E2170.htm> (accessed July 12, 2018).
- [17] USEPA, Fate, Transport and Transformation Test Guidelines OPPTS 835.3400 Anaerobic Biodegradability of Organic Chemicals, (1998) 10. <https://nepis.epa.gov/Exe/tiff2png.cgi/P100ID30.PNG?-r+75+g+7+D%3A%5CZYFILES%5CINDEXDATA%5C95THRU99%5CTIFF%5C00002810%5CP100ID30.TIF> (accessed July 12, 2018).
- [18] J.-D. Gu, D. Eberiel, S.P. McCarthy, R.A. Gross, Degradation and mineralization of cellulose acetate in simulated thermophilic compost environments, *J. Environ. Polym. Degrad.* 1 (1993) 281–291. doi:10.1007/BF01458295.
- [19] J. Pérez, J. Muñoz-Dorado, T. de la Rubia, J. Martínez, Biodegradation and biological treatments of cellulose, hemicellulose and lignin: an overview, *Int. Microbiol.* 5 (2002) 53–63. doi:10.1007/s10123-002-0062-3.
- [20] Metabolix unveils further PHA grades as additives for PVC and PLA; moves corporate HQ, *Addit. Polym.* 2016 (2016) 2–3. doi:10.1016/S0306-3747(16)30018-5.
- [21] U. Er, C. Suh, M.P. Marshak, A. An Aspuru-Guzik, Computational design of molecules for an all-quinone redox flow battery, *Chem. Sci.* 6 (2015) 845–1592. doi:10.1039/c4sc03030c.
- [22] Vinçotte, OK Compost EN 13432, (1995).

4.



Optimization of a paper-based capillary flow battery with flow-through electrodes

Overview

In this chapter, the design, fabrication and characterization of a capillary-based flow cell, working with organic redox species, paper matrices and carbon paper electrodes under controlled flow conditions is presented. This approach comes to represent an optimization in terms of fuel utilization for the powerPAD device presented previously in this thesis as a sustainable solution for single-use disposable applications. This improved platform proves the advantages of integrating hydrophilic porous carbon structures and a quasi-steady capillary flow to enhance the power density, operating time and fuel utilization.

4.1. INTRODUCTION

Continuing with the same line of developing sustainable power sources intensive efforts are being carried out in order to obtain efficient, eco-friendly, portable and low-cost energy storage solutions to power novel electronic devices as well as to reduce the environmental impact of e- waste.

Besides solid-state batteries, the most common approaches to store electrochemical energy include fuel cells and redox flow cells. In all of these, the electrical energy is produced by the conversion of chemical energy via redox reactions at their electrodes, which are separated by an ion exchange membrane.

Due to their cost and composition, these separation membranes are not typically suitable for disposable applications, which has led to the development of membrane-less cell designs based on microfluidics. In a microfluidic fuel cell, the fluid reactants, reaction sites and electrodes are confined within a microfluidic channel. Due to the laminar flow regime established inside a microchannel, microfluidic fuel cells can operate in a co-laminar flow regime without a physical barrier, such as an ion-exchange membrane, to separate the anode and the cathode[1–4]. Some of the reported examples include the use of liquid fuels such as ethanol,[5][6] methanol, formic acid, glucose and vanadium redox species[3,4].

Innovations in co-laminar flow cells configurations have resulted in remarkable enhancements in their performance, such as the implementation of flow through porous electrodes, which eliminated mass transport limitations and improved reactant conversion and power density[7,8]. However, in most cases the need of external pumps and other ancillary systems required to maintain the flow of reactants increases the device complexity and decreases the overall energy efficiency.[1][9] In this sense, microfluidic fuel cells have benefited from recent advances in capillary-based microfluidics, which rely on paper and other porous matrices to transport fluids without any external pumps[10–12]. Paper-based microfluidic devices have shown to be inexpensive, portable, easy to use and disposable. They have been under development for applications in the clinical sector,[13][14] especially for point-of-care diagnostics. These features have also been used in the development of paper-based microfluidic power sources[15][16] that include batteries[17], and fuel cells using methanol[18], glucose[19], or hydrogen as fuels[10].

A new concept of single use paper-based flow battery featuring a biotic degradation [20] was previously presented in this thesis. The device is completely aligned with the sustainability principles of circular economy as it is composed by organic renewable materials, can be produced by energy efficient processes and can be safely disposed of without environmental impact. The device is activated upon the addition of a drop of water, which dissolves internally stored redox species that flow through carbon electrodes reaching a cellulose absorbent pad. Organic quinone species were used as redox chemistry due to their electrochemical characteristics, water solubility, eco-friendliness, fast kinetics and low cost[21–25]. The device provides a high power density, even capable of substituting a Li coin cell battery in a portable water sensing device.



In this work, an open-concept capillary flow cell is introduced as an experimental platform for evaluation of paper-based capillary flow batteries under controlled flow conditions. In comparison with the previously powerPAD device, the present design provides improvements in output power, operating time, ending up in a final optimization of the fuel utilization with slightly variations of the components in the cell. The device embodies quasi-steady capillary flow design using a circular absorbent pad that counteracts the increase in viscous drag forces, avoiding decay in the flow rate. [26,27]

This device represents a platform for evaluating the influence of different flow cell parameters and operating reaction areas conditions on the device performance. Here, the effect of different electrode configurations and reactants flow rates using a quinone-based chemistry was studied.

4.2. CAPILLARY-BASED FLOW CELL DESIGN AND WORKING PRINCIPLE

The capillary flow cell here presented creates a steady and controlled flow rate of reactants based on capillarity in paper. This device represents a robust platform to evaluate different parameters affecting the cell performance, such as redox chemistries, porous membranes materials, electrode configurations, device geometries and operating conditions.

The device comprises two inlet paper channels consisted of glass fiber strips as inlet channels (Standard 17; 370 μm thick; 20 mm length; 5 mm wide) forming a U-shape (20 x 12 mm), and cellulose pieces (Whatman1; 180 μm thick) as outlet paper channels (5 mm-wide) with three different lengths (20; 40 and 60 mm) and a rounded paper absorbent pad (10 mm and 50 mm diameter) (both materials from GE Healthcare, Pittsburgh, PA, USA) and a pair of porous carbon electrodes. Porous carbon electrodes were cut to size (5, 10, 15 and 20 mm-wide x 10 mm-long) from sheets of Toray carbon paper (TGPH-120; E-TEK) with thickness 370 μm . For the purpose of this work, the porous carbon electrodes were annealed in a butane flame to confer the hydrophilic behavior needed for the flow-through configuration.[7] The device structure was assembled using pressure sensitive adhesives (PSA) (Adhesives Research, Glen Rock, PA, USA). A custom-made support was fabricated in 6 mm thick Poly(methyl methacrylate) (Plexiglas, Evonik Performance Materials GmbH, Darmstadt, Germany), shown in Figure 4.2. The device components were designed in a CAD program (CorelDRAW, Corel, Ottawa, ON, Canada). All the components were cut using a CO₂ laser cutter (Mini 24, Epilog Laser, Golden, CO, USA) and manually assembled layer by layer using templates and alignment pins.

Figure 4.1 shows a schematic representation of the paper-based capillary flow battery working principle and its main components.

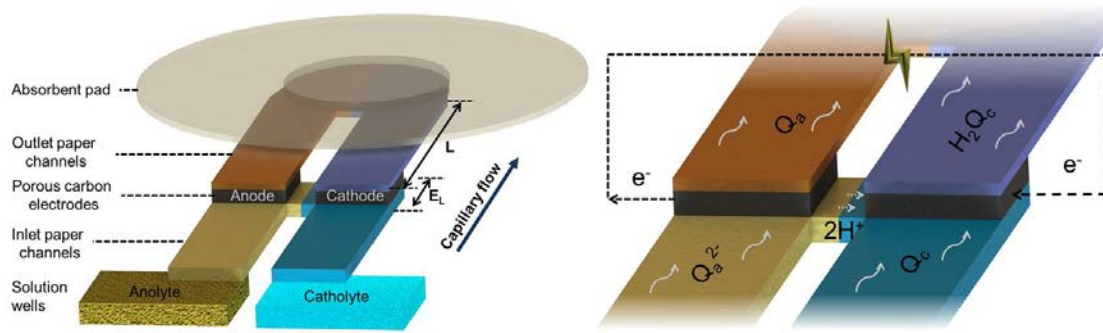


Figure 4.1. Paper-based capillary flow battery schematic representation and working principle.

The device was placed on a custom-made acrylic support that comprised two solution wells, facilitated electrical connection to the electrodes and included a lid to prevent evaporation while allowing purging of air as the absorbent pad is filled (Figure 4.2). Oxidized and reduced species are dissolved in their respective electrolytes and the solutions are stored in the support wells. The flow of reactants is established by immersing one inlet paper channel into each of these wells. A segment of paper perpendicular to the inlet channels is placed in contact with the electrodes, acting as a salt bridge. The two solutions are only in direct contact at this confined region, preventing interdiffusion of species before reaching the electrodes. The output channels converge the two reactants streams coming from the electrodes into an absorbent pad at the end of the cell. This absorbent pad has a fully circular shape in order to achieve a quasi-steady flow of reactants because the increasing area of the liquid front increases the capillary pressure and compensates the increment of viscous drag force, as has been shown in previous works.[27][13][28]

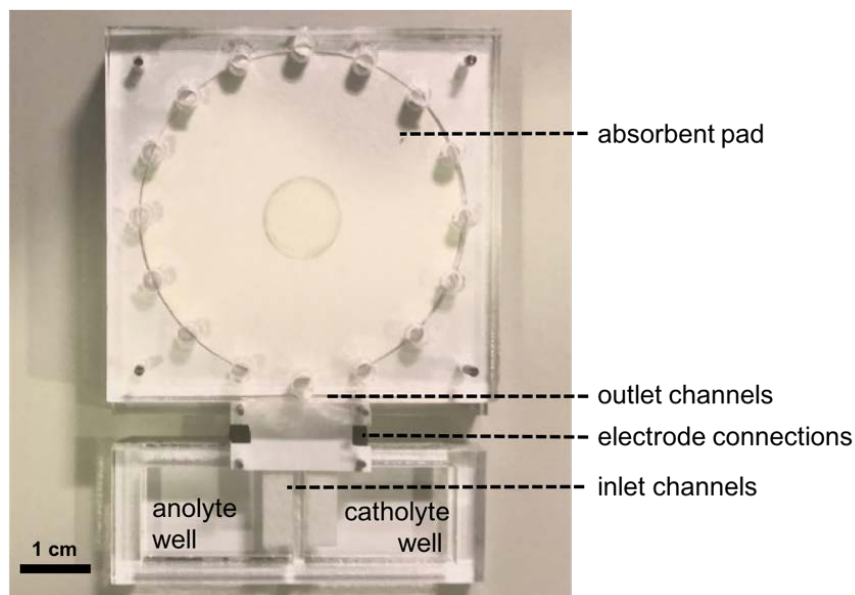


Figure 4.2. Setup of PMMA for the capillary-based flow rate evaluation.



The magnitude of the capillary flow rate depends on the materials and geometry of the entire microfluidic system. In this work, the flow rate of species has been modulated by changing the length of the outlet channels (L).

Moreover, the effect of two electrode configurations on the flow cell performance was studied. These electrode configurations, shown in Figure 4.3, have been named as flow-over (FO) and flow-through (FT). In the case of the flow-over electrode configuration, the reactants flow over the superficial surface of the electrode in their way to the absorbent pad. In the case of the flow-through electrode configuration, the electrodes are sandwiched between the inlet channels and the outlet channels, forcing the fluid to flow through the internal porous structure of the electrodes and taking advantage of their high effective area.

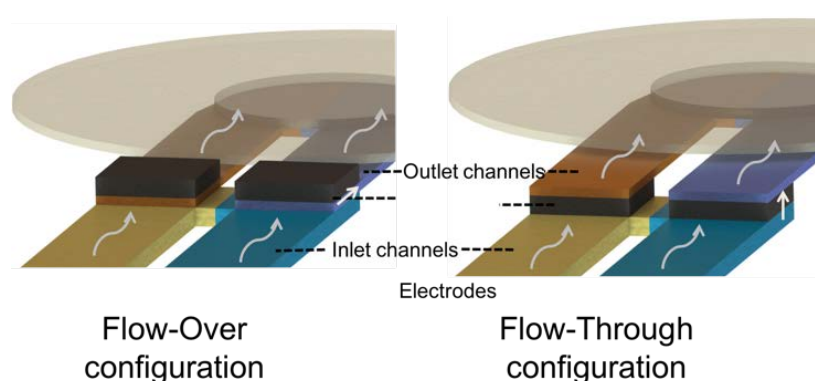


Figure 4.3. Flow over and flow through the electrode configurations.

4.3. QUASI-STEADY CAPILLARY FLOW CHARACTERIZATION

The capillary flow rate of the solutions in the flow cell was characterized by visual inspection of the change in fluid area within the absorbent pad over time.[13] For these measurements, 100 mM solutions of euroglaucine disodium salt and tartrazine dyes were used to simulate and visualize the flow of redox species in paper. In these experiments, the inlet paper channels were dipped into the solution wells of the acrylic support while recording images of the entire device with a web camera (C920, Logitech, Fremont, CA, USA) controlled by a time-lapse software (VideoVelocity, CandyLabs, Vancouver, BC, Canada), saved images at a rate of 1 frame/5 s. The flow rates were calculated from the captured images by measuring the increase in the area covered by the dyed solutions in the absorbent pad using ImageJ software (US National Institutes of Health, Bethesda, Maryland, USA), knowing the absorbent capacity of the Whatman 1 pad ($7\mu\text{l}/\text{mm}^2$), the flow rate can be calculated with equation (3).

$$Q = v \cdot A = \frac{\Delta A}{\Delta t} \cdot C \quad (3)$$

where Q = flow rate ($\mu\text{l}/\text{s}$), v = flow velocity (mm/s), A = cross-sectional vector area (mm^2) t = time (s) and C = absorbent capacity ($\mu\text{l}/\text{mm}^2$).

Before performing the electrochemical characterization of the cell, the flow rates established by capillarity were measured. The evolution of the flow rate along the paper channels in time was characterized by measuring the progress of the liquid front in the absorbent pad. As the absorbent pad has a measured volumetric capacity of $7 \mu\text{L cm}^{-2}$, the volume absorbed by the pad at a particular time can be directly computed by measuring the area covered by the liquid. In order to enhance image contrast, solutions with yellow (tartrazine) and blue (euroglaucine disodium salt) dyes were used to simulate and visualize the flow of redox species in paper.[29] All chemicals were purchased from Sigma-Aldrich (Sigma Aldrich, St Louis, Missouri, USA).

Figure 4.4a shows a sequence of photographs of the device as the absorbent pad fills up. The device starts to operate when the reactant solutions are deposited on the wells (1). A flow of reactants is established by immersing the inlet paper channels into these wells, then it advances towards the absorbent pad and starts to fill it up (2-3). A stationary flow is maintained in the cell until the absorbent pad gets completely saturated (4). Maintaining a steady or a quasi-steady flow rate in a capillary system is an important issue to consider as the flow decreases over time when there is a constant cross-sectional area of the liquid front. This happens because despite the capillary force remains constant, there is an increase in the viscous drag force or viscous resistance in response to the increase of the distance of the fluid front with respect the input source.

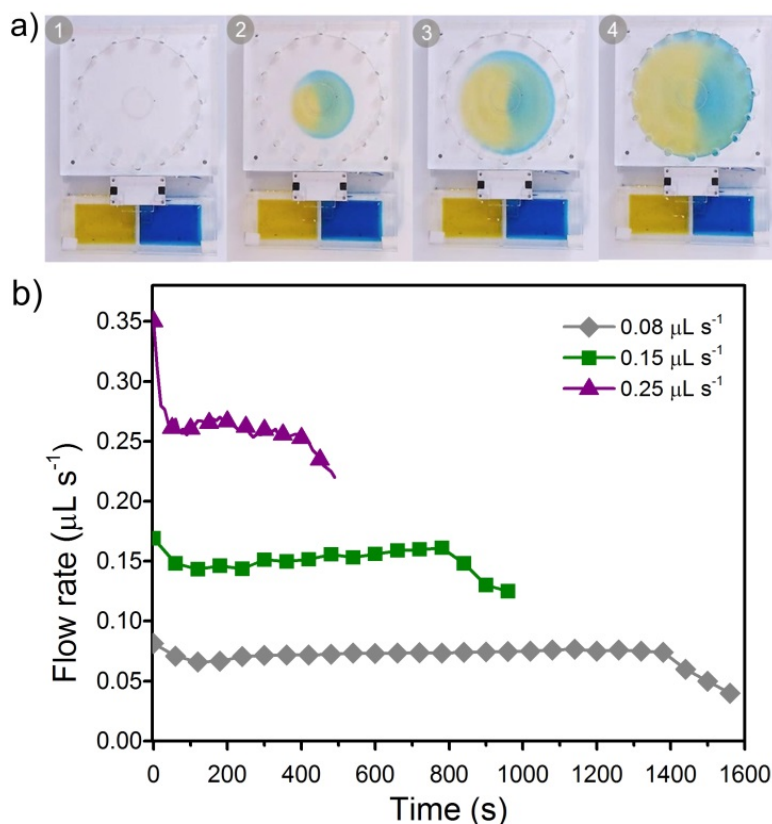


Figure 4.4. Characterization of capillary flow rate. (a) Image sequences for flow rate characterization. (b) Resulting capillary flow rates for different output channel lengths (L). Data points represent mean values for $n = 3$.



A good strategy to counteract this phenomenon is to gradually increase the area of the liquid front by changing the geometry of the outlet channel (eg. 270° fan shape) [33] so the capillary force and the viscous drag force will synchronously increase and cancel out, leading to a sustained flow rate over time. Moreover, when dealing with single use devices, achieving a constant flow rate is not the only important requirement. Maintaining this sustained flow for a considerable time is an important condition to accomplish as it is appealing to extend the operation time of the device for as long as possible. Figure 4.4b shows the flow rates obtained in the devices having different output channel lengths (20, 40 and 60 mm). Results show that a quasi-steady flow of reactants is effectively established and as expected, the magnitude of this flow rate decreases at increasing channel lengths. Generated flow rate values were $0.25 \mu\text{L s}^{-1}$, $0.15 \mu\text{L s}^{-1}$ and $0.08 \mu\text{L s}^{-1}$. As the capacity of the absorbent pad was fixed to $140 \mu\text{L}$, the operational time of the device is inversely proportional to the established flow rate.

4.4. ELECTROCHEMICAL BATTERY CHARACTERIZATION

The redox chemistry was first characterized *ex-situ* using voltammetry techniques to assess the electrochemical reaction kinetics for the specific redox species and electrolytes. Linear sweep voltammeteries of the aqueous quinone redox couple were performed in a conventional three-electrode electrochemical cell. The potential was swept from open circuit potential in the direction of the intended discharge reaction of the measured half-cell at a scan rate of 50 mV s^{-1} . Glassy carbon electrode (0.07 cm^2), platinum wire electrode and silver-silver chloride electrode (Ag/AgCl) (Metrohm AG, Herisau, Switzerland) were used as working electrode, counter electrode and reference electrode, respectively. For battery characterization, the open circuit voltage (OCV) of each cell was measured before polarization. Polarization curves were performed in potentiodynamic mode at a scan rate of 50 mV s^{-1} . Chronopotentiometric curves were measured using external loads selected for each kind of electrode configuration. All electrochemical characterization curves were recorded with a potentiostat Dropsens $\mu\text{Stat 400}$ (Dropsens, Oviedo, Spain).

4.4.1 Electrode configuration

The capillary flow battery performance was tested with a solution of 0.1 M p-Benzoquinone (pBQ) in 0.5 M oxalic acid ($\text{C}_2\text{H}_2\text{O}_4$) (oxide form) as catholyte and 0.1 M hydroquinonesulfonic acid potassium salt (H_2BQS) (reduced form) in 1 M potassium hydroxide (KOH) as anolyte under capillary flow at quasi-steady state. The electrolyte concentrations were balanced in order to keep a neutral pH at the absorbent pad. The open circuit voltage of the cell was measured once the liquid front reached the absorbent pad and a steady value of $0.75 \pm 0.05 \text{ V}$ was obtained in all cases, which is in good correlation to prior studies. Polarization curves of the battery were measured at room temperature under potentiostatic control. Measurements were performed by triplicate for each cell. Figure 4.5a shows the I-V curves obtained at $0.25 \mu\text{L s}^{-1}$ for the flow-through and flow-over configuration. A maximum power of $0.47 \pm 0.02 \text{ mW}$ was obtained in the flow-through cells whereas the power output in the flow-over configuration reached a maximum value of $0.020 \pm 0.005 \text{ mW}$. These results show that using hydrophilic porous carbon electrodes that allow the reactant

species to flow through the electrodes leads to a 20-fold improvement in the power delivered by the cell.

In order to evaluate the continuous operation of the batteries, the different cell configurations were tested by connecting them to an external resistive load that set them to operate at their maximum power (flow-over devices required a load of 1.6 k Ω , while flow-through cells were connected to a 230 Ω ohmic load) (Figure 4.5b).

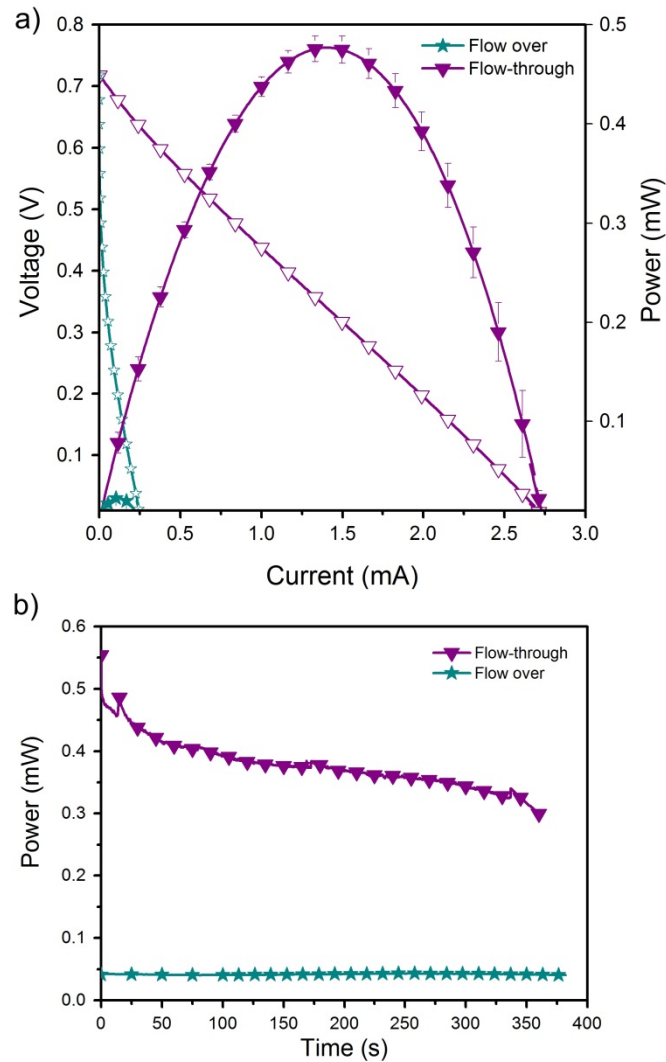


Figure 4.5. a) Polarization curves of the capillary flow battery designs with flow-over and flow-through electrode configurations. Data points represent mean values and error bars represent \pm one standard deviation, for $n = 3$. b) Discharge curves of the capillary paper-based flow battery subjected to fixed external loads. Data points and lines represent mean values for $n = 3$.

The results obtained from the characterization of the flow battery under a continuous operation allowed assessing its efficiency at the different configurations and tested conditions[30]. The faradaic efficiency allows evaluating the electroactive material utilization, which is the percentage of the theoretical species capacity that is actually being converted to current, and it is computed by the following expression:



$$\varepsilon_F = \frac{\int_0^t i(t) dt}{n C_0 V F} \quad (4)$$

where t is the measurement time, $i(t)$ the current calculated from the measured voltage divided by the resistance of the fixed load, n is the number of electrons per mole, F is the Faraday constant, C_0 is the initial species concentration, V is the volume of diluted redox species.

Moreover, the energy efficiency of the capillary flow cell can be evaluated by comparing the power delivered by the device when it is discharged to the energy that the flow cell could delivery ideally, that is, when working at its theoretical voltage:

$$\varepsilon_E = \frac{\int_0^t i(t) \cdot E(t) dt}{n C_0 V F E_T} \quad (5)$$

where $E(t)$ is the operating voltage and E_T is the theoretical open circuit voltage of the battery. The efficiencies were calculated from the chronopotentiometric curves from Figure 3b, 4b and 5b considering the load used for each electrode configuration.

It can be seen in Table 4.1 that the configuration of flow-through electrodes allows to improve significantly the faradaic efficiency when compared to the traditional flow-over configuration (from 7.9% to 28%) at the same flow rate. This also translates into a better energy efficiency that increases from 0.3% to 0.7%.

Table 4.1. Values of faradaic and energy efficiency yielded for the flow-over and flow-through electrodes configuration.

	Flow rate	ε_F (%)	ε_E (%)
Flow-Over Convective Flow	0.25 $\mu\text{L s}^{-1}$	7.9	0.3
Flow-Through Convective Flow	0.25 $\mu\text{L s}^{-1}$	28	0.7

4.4.2. Flow-through electrode flow rate modification

The performance of the flow-through cells were then tested at the flow rates reported in the previous section. Figure 4.6a shows the maximum power values recorded at each flow rate yielding 0.47 ± 0.2 mW at $0.15 \mu\text{L s}^{-1}$ and 0.44 ± 0.01 mW cm^{-2} at $0.08 \mu\text{L s}^{-1}$. For comparison, the cell performance at zero flow rate (diffusive flow of species) was also tested, yielding a value of 0.36 ± 0.01 mW.

All the flow-through regimens were put to work under a fixed ohmic load of 230Ω in order to generate a discharge curve of the batteries. All the devices reached an OCV of 0.75 ± 0.05 V that dropped to approximately 0.3 V when the load was connected, which yields peak power output for both flow configurations, as shown in Fig. 4.5. Figure 4.6b depicts the power delivered by the capillary flow cells until the absorbent pad was completely saturated (500 s for the highest flow rate system and up to 1600 s for the lowest flow rate).

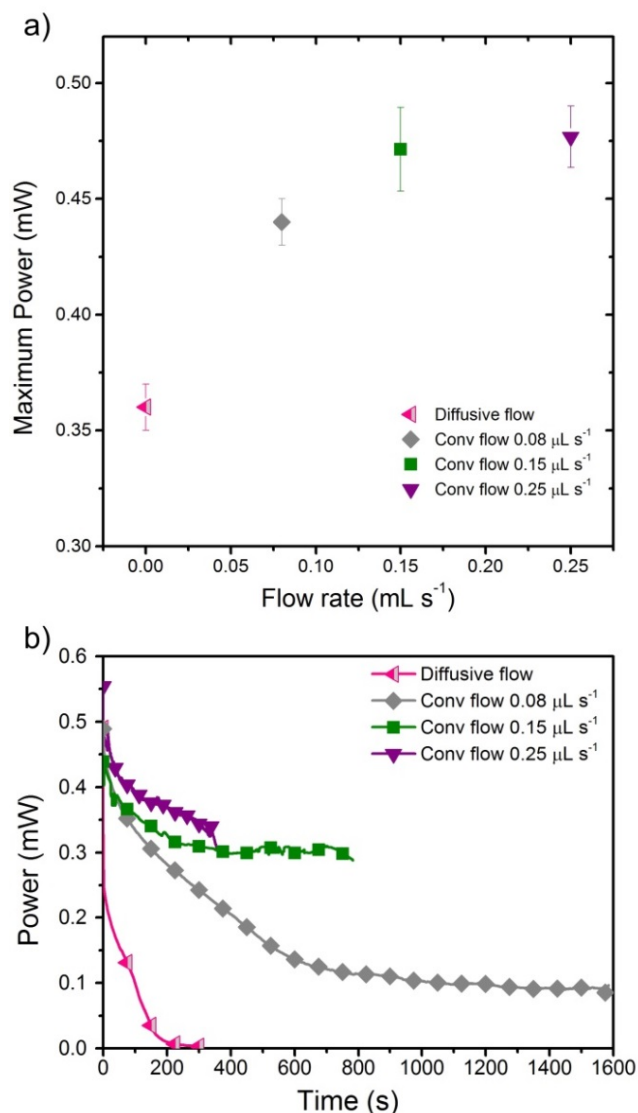


Figure 4.6. a) Maximum powers of capillary flow battery at different reactants flow rates. Data points represent mean values and error bars represent \pm one standard deviation, for $n = 3$. b) Discharge curves of the capillary paper-based flow battery subjected to fixed external loads. Data points and lines represent mean values for $n = 3$.

All the flow-through configurations yielded an initial power ranging between 0.45 and 0.55 mW. It can be seen that the cell configuration based on diffusive flow shows rapid performance decay, dropping to 0.03 mW within the first minute of operation. Conversely, the cells working with a convective flow of reactants showed a mild and continuous decrease in time until they reached a plateau at 0.36 mW at 0.25 $\mu\text{L s}^{-1}$, at 0.32 mW in the cell at 0.15 $\mu\text{L s}^{-1}$ and 0.12 mW in the cell at 0.08 $\mu\text{L s}^{-1}$. In this case, this power decay in time could be due to the oxidation of hydroquinone species when exposed to atmosphere.

The values of the energy and faradaic efficiencies obtained from the discharge curves of the convective and diffusive flow regimes are shown in table 4.2. The establishment of a slower flow rate makes it possible for the species involved to pass slowly through the electrodes, therefore, the redox have more time to take place. It is clear that



maintaining a convective flow in the system leads to an increase in the fuel utilization of 25 %

It can be seen that lower flow rates yield better efficiencies with a maximum of 48% of fuel conversion at $0.08 \mu\text{L s}^{-1}$. It should be noted that within the tested quasi-steady flow rates in the flow-through electrode configuration ($0.25 \mu\text{L s}^{-1}$, $0.15 \mu\text{L s}^{-1}$ and $0.08 \mu\text{L s}^{-1}$) there is a trade-off between delivered power and efficiencies. As mentioned before, higher flow rates result in higher power, however the electroactive material utilization decreases with increasing flow rate.

Table 4.2. Values of faradaic and energy efficiency yielded for the diffusive and convective regimes.

	Flow rate	ϵ_F (%)	ϵ_E (%)
Diffusive flow		3	0.1
	$0.25 \mu\text{L s}^{-1}$	28	0.7
Flow-Through Convective Flow	$0.15 \mu\text{L s}^{-1}$	31	1.2
	$0.08 \mu\text{L s}^{-1}$	48	1.2

4.4.3. Electrode length modification

With the prior knowledge of the relationship existent between the lower flow rates, the higher the percentage of energy efficiencies is, a maximum optimization in terms of fuel utilization was explored. For this, the reaction zone was modified by increasing the length of the porous carbon electrode (E_L) and the intersection area in the inlet canal (bridge) where the electrodes rest (Figure 4.7).

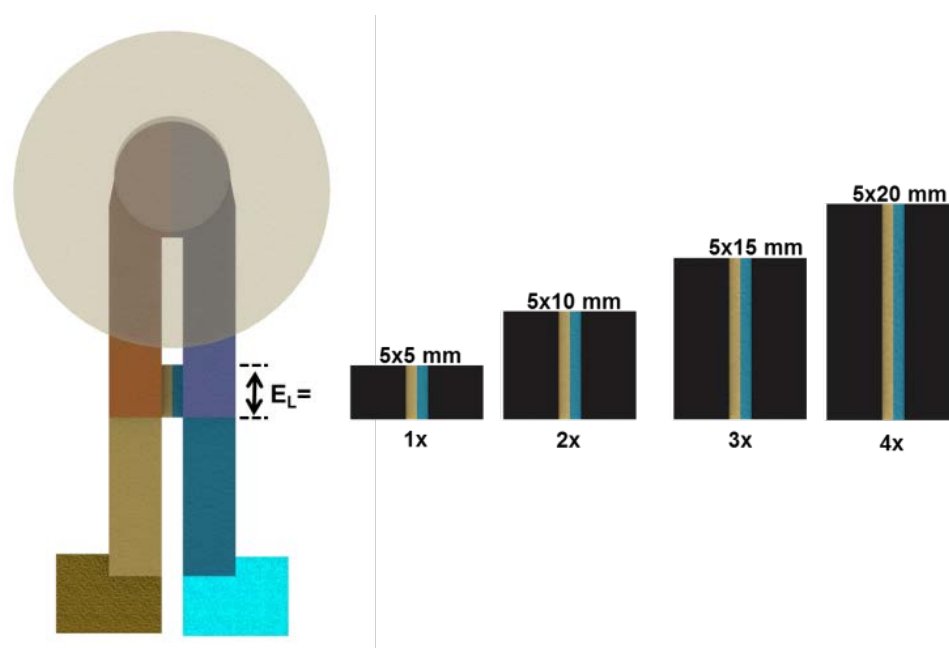


Figure 4.7. Electrode (E_L) and bridge length modification.

The reaction areas evaluated were using electrodes of different dimensions, 5 mm length (1x), 10 mm length (2x), 15 mm and 20 mm length (3x and 4x respectively). Consecutively, polarization curves of the cells were made. Figure 4.8 shows the expected trend, the power increases as the reaction area increases, however, the greatest change is observed from the 1x to 2x configuration, increasing from 0.45 mW to 0.61 mW. While in the 3x and 4x configurations, the rate of increase was slower, a maximum power of 0.7 mW was reached for the 4x configuration.

Once the maximum powers of the different cells were known, the batteries were put to work at their point of maximum power, again using a fixed external ohmic load. The results of the discharge curves can be seen in figure 4.8b, all the discharge curves begun in the maximum power output and were decreasing over time, keeping the cells with more than $2xE_L$ above 0.2 mW for up to a 20-minute period.

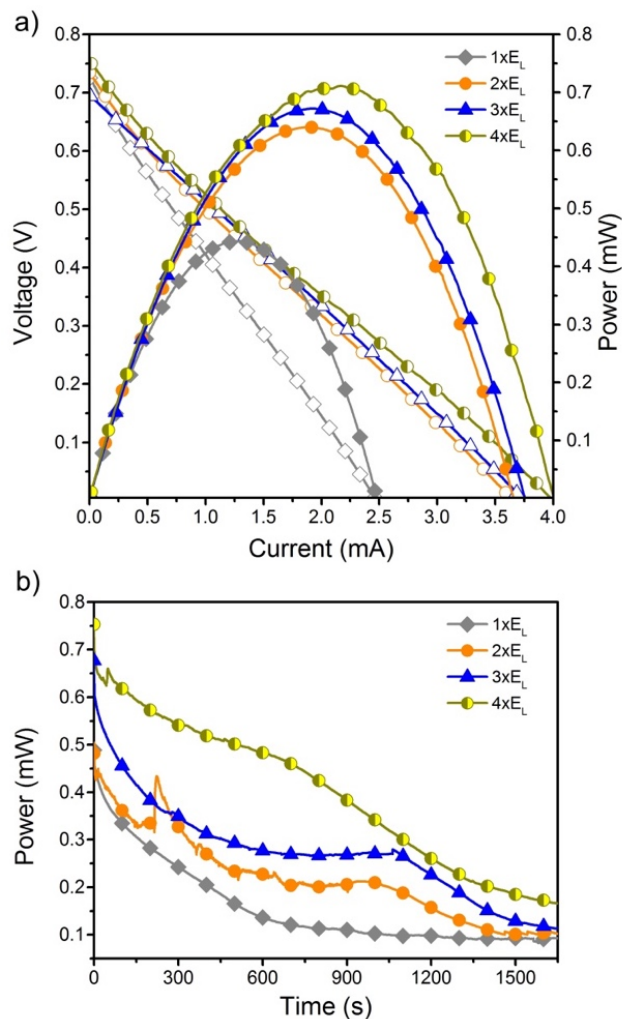


Figure 4.8. a) Polarization curves of the capillary flow battery designs with the 1x, 2x, 3x and 4x E_L configuration. Data points represent mean values and error bars represent \pm one standard deviation, for $n = 3$. b) Discharge curves of the capillary paper-based flow battery subjected to fixed external loads. Data points and lines represent mean values for $n = 3$.



Finally, following the same procedure, fuel utilization efficiency was calculated. Table 4.3 shows the dramatic increase in efficiency as the reaction zone grew. It is possible to observe that increasing the length of the electrodes it was possible enhance the efficiency of the cell reaching a 96% value ($4x E_L$) with the simple modification of the size of the electrodes, this represents the same volume of fuel in the cell but carrying out its optimal custom, without affecting the costs, weight or size of the device.

Table 4.3. Values of faradaic and energy efficiency yielded flow-through electrodes configuration with variation in the electrode length size.

E length	ϵ_F (%)	ϵ_E (%)
1x	48	1.5
2x	70	2.2
3x	89	3.2
4x	96	3.9

4.5. CONCLUSIONS

This work presents the design, fabrication, characterization in fuel utilization efficiency optimization of a capillary-based flow battery, working with organic redox species, paper matrices and flow-through porous electrodes under controlled flow conditions. This capillary flow cell embodies a quasi-steady capillary flow regime and takes advantage of the integration of different sizes of porous carbon hydrophilic structures. This device represents a robust platform for evaluating the influence of different cell parameters and operating conditions on the device performance. The reactants flow rate in these capillary flow cells was tuned by modifying the length of the paper channels. The effect of different electrode configurations and areas as well as different reactants flow rates using a quinone-based chemistry showed significant improvements in both power density and fuel utilization, leading to almost 100% utilization of the redox-reactants passing through the reaction zone of the cell, by establishing a slow flow rate modifying the length of the outlet channels and a larger reaction zone, as mentioned above, these modifications do not represent an additional expense in the development of the capillary-based flow cell configuration. Additional parameters affecting the device performance such as further engineering of the absorbent pad to expand the operation time will be subject to future work. The microfluidic platform presented provides a reliable cell design suitable for optimization of capillary flow batteries as well as other capillary-based electrochemical devices.

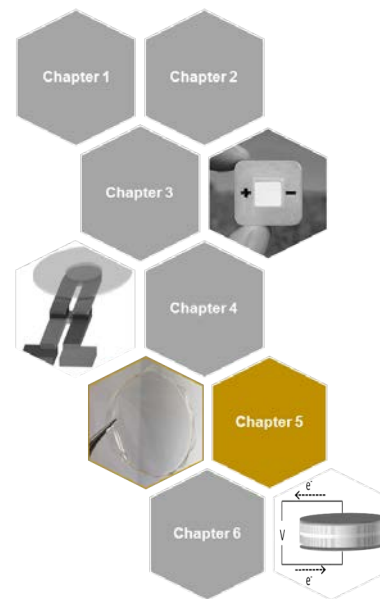
References in Chapter 4.

- [1] E. Kjeang, N. Djilali, D. Sinton, Microfluidic fuel cells : A review, 186 (2009) 353–369. doi:10.1016/j.jpowsour.2008.10.011.
- [2] J. Yang, S. Ghobadian, P.J. Goodrich, R. Montazami, N. Hashemi, Miniaturized biological and electrochemical fuel cells: challenges and applications, *Phys. Chem. Chem. Phys.* 15 (2013) 14147–14161. doi:10.1039/c3cp50804h.
- [3] R. Ferrigno, A.D. Stroock, T.D. Clark, M. Mayer, G.M. Whitesides, Membraneless Vanadium Redox Fuel Cell Using Laminar Flow, *J. Am. Chem. Soc.* 2 (2002) 12930–12931.
- [4] E. Kjeang, B.T. Proctor, A.G. Brolo, D.A. Harrington, N. Djilali, D. Sinton, High-performance microfluidic vanadium redox fuel cell, *Electrochim. Acta.* 52 (2007) 4942–4946. doi:10.1016/j.electacta.2007.01.062.
- [5] T.J. Yen, N. Fang, X. Zhang, A micro methanol fuel cell operating at near room temperature, *Appl. Phys. Lett.* 83 (2003) 4056–4058. doi:10.1063/1.1625429.
- [6] R.S. Jayashree, L. Gancs, E.R. Choban, A. Primak, D. Natarajan, L.J. Markoski, P.J.A. Kenis, Air-Breathing Laminar Flow-Based Microfluidic Fuel Cell, *J. Am. Chem. Soc.* 127 (2005) 16758–16759.
- [7] E. Kjeang, R. Michel, D.A. Harrington, N. Djilali, D. Sinton, A Microfluidic Fuel Cell with Flow-Through Porous Electrodes, *J. Am. Chem. Soc.* 130 (2008) 4000–4006. doi:10.1021/JA078248C.
- [8] M.A. Goulet, O.A. Ibrahim, W.H.J. Kim, E. Kjeang, Maximizing the power density of aqueous electrochemical flow cells with in operando deposition, *J. Power Sources.* 339 (2017) 80–85. doi:10.1016/j.jpowsour.2016.11.053.
- [9] S.A. Mousavi Shaegh, N.T. Nguyen, S.H. Chan, A review on membraneless laminar flow-based fuel cells, *Int. J. Hydrogen Energy.* 36 (2011) 5675–5694. doi:10.1016/j.ijhydene.2011.01.063.
- [10] J.P. Esquivel, J.R. Buser, C.W. Lim, S. Rojas, P. Yager, Single-use paper-based hydrogen fuel cells for point-of-care diagnostic applications, *J. Power Sources.* 342 (2017) 442–451. doi:10.1016/j.jpowsour.2016.12.085.
- [11] R.K. Arun, S. Halder, N. Chanda, S. Chakraborty, A paper based self-pumping and self-breathing fuel cell using pencil stroked graphite electrodes., *Lab Chip.* 14 (2014) 1661–4. doi:10.1039/c4lc00029c.
- [12] A.K. Yetisen, M.S. Akram, C.R. Lowe, Paper-based microfluidic point-of-care diagnostic devices, *Lab Chip.* 13 (2013) 2210–2251. doi:10.1039/c3lc50169h.
- [13] J.A. Adkins, E. Noviana, C.S. Henry, Development of a Quasi-Steady Flow Electrochemical Paper-Based Analytical Device, *Anal. Chem.* 88 (2016) 10639–10647. doi:10.1021/acs.analchem.6b03010.
- [14] I. Jang, S. Song, Lab on a Chip Facile and precise flow control for a paper-based, *Lab Chip.* 15 (2015) 3405–3412. doi:10.1039/C5LC00465A.
- [15] H. Liu, R.M. Crooks, Paper-based electrochemical sensing platform with integral battery and electrochromic read-out, *Anal. Chem.* 84 (2012) 2528–2532. doi:10.1021/ac203457h.
- [16] A. Fraiwan, L. Kwan, S. Choi, A disposable power source in resource-limited environments: A paper-based biobattery generating electricity from wastewater, *Biosens. Bioelectron.* 85 (2016) 190–197. doi:10.1016/j.bios.2016.05.022.
- [17] N.K. Thom, G.G. Lewis, M.J. DiTucci, S.T. Phillips, Two general designs for fluidic batteries in paper-based microfluidic devices that provide predictable and tunable sources of power for on-chip assays, *RSC Adv.* 3 (2013) 6888–6895. doi:10.1039/C3RA40701B.
- [18] J.P. Esquivel, F.J. Del Campo, J.L. Gómez de la Fuente, S. Rojas, N. Sabaté, Microfluidic fuel cells on paper: meeting the power needs of next generation lateral flow devices, *Energy Environ. Sci.* 7 (2014) 1744. doi:10.1039/c3ee44044c.



- [19] M.J. González-Guerrero, F.J. del Campo, J.P. Esquivel, D. Leech, N. Sabate, Paper-based micro fluidic biofuel cell operating under glucose concentrations within physiological range, *Biosens. Bioelectron.* 90 (2017) 475–480. doi:10.1016/j.bios.2016.09.062.
- [20] J.P. Esquivel, P. Alday, O.A. Ibrahim, B. Fernández, E. Kjeang, N. Sabaté, A Metal-Free and Biotically Degradable Battery for Portable Single-Use Applications, *Adv. Energy Mater.* (2017) 1700275. doi:10.1002/aenm.201700275.
- [21] Y. Ding, Y. Li, G. Yu, Exploring Bio-inspired Quinone-Based Organic Redox Flow Batteries: A Combined Experimental and Computational Study, *Chem.* 1 (2016) 790–801. doi:10.1016/j.chempr.2016.09.004.
- [22] B. Yang, L. Hooper-Burkhardt, F. Wang, G.K. Surya Prakash, S.R. Narayanan, An Inexpensive Aqueous Flow Battery for Large-Scale Electrical Energy Storage Based on Water-Soluble Organic Redox Couples, *J. Electrochem. Soc.* 161 (2014) A1371–A1380. doi:10.1149/2.1001409jes.
- [23] B. Huskinson, M.P. Marshak, C. Suh, S. Er, M.R. Gerhardt, C.J. Galvin, X. Chen, A. Aspuru-Guzik, R.G. Gordon, M.J. Aziz, A metal-free organic–inorganic aqueous flow battery, *Nature.* 505 (2014) 195–198. doi:10.1038/nature12909.
- [24] S. Nawar, B. Huskinson, M. Aziz, Benzoquinone-Hydroquinone Couple for Flow Battery, *Mater. Res. Soc. Symp. Proc.* 1737 (2013) 2–7. doi:10.1557/opl.2012.1737.
- [25] O.A. Ibrahim, P. Alday, N. Sabaté, J.P. Esquivel, E. Kjeang, Evaluation of Redox Chemistries for Single-Use Biodegradable Capillary Flow Batteries, *J. Electrochem. Soc.* 164 (2017) A2448–A2456. doi:10.1149/2.0971712jes.
- [26] K. Li, D. Zhang, H. Bian, C. Meng, Y. Yang, Criteria for Applying the Lucas-Washburn Law, *Sci. Rep.* 5 (2015) 1–7. doi:10.1038/srep14085.
- [27] S. Mendez, E.M. Fenton, G.R. Gallegos, D.N. Petsev, S.S. Sibbett, H.A. Stone, Y. Zhang, P.L. Gabriel, Imbibition in Porous Membranes of Complex Shape: Quasi-stationary Flow in Thin Rectangular Segments, *Langmuir.* 26 (2010) 1380–1385. doi:10.1021/la902470b.
- [28] B.M. Cummins, R. Chinthapatla, B. Lenin, F.S. Ligler, G.M. Walker, Modular pumps as programmable hydraulic batteries for microfluidic devices, *Technology.* 5 (2017) 21–30. doi:10.1142/S2339547817200011.
- [29] J.L. Osborn, B. Lutz, E. Fu, P. Kauffman, D.Y. Stevens, P. Yager, Microfluidics without pumps: reinventing the T-sensor and H-filter in paper networks, *Lab Chip.* 10 (2010) 2659–2665. doi:10.1039/c004821f.
- [30] D.C. Rongzhong Jiang*, Charles Rong, Determination of energy efficiency for a direct methanol fuel cell stack by a fuel circulation method, *J. Power Sources.* 126 (2004) 119–124. doi:10.1016/j.jpowsour.2003.08.022.

5.



Bio-Polymer Electrolyte Membranes (BioPEMs) for primary redox batteries

Overview

Nowadays, the need for alternative power sources environmentally friendly and efficient substitutes for conventional fossil fuels has become of the utmost importance. Redox batteries turned out to lay the foundation for the generation of portable power applications, but there are some economic and technical problems involved. Among such problems is the fact that these devices typically use proton exchange membrane (PEM), like Nafion[®] (a perfluorosulfonic acid copolymer). However, Nafion[®] presents some drawbacks, such as being non-environmentally friendly and high-priced.

In this chapter, a novel eco-friendly and sustainable bio-polymeric membranes (BioPEMs) were synthesized from bio-polymers like chitosan, cellulose and starch. These BioPEMs should possessed good chemical and mechanical stability, among some other characteristics with the purpose of being a naturally driven component in the integration to biodegradable batteries[1],[2] bringing forth advantages in terms of operation, functionality, sustainability and cost.

5.1. INTRODUCTION

The progress of a society is based to a large extent on the search and execution of new sources of energy that can solve the deficit of fossil fuels, rising oil, coal and gas prices and contribute to a more sustainable and eco-friendly energy consumption.

Redox batteries are open systems where redox reactions take place at the anode and the cathode, indicated as the negative and positive electrodes, respectively and the active masses undergoing the redox reaction are delivered from outside the cell [3]. On the other hand, fuel cells are electrochemical devices in which a continuous flow of fuel and oxidant undergo a controlled chemical reaction that gives rise to the products and directly supplies electric current to an external circuit, allowing the continuous supply of consumed reagents using catalytic electrodes. In the redox flow cells, the flow of reactants is unlimited, recirculating from one compartment to the other as the cell is recharged and discarded, and while in the fuel cell the fuel is used using catalytic electrodes in its systems. Both of these systems incorporate an electrolyte membrane, which allows the protons to flow through the membrane from the anode to the cathode and acts as a non-conductor electrons material [4],[5].

The membrane is a semipermeable membrane made from an ionomeric polymer, which must fulfill the following properties: (i) transport of protons by their matrix, (ii) separate the reactants of the two half-cells, (iii) low permeability to the redox reagents involved (iv) adequate mechanical properties, tolerating to obtain a membrane thickness of 10-250 μm , (v) long lifetime, (vi) low cost and (viii) the capability of fabrication into membrane electrode assemblies[6]. Nowadays, the Nafion[®] (a perfluorosulfonic acid copolymer) and its derivative membranes dominate the market, particularly in PEMFCs[7]. However, Nafion[®] has some serious drawbacks, Nafion[®]-based membranes are expensive because of their complex and high manufacturing process cost, low conductivity at low humidity, loss of mechanical stability at high temperature (100°C) [8].

At present, exist the aim to develop more bio-solid polymer electrolyte based on natural polymers due to their abundance, low-cost and environmentally friendly nature as alternative candidates to substitute synthetic polymer-based membranes (particularly Nafion[®]). Such natural-based polymers include agar[9,10], gelatin[11,12], starch[13], cellulose[14] or chitosan[15–21]. Chitosan (CH) and its derivatives are extensively investigated as some of the most attractive “green” materials for power sources applications due to its biodegradability, biocompatibility, non-toxicity and low-cost polymer as well as the simple and easy chemical modifications allow. Barros et al evaluated hydrogel films based on the polysaccharides CH and cellulose [21]. Chitosan has been used for the synthesis of membranes for applications as alternative proton exchange membrane materials in fuel cells[16]. Some other membranes based on natural polymers, such as gelatin networks, have been doped with compounds to improve their electronic properties for applications in biotechnology[11].



During this work the objective was to develop membranes based on bio-polymers that represent an eco-friendly, sustainable and naturally driven components of portable power sources. This power source would be based on a redox flow battery working principle with particular features. In this case the redox species would not circulate through the cell, eliminating the need of pumps and the energy consumption associated with them. Also, this battery would be conceived for single-use applications so rechargeability is not initially pursued. Therefore, we have called this particular power source as passive *primary redox battery*.

In this chapter, we present a new concept of bio-polymer membranes (BioPEMs) for electrochemical power sources, which not only serve to separate the anolyte from the catholyte but also possess high ionic conductivity for the ion exchange between both sides of the cell, thus improving its efficiency, mechanical robustness and sustainability.

The new membranes should fulfill certain essential aspects for their incorporation in these primary redox batteries, such as the following: good chemical and mechanical stability, high ionic conductivity, present low crossover of the redox species and favor having high power output in the device.

The synthesis of the bio-polymer membranes, their ionic conductivity characterization and performance of the BioPEMs in primary redox batteries are presented in the current chapter.

5.2. POLYMER ELECTROLYTES PREPARATION

Two main bio-polymeric electrolyte membranes were synthesized: chitosan-based electrolytic films and starch-based electrolyte membranes.

5.2.1. Chitosan-based electrolytes

The synthesis of the chitosan (medium molecular weight, 75 – 85 % deacetylated, 448877), and hydroxypropyl methyl cellulose (09963) (CH:HPMC) matrix were prepared by solvent casting (SC). Firstly, the stock solutions of the natural polymers were obtained to subsequently carry out the different BioPEMs preparation. Briefly, 1 g of CH was dissolved in 50 mL aqueous acetic acid (99.8%) and 1 g of HPMC 50 mL ultra- pure water, to prepare 1 wt. % and 2 wt. % solutions, respectively. All these products were purchased by Sigma-Aldrich Company, Ltd (St. Lois, MO, US) and were used as received without further purification. These polymeric mixtures were stirred overnight at room temperature until a homogeneous and viscous solution was formed. The pH of the solutions was adjusted to 4.

For the bio-polymer electrolytic membrane the CH and HPMC solutions were mixed together in 25:75(w:w) ratio resulting in the general matrix. Samples of 10 mL were prepared by mixing 2.5 mL of CH and 7.5 mL of HPMC, for the preparation of three-BioPEMs. To provide a more suitable ionic conductivity, the compounds used for doping the matrixes were glycerol (gly) (Himedia, 99.5 %), urea (U5378, Sigma

Aldrich, Germany) and the ionic liquids [C₂C₁C₁im] [NTf₂] (IL1) and [[N111(2OH)]Cl] (IL2) were supplied from the University of Aveiro, Portugal.

Then 0.2 g of glycerol was added as plasticizer, and 0.2 g of the IL1, IL2 were added to each solution in order to get different doped polymer electrolytes. The resulting solutions were stirred for 2h at room temperature. After this time the solutions were cast into 5.5 mm diameter Petri dishes (BP50-01, Gosselin, Hazebrouck, FR) and left to dry in an incubator (Thermo Fisher Scientific, Massachusetts, USA) for 96 h at 25°C, except for the one with urea that required a 7-day period of drying.

The synthesized BioPEMs must meet certain requirements as good chemical and mechanical stability, high ionic conductivity ($1 \times 10^{-5} \text{ S cm}^{-1}$, defined as the minimum threshold), present low crossover of redox species and favor having high power output in the device. There were obtained three chitosan-based BioPEMs: CH:HPMC+gly, CH:HPMC+IL1 and CH:HPMC+IL2. However, at the time of the addition of IL1 to the chitosan-acetic acid solution, the mixture went from transparent to opaque, this can be explained due to the insolubility of chitosan in alkaline media as a result of the basic pH of the ionic liquid IL1. The rest of the CH:HPMC BioPEMs resulted as mechanically robust, flexible, transparent, and completely amorphous films as is shown in Figure 5.1, favorable to the aims pursued.

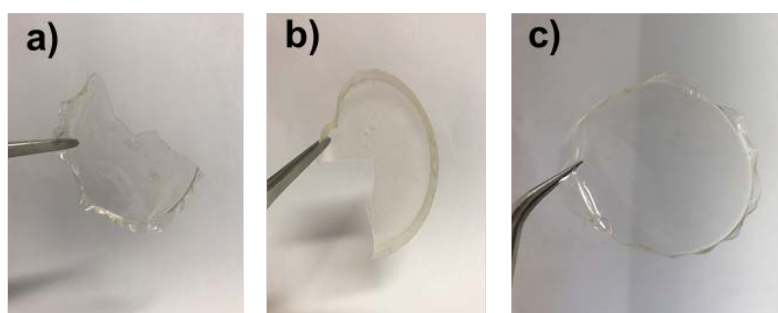


Figure 5.1. Physical appearance of the chitosan BioPEM: a) CH:HPMC+gly; b) CH:HPMC+IL1; c) CH:HPMC+IL2.

5.2.2. Starch-based electrolytes

In order to obtaining polymeric membranes from another natural source, starch-based BioPEMs were prepared, starch (cationic, Brazil) was used as received. Two main starch matrixes were synthesized and were doped with different compounds to increase their ionic conductivity. On the one hand, glycerol was used as plasticizer and the samples were doped with IL1 and IL2 and a third one was prepared only with the addition of glycerol. On the other hand, a second starch-based BioPEM was prepared with the addition of urea (U5378, Sigma Aldrich, Germany) as a plasticizer and was doped with IL2.

The samples were prepared by dispersion of 1.2 g of starch in 30 mL of ultra-pure water (Mili-Q) and stirred for 2h at 70-80 °C, until a homogeneous and viscous solution was formed. An extra water sample was located in the stirring plate as a



temperature control. The solution was brought to room temperature. After this, 0.6 g of glycerol were added the starch-gly BioPEMs and doped with 0.4 g of IL1 and IL2. In the other side, for urea samples, 0.6 g of urea as matrix was added and was doped with 0.4 g of IL2. The resulting solutions were cast into Teflon dishes and dried for 72 h at 25 °C. After this time, it was observed that samples needed more drying time, therefore sample A doped with IL1 was put it overnight at 40 °C to get a dried film. However, starch-BioPEM with urea and IL2 were left for 7 days at 25 °C and were not able to get a working film.

The starch based BioPMEs obtained were: Starch+gly, Starch+IL1, Starch+IL2 and Starch+urea. The starch films were not as easily handled as the chitosan-based BioPEMs, presenting a higher viscous consistency at room temperature. The films doped with urea and IL2 could not be removed from the Teflon molds, preserving a rubbery appearance attached to the mold, impossible to perform the coming tests of ionic conductivity. In Figure 5.2 is observed the appearance of the starch films doped with glycerol and IL1 once they were removed from the mold.

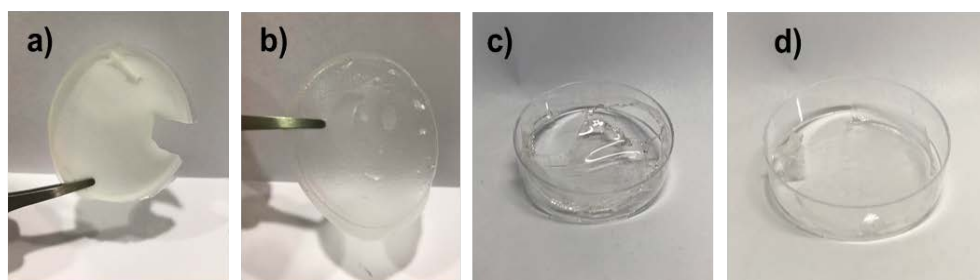


Figure 5.2. Physical appearance of the starch BioPEMs. a) Starch+IL1; b) Starch+gly; c) Starch+IL2; d) Starch+urea.

The measurement of the thickness of the BioPEMs was performed using a digital micrometer (Mitutoyo 293 series, MDC-25P, Kanagawa, JP) obtaining values ranged between 65–244 and 154–348 μm , for the CH:HPMC hydrogels and starch-based films, respectively.

Due to the physical limitations that certain BioPEMs presented in this step, the ionic conductivity evaluation was carried out to three chitosan-based BioPEMs (CH:HPMC+gly, CH:HPMC+IL1 and CH:HPMC+IL2) and two starch-based membranes (starch+IL1 and Starch+gly).

5.3. BIOPEMS IONIC CONDUCTIVITY CHARACTERIZATION

In order to assess the functionality of the BioPEMs as proton conducting electrolyte, Electrochemical Impedance Spectroscopy (EIS) technique was used to evaluate the samples. The total ionic conductivity of the polymer electrolytes was determined by introducing the membranes between two ion-blocking gold electrodes (10 mm diameter) (Goodfellow, > 99.95%) as is shown in Figure 5.3. The symmetrical cell obtained of electrode/ polymer electrolyte/ electrode was secured in a suitable constant volume support and installed in a Buchi TO51 tube oven with a type K

thermocouple localized close to electrolyte disk to measure the sample temperature. An Autolab PGSTAT-12 potentiostat (Eco Chemie) was used to obtain bulk ionic conductivities during heating cycles between room temperature ($\sim 21^\circ\text{C}$) to 50°C at approximately 7°C intervals and over the frequency range of 65 kHz to 500 mHz. The ionic conductivity (σ) determined according to equation:

$$\sigma = \frac{d}{R_b A} \quad (1)$$

where σ_1 is the ionic conductivity, d is the thickness, A is the electrode contact area, and R_b is the bulk resistance of the sample. R_b was obtained from the intercept of the imaginary part of the impedance (minimum value of Z'') with the slanted line in the real part of the impedance (Z'). The plot of Z'' vs Z' , the Nyquist plot, is described by three distinct parts: a semicircle at higher frequencies, a straight line at lower frequencies, and the transition between these two.

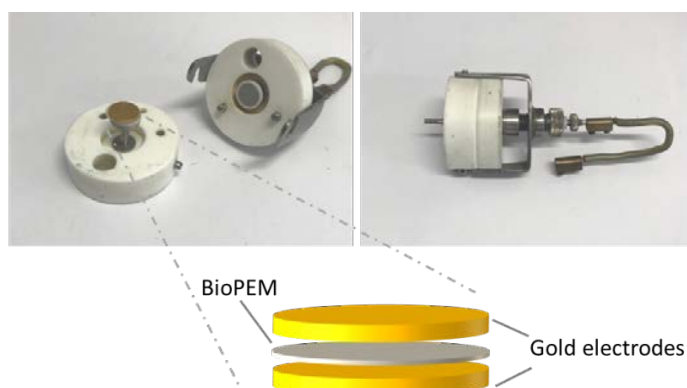


Figure 5.3. Symmetrical cell of gold-electrode/ polymer electrolyte / gold-electrode for impedance spectroscopy evaluation.

The measurement values of ionic conductivity as a function of temperature are shown in Figure 5.4.

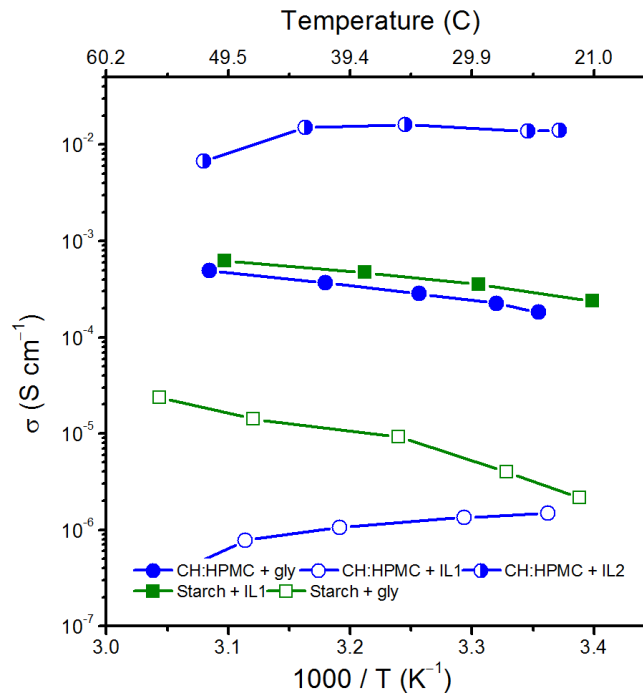


Figure 5.4. Variation of the ionic conductivity of the chitosan and starch BioPEMs with the inverse of temperature.

The conductivity study of the BioPEMs with glycerol shows that the addition of glycerol results in an increase in conductivity. Other researchers have studied the influence of glycerol in some other electrolytes containing LiBF [23]. They concluded that the increase of plasticizer promoted greater mobility of ions due to better solvation of the lithium ion. On the other hand, as the electrolyte is more malleable, it promotes a decrease in intra- and intermolecular interactions in the plasticizer and chitosan induced by hydrogen bonding of OH⁻ groups of glycerol with the chains of monosaccharides presented in chitosan and starch. As expected, the incorporation of more glycerol into the matrix rises the ionic conductivity over the temperature range evaluated [24]. The temperature dependence of the ionic conductivity was well described by the Vogel–Tamman–Fulcher (VTF) equation in the temperature range from 25°C to 100°C, exhibiting proportionality between temperature and conductivity.

From the measured membranes the highest ionic conductivity of $1.4 \times 10^{-2} \text{ S cm}^{-1}$ was obtained for the CH:HPMC+IL2 BioPEM at room temperature resulting in the highest ionic conductivity, value in the same order of magnitude of the values reported for Nafion[®] membranes[11] ($10^{-2} \text{ S cm}^{-1}$) and same range value reported for gellan-based polymer electrolytes as promising candidates to be used as electrolytes in Li conducting electrochemical devices[25]. The membranes that followed with high ionic conductivity values were the Starch+IL1 ($6.2 \times 10^{-4} \text{ S cm}^{-1}$) and CH:HPMC+gly ($4.9 \times 10^{-4} \text{ S cm}^{-1}$) BioPEMs. Even though the Starch+IL1 BioPEM exhibited one of the highest ionic conductivity values, the film is not very promising as a BioPEM because of its mechanical characteristics showing a brittle structure resulting in a material that doesn't meet the expected regarding to the mechanical properties of flexibility. It can

be seen that the levels of ionic conductivity evaluated for the starch+gly and starch+IL1 BioPEMs were to be below 10^{-4} S cm^{-1} , which are inadequate as electrolyte membrane applications.[26]

Based on the EIS results, the CH:HPMC+gly and CH:HPMC+IL2 BioPEMs as they presented the highest ionic conductivity values and exhibited physical characteristics render them adequate for this work purpose were selected for the following tests. In the following sections, the viability of these materials as electrolytic membranes is investigated in primary redox batteries.

Because the conductivities presented for these materials confirmed the correct operation of the proton conductive polymeric electrolytes similar to the lithium doped polymer electrolytes at room temperature [27],[17],[28]; it is interesting to investigate used in PEM-cell systems as polymer exchange membranes. This capability was carried out in the following sections of this work.

5.4. PERFORMANCE OF THE BIOPEMS IN REDOX BATTERIES

Once the BioPEMs were synthesized, the next step was to evaluate and validate the crossover of the redox species across the membranes and the performance of a BioPEM-battery. The redox compounds involved during this work consisted of hydroquinonesulfonic acid potassium salt (H_2BQ , H18402), p-benzoquinone (p-BQ, B10358), oxalic acid dihydrate ($\text{C}_2\text{H}_2\text{O}_4$, O0376), potassium hydroxide (KOH, P1767), ascorbic acid (AA, A92902) (all from Sigma Aldrich, St Louis, Missouri, USA), and iron nitrate (Fe^{3+} , 103883) acquired to Merck KGaA (Darmstadt, Germany). For the experiments redox electrolytes solution reagents, were prepared at concentrations of 0.1 M H_2BQ and 0.1 M AA in 1.0 M KOH and 0.1 M pBQ and 0.5M Fe^{3+} in 0.5 M $\text{C}_2\text{H}_2\text{O}_4$.

5.4.1. Experimental setup design

For this purpose, a two half cells setup that allowed the incorporation of the BioPEM was fabricated using Poly(methyl methacrylate) (Plexiglas, Evonik Performance Materials GmbH, Darmstadt, Germany) layers assembled using pressure sensitive adhesives (PSA) (Adhesives Research, Glen Rock, PA, USA). The device components were designed in a CAD program (CorelDRAW, Corel, Ottawa, ON, Canada). All the components were cut using a CO_2 laser cutter (Mini 24, Epilog Laser, Golden, CO, USA) and manually assembled layer by layer using screws that allow the pieces to be firmly joined. For this purpose, homemade screen-printed electrodes (SPEs) were fabricated as described by Del Torno et al.[29] using carbon inks (Gwent ink C1090D14, Gwent Electronic Materials, Gwent, U.K.) for the working and counter electrode and silver silver chloride (Ag/AgCl) ink for the reference electrode.

The strategy to evaluate the crossover of species across the BioPEMs materials and its performance in a BioPEM-cell was the fabrication of a double half-cell setup made of PMMA and PSA materials. Briefly, a half-cell for the anode was fabricated with PMMA and PSA pieces, one of these pieces had a space for the incorporation of the



SPE, in the same way a second half-cell was fabricated for the cathode electrode. In the middle of both half-cells a cavity to fit the BioPEM was defined. Figure 5.5 shows the design and assembly of the setup.

The transparency of the PMMA setup allows the direct observation of the anolyte and catholyte separated by the membrane into the cell. In-house fabricated screen printed electrodes were used to measure the redox species concentrations in the half-cells by the current output generated. The SPE consisted of Ag/AgCl ink as the reference electrode (R) and a carbon ink for the counter (C) and working electrode (W) with 0.07 cm² of area. A semi-automatic screen-printing machine was used for the fabrication of screen-printed electrodes. Initially a layer of silver ink was screen-printed on the PEM substrate, and then the carbon ink was screen-printed over the silver ink to expose the area of 0.70 cm² (working electrode). After screen-printing, the electrodes were dried at 80°C for 2 h in an oven.

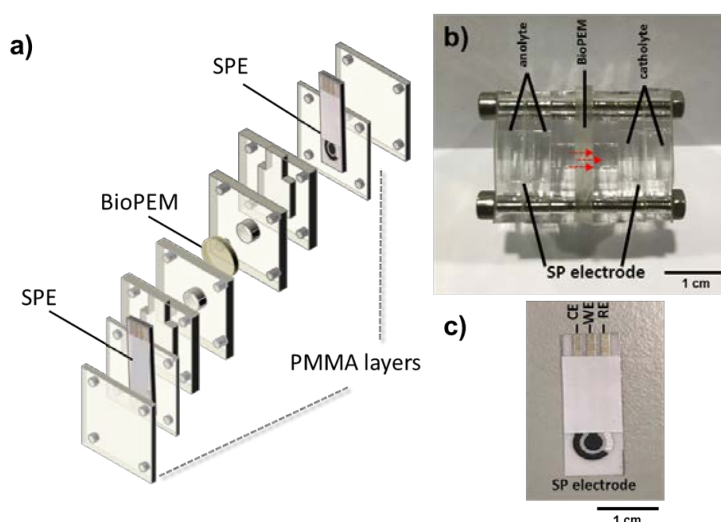


Figure 5.5. Exploded view of components of the cell setup. b) Picture of assembled cell. c) screen printed carbon electrode.

5.4.2. Characterization of redox species crossover

The crossover of the species across the two selected BioPEMs was evaluated towards the four redox compounds: H₂BQ, p-BQ, AA and Fe³⁺. Permeability was calculated by carrying out linear sweep voltammeteries (LSV) in potentiodynamic mode at a scanning speed of 10 mV s⁻¹, placing in one chamber the redox specie and its electrolyte and in the other half-cell only the correspondent electrolyte was placed. The LSV were measured in each chamber over time. Based on the voltammeteries, the maximum current generated in each BioPEM FC was calculated. Then, the cells were fixed with each of the redox species in one half-cell and in the other half-cell was placed its corresponding electrolyte, in this way, the voltamograms of each half-cell was made, fixing the battery maximum current as a cut point, the percentage of current present in each half-cell of the electrolyte was calculated, corresponding to the migrated redox compound.

In order to calculate the percentage (%) of the redox species that was consumed and migrated to the other half- cell in the period of time, the polarization curves of the redox species were measured for a 3-4 h period and based on their current output variation over time. Figure 5.6 shows the polarization curves of the redox species for BioPEM-batteries. The chart *a* and *b* correspond to the oxidation currents of the anolytes (H_2BQ and AA), while *c* and *d* show the evolution of the reduction currents of the catholytes (p-BQ and Fe^{3+}) over time.

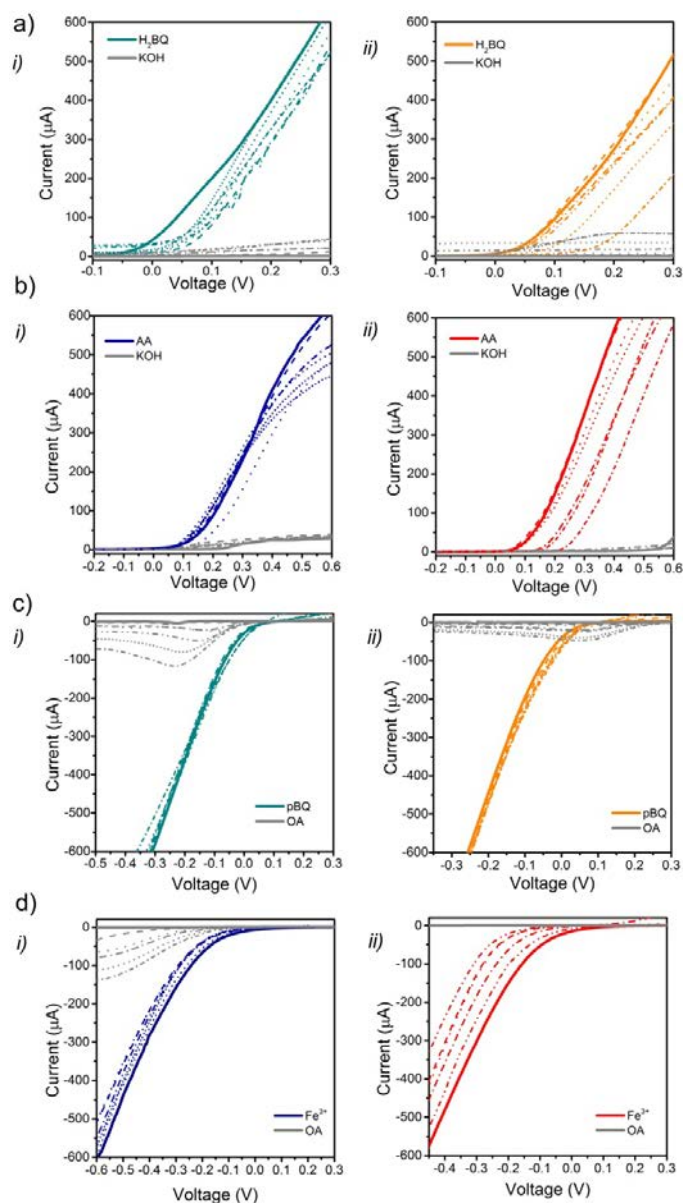


Figure 5.6. Polarization curves over time of the half-cell molecules involved in the redox reactions (time=0 solid line; dash line every 30 min). a) H_2BQ ; (i) CH:HPMC+gly BioPEM (ii) CH:HPMC+IL2 BioPEM. b) AA; (i) CH:HPMC+gly BioPEM cell, (ii) CH:HPMC+IL2 BioPEM. c) p-BQ; (i) CH:HPMC+gly BioPEM, (ii) CH:HPMC+IL2 BioPEM d) Fe^{3+} ; (i) CH:HPMC+gly BioPEM cell, (ii) CH:HPMC+IL2 BioPEM.



Firstly, it can be observed that in the case of the anolytes, H₂BQ and AA, lower levels of migration across the membrane based on CH:HPMC+gly in a 4-hour period of evaluation were presented. However, for the redox specie pBQ, the crossovers in both membranes were similar, showing a very low level of migration. While for the Fe³⁺ the trend was similar to that one detected for the anolytes, with less crossover across the CH:HPMC+gly BioPEM in comparison with the CH:HPMC+IL2 BioPEM.

During the evaluation of the crossover of the redox compounds across the BioPEMs, little migration was found by the p-BQ, a molecule that presents a neutral charge, while the ionically charged molecules such as the H₂BQ, Fe³⁺ and AA species presented higher crossover through the membranes. A summary of the crossover across the BioPEMs is presented in Figure 5.7. Evaluated BioPEMs are proton exchange membranes and present ion selectivity since they are not very permeable to non-polar molecules. The CH:HPMC+IL2 BioPEM is presented as the polymer electrolyte membrane with higher crossover; possibly because the chlorides present in its structure are responsible for the transport of protons through its matrix. It was observed that for both tested membranes is possible to hold more than 50% of the species in the reservoir for at least the first 3-hour period of evaluation.

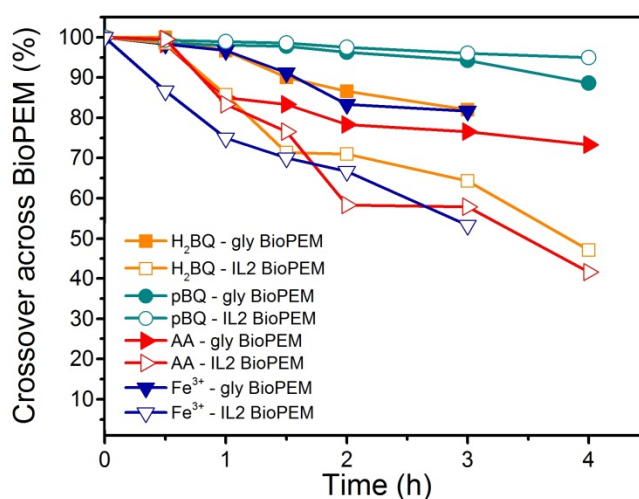


Figure 5.7. Crossover across the gly and IL2-BioPEMs for the evaluated redox species: H₂BQ, AA, p-BQ, Fe³⁺.

5.5. BIOPEM-BATTERY CHARACTERIZATION

In order to test the synthesized electrolyte membranes in the battery cell system, polarization curves were performed in complete cells with the incorporation of the membranes: CH:HPMC+gly and CH:HPM+IL2 BioPEMs in the PMMA setup. The potential was swept from open circuit potential to zero volts at a scan rate of 10 mV s⁻¹ (chronopotentiometric curves were measured using an external load selected). All electrochemical characterization curves were recorded with a potentiostat Dropsens μ Stat 400 (Dropsens, Oviedo, Spain).

Measurements were performed every 20 min for a 2-hour period utilizing SPE, using all-quinone and AA/Fe³⁺ chemistry redox couple. The open circuit voltage of the cell was measured once the liquid species were added to both half cells and a steady value of 0.75 ± 0.05 V and 0.90 ± 0.05 V in all-quinone and AA/Fe³⁺, respectively, were achieved. Figure 5.8 shows the I-V curves obtained at a scan rate of 10 mV s^{-1} . The figure shows that the two redox couples have been benefited in terms of current and power outputs using the Gly-BioPEM. On one hand, the battery of quinones with gly-BioPEM presents a power output of 2.4 mWcm^{-2} and a stability of 87% in its performance over time. The battery with the same gly-BioPEM using the chemistry of AA/Fe³⁺, presented a performance stability of 91% and the highest power output of 2.5 mWcm^{-2} . On the other hand, the batteries with the two redox couples using IL2-BioPEMs generated current and power values below the system using gly-BioPEM. However, the performance stability for the AA/Fe³⁺ with IL2-BioPEM battery was 95% during the 2-hour period, while the quinone chemistry with the IL2-BioPEM was the least stable, with 74% stability over time. The calculations of the internal resistance of the cells agree in the same range of ionic conductivity measured by EIS for the BioPEM.

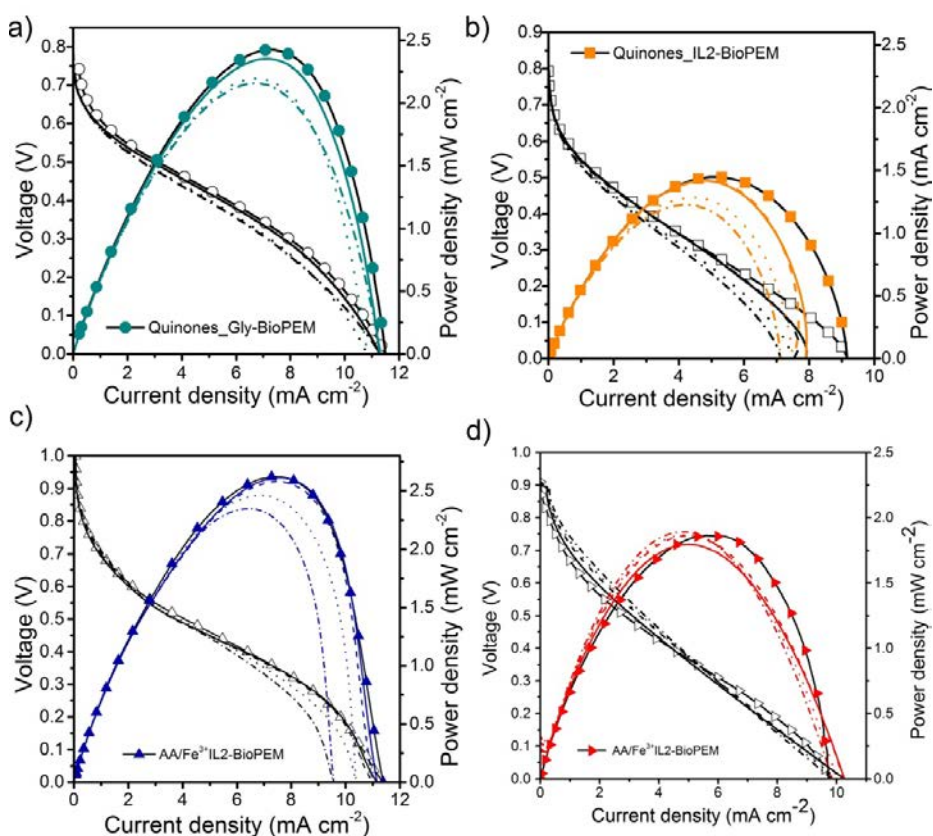


Figure 5.8 . Discharge polarization curves of redox flow battery with: a) CH:HPMC+gly BioPEM, b) CH:HPMC+IL2 BioPEM, supplied with species of 0.1 M H2BQ in 1 M KOH and 0.1 M pBQ in 0.5 M C2H2O4 at the negative and positive electrodes, respectively, at room temperature. (time=0 solid line; dash line every 30 min).



5.6. CONCLUSIONS

This work presents the developed of polymeric electrolytic membranes and its successful incorporation in primary passive redox batteries.

It was observed that CH:HPMC+IL2 membrane had the highest conductivity in the impedance tests. Since the addition of salts and plasticizers as the glycerol can achieve the amorphization of the chitosan matrix and increased its conductivity[16], both BioPEMs (CH:HPMC+gly and CH:HPM+IL2) resulting in materials with good ionic conductivity and presented low crossover of the redox species evaluated, being the glycerol membrane the one allowing less migration of species. Despite the high ionic conductivity shown by the membrane with ionic liquid, it is clear that regarding to the incorporation of the membranes in the cell, the membrane doped with glycerol provided the best performance of the BioPEM redox battery presenting less species lost through its matrix. Therefore, the membrane with glycerol is shown as the best option of the BioPEMs evaluated for this type of device.

The successful incorporation of biopolymer membranes into a primary passive redox battery systems was achieved, after being individually characterized in terms of ionic conductivity, redox compounds crossover and electrochemical performance suitable for all applications.

These membranes based on natural polymers are a promising alternative to replace Nafion membranes in sustainable electrochemical systems. These materials seek to have a harmony with the environment and provide sustainable biodegradable devices[22] without a negative impact.

These new bio-polymer membranes set the guidelines for the development of the power sources devices based on biopolymers that are presented in chapter 6 of this thesis.

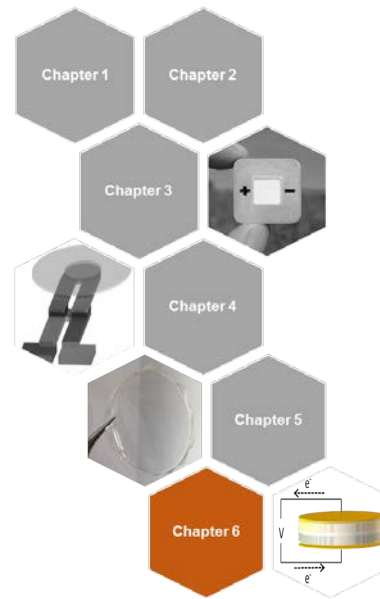
References in Chapter 5.

- [1] Y. Yang, E. Noviana, M.P. Nguyen, B.J. Geiss, D.S. Dandy, C.S. Henry, Paper-Based Microfluidic Devices: Emerging Themes and Applications, (n.d.). doi:10.1021/acs.analchem.6b04581.
- [2] J.A. Adkins, E. Noviana, C.S. Henry, Development of a Quasi-Steady Flow Electrochemical Paper-Based Analytical Device, *Am. Chem. Soc.* 88 (2016) 10639–10647. doi:10.1021/acs.analchem.6b03010.
- [3] M. Winter, R.J. Brodd, What Are Batteries, Fuel Cells, and Supercapacitors?, *Chem. Rev.* 104 (2004) 4245–4269. doi:10.1021/CR020730K.
- [4] J. Walkowiak-Kulikowska, J. Wolska, H. Koroniak, Polymers application in proton exchange membranes for fuel cells (PEMFCs), *Phys. Sci. Rev.* 2 (2017). doi:10.1515/psr-2017-0018.
- [5] A. Kirubakaran, S. Jain, R.K. Nema, A review on fuel cell technologies and power electronic interface, *Renew. Sustain. Energy Rev.* 13 (2009) 2430–2440. doi:10.1016/J.RSER.2009.04.004.
- [6] S. Cheng, H. Liu, B.E. Logan, Power Densities Using Different Cathode Catalysts (Pt and CoTMPP) and Polymer Binders (Nafion and PTFE) in Single Chamber Microbial Fuel Cells, *Environ. Sci. Technol.* 40 (2006) 364–369. doi:10.1021/es0512071.
- [7] M.A.R. Sadiq Al-Baghdadi, Prediction of deformation and hygro-thermal stresses distribution in PEM fuel cell vehicle using three- dimensional CFD model, 3 (2012) 485–504. https://www.ijee.ieefoundation.org/vol3/issue4/IJEE_01_v3n4.pdf (accessed March 26, 2018).
- [8] N. Cele, S. Sinha Ray, Recent Progress on Nafion-Based Nanocomposite Membranes for Fuel Cell Applications, (n.d.). doi:10.1002/mame.200900143.
- [9] E. Raphael, C.O. Avellaneda, B. Manzolli, A. Pawlicka, Agar-based films for application as polymer electrolytes, *Electrochim. Acta.* 55 (2010) 1455–1459. doi:10.1016/j.electacta.2009.06.010.
- [10] E. Lima, E. Raphael, F. Sentanin, L.C. Rodrigues, R.A.S. Ferreira, L.D. Carlos, M.M. Silva, A. Pawlicka, Photoluminescent polymer electrolyte based on agar and containing europium picrate for electrochemical devices, *Mater. Sci. Eng. B.* 177 (2012) 488–493. doi:10.1016/j.mseb.2012.02.004.
- [11] G. Ribeiro, M. Conde, J. Carvalho, L.C. Rodrigues, R. Alves, R.A.S. Ferreira, A. Pawlicka, L.D. Carlos, M.M. Silva, Natural membranes for application in biomedical devices, *Mol. Cryst. Liq. Cryst.* 562 (2012) 147–155. doi:10.1080/15421406.2012.679172.
- [12] A. Pawlicka, R.I. Mattos, J.F. Lima, C.E. Tambelli, C.J. Magon, J.P. Donoso, Magnetic resonance and conductivity study of a gelatin-based polymer gel electrolyte, *Electrochim. Acta.* 57 (2011) 187–191. <http://www.producao.usp.br/handle/BDPI/49805> (accessed March 26, 2018).
- [13] B. Chatterjee, N. Kulshrestha, P.N. Gupta, Nano composite solid polymer electrolytes based on biodegradable polymers starch and poly vinyl alcohol, *Measurement.* 82 (2016) 490–499. doi:10.1016/J.MEASUREMENT.2016.01.022.
- [14] L.V.S. Lopes, G.O. Machado, A. Pawlicka, J.P. Donoso, Nuclear magnetic resonance and conductivity study of hydroxyethylcellulose based polymer gel electrolytes, *Electrochim. Acta.* 50 (2005) 3978–3984. doi:10.1016/j.electacta.2005.02.056.
- [15] S.C. Barros, A.A. da Silva, D.B. Costa, C.M. Costa, S. Lanceros-Méndez, M.N.T. Maciavello, J.L.G. Ribelles, F. Sentanin, A. Pawlicka, M.M. Silva, Thermal–mechanical behaviour of chitosan–cellulose derivative



- thermoreversible hydrogel films, *Cellulose*. 22 (2015) 1911–1929. doi:10.1007/s10570-015-0603-5.
- [16] P. Mukoma, B.R. Jooste, H.C.M. Vosloo, Synthesis and characterization of cross-linked chitosan membranes for application as alternative proton exchange membrane materials in fuel cells, *J. Power Sources*. 136 (2004) 16–23. doi:10.1016/j.jpowsour.2004.05.027.
- [17] R. Alves, A.S.S. de Camargo, A. Pawlicka, M.M. Silva, Luminescent polymer electrolytes based on chitosan and containing europium triflate, *J. Rare Earths*. 34 (2016) 661–666. doi:10.1016/S1002-0721(16)60076-5.
- [18] J. Ma, Y. Sahai, Chitosan biopolymer for fuel cell applications, *Carbohydr. Polym.* 92 (2013) 955–975. doi:10.1016/j.carbpol.2012.10.015.
- [19] N. Li, R. Bai, Novel chitosan-cellulose hydrogel adsorbents for lead adsorption, (n.d.).
<https://pdfs.semanticscholar.org/7dec/de1d7419c475bfd878264f68b1ad46302f85.pdf> (accessed November 28, 2017).
- [20] A. Pawlicka, J.P. Donoso, Polymer electrolytes based on natural polymers, in: *Polym. Electrolytes*, Elsevier, 2010: pp. 95–128. doi:10.1533/9781845699772.1.95.
- [21] S.C. Barros, A.A. da Silva, D.B. Costa, I. Cesarino, C.M. Costa, S. Lanceros-Méndez, A. Pawlicka, M.M. Silva, Thermo-sensitive chitosan-cellulose derivative hydrogels: swelling behaviour and morphologic studies, *Cellulose*. 21 (2014) 4531–4544. doi:10.1007/s10570-014-0442-9.
- [22] J.P. Esquivel, P. Alday, O.A. Ibrahim, B. Fernández, E. Kjeang, N. Sabaté, A Metal-Free and Biologically Degradable Battery for Portable Single-Use Applications, *Adv. Energy Mater.* (2017) 1700275. doi:10.1002/aenm.201700275.
- [23] M. Naya, J. Nakanishi, Risk assessment of formaldehyde for the general population in Japan, *Regul. Toxicol. Pharmacol.* 43 (2005) 232–248. doi:10.1016/j.yrtph.2005.08.002.
- [24] R. Alves, M.M. Silva, The Influence of Glycerol and Formaldehyde in Gelatin-Based Polymer Electrolytes, *Mol. Cryst. Liq. Cryst.* 591 (2014) 64–73. doi:10.1080/15421406.2013.822739.
- [25] I.S.M. Noor, S.R. Majid, A.K. Arof, D. Djurado, S.C. Neto, A. Pawlicka, Characteristics of gellan gum–LiCF₃SO₃ polymer electrolytes, *Solid State Ionics*. 225 (2012) 649–653. doi:10.1016/j.ssi.2012.03.019.
- [26] T.D.O. Gadim, A.G.P.R. Figueiredo, N.C. Rosero-Navarro, C. Vilela, J.F. Gamelas, A. Barros-Timmons, C.P. Neto, A.J.D. Silvestre, C.S.R. Freire, F.M.L. Figueiredo, Nanostructured Bacterial Cellulose–Poly(4-styrene sulfonic acid) Composite Membranes with High Storage Modulus and Protonic Conductivity, (n.d.). doi:10.1021/am501191t.
- [27] N.A. Aziz, S.R. Majid, A.K. Arof, Synthesis and characterizations of phthaloyl chitosan-based polymer electrolytes, *J. Non. Cryst. Solids*. 358 (2012) 1581–1590. doi:10.1016/J.JNONCRY SOL.2012.04.019.
- [28] S. Tang, A. Babai, A.-V. Mudring, Europium-Based Ionic Liquids as Luminescent Soft Materials, *Angew. Chemie Int. Ed.* 47 (2008) 7631–7634. doi:10.1002/anie.200801159.
- [29] L. del T. Román, M. Navarro, G. Hughes, J.P. Esquivel, R.D. Milton, S.D. Minter, N. Sabaté, Improved performance of a paper-based glucose fuel cell by capillary induced flow, *Electrochim. Acta.* (2018). doi:10.1016/j.electacta.2018.05.074.

6.



Biodegradable button cell battery based on redox biopolymers

Overview

The existence of electrochemically active polymers is well known. These natural materials can be classified into two main classes: electron-conducting polymers and proton-conducting polymers. In turn, within the first class, two main categories can be distinguished based on the mode of electron transport: the redox polymers and the electronically conductive polymers.

In this chapter, the manufacture of a passive primary battery will be presented. Such battery is based on natural redox polymers, bio-polymeric membranes, carbon electrodes, organic materials and an iron salt, together with water-based electrolytes, which has proved to be a safe, inexpensive and sustainable alternative. In this study, two conducting redox polymers based on ascorbic acid and iron nitrate have been synthesized and characterized.

This battery is presented as a promising source of power in the search for sustainable alternatives of devices for feeding single-use devices.

6.1. INTRODUCTION

The constant demand of power sources for the power supply of portable electrical devices is increasing at an alarming speed. Much of this demand is being met by lithium-ion batteries, which have high energy storage. However, lithium has disadvantages such as limited material resources, high energy consumption during production, high cost and requires flammable electrolytes. Therefore, the need to develop high performance batteries which are based on low cost abundant and renewable elements is mandatory.

Batteries are closed systems, with the anode and cathode being the charge-transfer medium and taking an active role in the redox reaction as “active masses”. The positive electrode is an electron acceptor such as lithium cobalt oxide, manganese dioxide, or lead oxide. The negative electrode is a good reducing agent (electron donor) such as lithium, zinc, or lead[1]. Currently, batteries represent a large volume of toxic and hazardous materials in common use, and these materials must be managed throughout their life cycle to avoid harm to the environment and human health[2]. The development of new battery prototypes, based on naturally found materials, is the starting point for the realization of this research work.

Many organic battery constituents have also been studied, including conducting redox polymer (CRP) [3–5]. A CRP consists of a conducting polymer backbone, a redox active pendant group which can store charge, and a linker connecting the pendant group to the backbone (Figure 6.2). Redox hydrogels conduct electrons by self-exchange of electrons or holes between rapidly reduced and rapidly oxidized redox functions tethered to backbones of cross-linked polymer networks. The redox polymers conduct electrons, through self-exchange in the water-swollen hydrogels[6].

The development of redox polymers has undoubtedly been an application-oriented field. Historically, the most important applications have been (and still are) batteries and (bio)sensors[7]. The electron-conducting redox hydrogels serve to electrically connect the redox centers of enzymes to electrodes. This is the case in glucose concentration monitoring electrodes implanted in diabetic people[8].

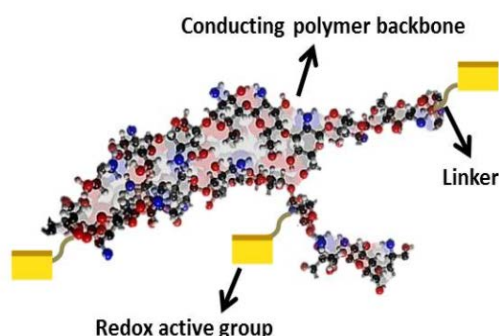


Figure 6.2. Schematic representation of the conducting redox polymer (CRP).



Previous studies have used polypyrrole (PPy) as the polymer backbone and a quinone pendant group as the redox active group. They observed that the conductivity of the polymer was affected by the redox activity of the quinones [9]. In the present study, the use of quinones was unlikely due to the reaction of hydroquinone with chitosan and hydroxypropylmethyl cellulose used as backbone.

The electrochemical properties of the redox polymers will be directly related to the properties of the redox system incorporated into the polymer. Polymers can incorporate redox active groups such as ferrocene/ferrocenium into the polymer backbone [7]. With regard to the reduced compounds to be proposed for batteries, a unique class of carbonyl compounds [10] that has been extensively studied in the field of organic matter based polymer electrolytes is constituted by the ascorbic acid. The ascorbic acid, or vitamin C, is a natural occurring compound which consists of two enol hydroxyl groups, as well as a primary and secondary alcohol group. The enediol structure motivates its antioxidant qualities, since enediols can easily be oxidized. The ascorbic acid forms two bonds of intramolecular hydrogen bonds (shown in red in the Figure 6.1) that contribute decisively to the stability, thus enhancing the chemical qualities of the enediol structure.

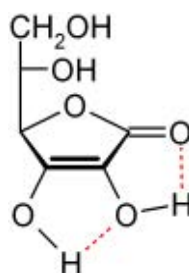


Figure 6.1. Structures of ascorbic acid with enediol group in red.

We have studied the electrochemical performance of the ascorbic acid in the previous chapters, proving that it presents a very good stability and high negative redox potential. However, ascorbic acid shows low electronic conductivity and is easily dissolved in water electrolytes. To increase the conductivity, ascorbic acid can be connected to a conducting polymer forming a conducting redox polymer. Hence the challenge followed was developing a polymer backbone of chitosan and cellulose by coupling it with a redox couple that we had found to work perfectly, presently ascorbic acid as an anode and iron nitrate as a cathode.

In this way the obtaining of redox-hydrogels would be coupled to porous paper electrodes and as a proof of concept, it was given a button cell battery form, a commonly used battery to power portable devices. In this chapter, the framework for obtaining this power source is presented.

The synthesis of the redox polymers, their electrochemical characterization, the manufacture of the device, the battery performance and the cells connection in series to increase de cell voltage are presented in this chapter.

6.2 PREPARATION OF HYDROGELS

The implementation of natural polymers that serve as a matrix for the synthesis of redox hydrogels is presented below. These backbones have been synthesized from three biopolymers for the subsequent incorporation of chemical compounds that provide redox activity to the hydrogel backbones, because the redox hydrogels envelope the redox compounds, they electrically connect the reactant reaction centers to electrodes.

6.2.1. Synthesis of the hydrogel backbones

For the synthesis of the hydrogel backbone, the natural polymers used were: chitosan (CH), which has a molecular weight of 75-85% (deacetylated, 448877) and hydroxypropyl methyl cellulose (HPMC, 09963) used as received without further purification. Acetic acid (33209, 99.8% C) was used for the chitosan dissolution, since this polymer requires acidic conditions for suspension; These three compounds were acquired from Sigma-Aldrich Company, Ltd (St. Louis, MO, US). On the other hand, to dissolve the HPMC and the rest of the compounds, high-purity distilled water was used in all experiments. Glycerol (Himedia, 99.5%) was used as a convenient crosslinker because of its solubility in water and an enhancer of ionic conductivity in the biopolymer backbone.

The synthesis of the Chitosan:Hydroxypropylmethyl cellulose (CH:HPMC) bio-polymer backbone was prepared in the same way as the BioPEM (bio-polymeric membranes) synthesized in the previous chapter. To explain it briefly, 1 g of CH and HPMC were dissolved in 50 mL aqueous acetic acid (1 wt. %) and 50 mL ultra- pure water, respectively, to prepare 2 wt. %. These polymeric mixtures were stirred overnight at room temperature until a homogeneous and viscous solution was formed. The CH and HPMC solutions were mixed together in 25:75(w:w) ratios for the polymer electrolytic membrane proportion. The pH of the solutions was adjusted to 4. Then 2% of glycerol was added as plasticizer and stirred for 2 h at room temperature.

6.2.2. Synthesis of the redox hydrogels

Since the objective of this work was obtaining hydrogels with redox activity, the integration of redox species into the hydrogels backbone was carried out. For this, the chemicals involved during this work consisted of the redox couple of ascorbic acid (AA, A92902, Sigma Aldrich, USA), and iron nitrate (Fe^{3+} , 103883) acquired from Merck KGaA (Darmstadt, Germany) as anolyte and catholyte, respectively.

As electrolyte compounds oxalic acid dihydrate ($\text{C}_2\text{H}_2\text{O}_4$, 00376), potassium hydroxide (KOH, P1767), ammonium chloride (NH_4Cl , 254134) and sodium chloride (NaCl, 450006) were implemented, all of these compounds were acquired from Sigma Aldrich, USA.

The formulation of the redox-hydrogels was carried out by preparing concentrations of 0.1 M AA and 0.2 M Fe^{3+} with 0.2% KOH. Ascorbic acid (0.88 g, 0.1M) was stirred in a



round-bottom flask and dissolved and diffused in 50 mL of CH:HPMC (25:75 + gly) mixture as a negative redox polymer. The same treatment was given to the catholyte redox polymer. Iron nitrate (4.04 g, 0.2 M) was added to 50 mL of the polymer backbone. Both mixtures were stirred at room temperature for 1 h. The synthesis of the redox hydrogels was carried out by solvent casting (SC), where 50 mL of the redox sample of AA and Fe^{3+} hydrogel was placed in Petri dishes (diameter: 11 cm) and incubated at 25 ° C for 48 h. This thermal procedure was used to minimize the effects of a fast solvent evaporation.

The redox couples were bound to the cross-linked polymer network through covalent or coordinative bonds. The aspect of the redox hydrogels is shown in Figure 6.3. Because the hydrogels are permeable to water-soluble chemicals as the ones used during this work, particularly ascorbic acid, can be electrooxidized or electroreduced in their three-dimensional matrices [11].

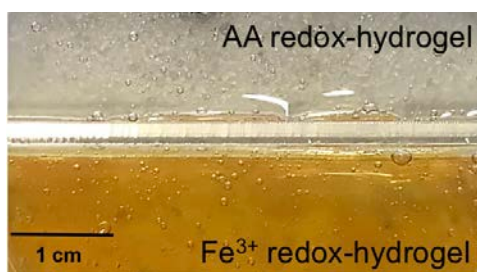


Figure 6.3. Top view of a petri dish with ascorbic acid (AA) and iron nitrate (Fe^{3+}) hydrogels aspect.

Due to the high ionic conductivity and low crossover of redox species demonstrated in the previous work of this thesis, the CH:HPMC+gly (chitosan:hidroxy cellulose with glycerol) BioPEM was selected for the experiments carried out during this current work.

6.3. PREPARATION OF REDOX HYDROGEL ELECTRODES

To obtain a battery made of redox hydrogels, it was necessary to incorporate materials for electronic conduction. Two different classes of electrodes were evaluated: two-dimensional (2D) and three-dimensional (3D) electrodes. On the one hand, the 2D electrodes were screen printed electrodes (SPE) in which the redox hydrogel was deposited on the top surface of the working electrode (WE). On the other hand, for the three-dimensional electrodes the redox hydrogel permeates into the porous electrode structure to take advantage of a larger active area.

For this step, screen-printed electrode were fabricated using carbon inks (Gwent ink C1090D14, Gwent Electronic Materials, Gwent, U.K.) for the working and counter electrode and silver-silver chloride (Ag/AgCl) ink for the reference electrode, in the same way as the SPEs obtained[12] in the previous chapter. Besides, porous carbon electrodes were also used and were cut to size from sheets of Toray carbon paper (TGPH-120; E-TEK) with a thickness of 370 μm .

All the redox-hydrogel electrode preparations were submitted to incubation for 48 h at 25 ° C so that the solvent could evaporate slowly and the excessive formation of bubbles or dryness in the electrode could be avoided.

As a consequence, the redox-hydrogel electrodes structure results in the schematic representation shown in Figure 6.4. The redox species are linked to the hydrogel backbone and crosslinked to the complete electrode area, since it has been coated with this mixture creating the final version of the redox-electrode.

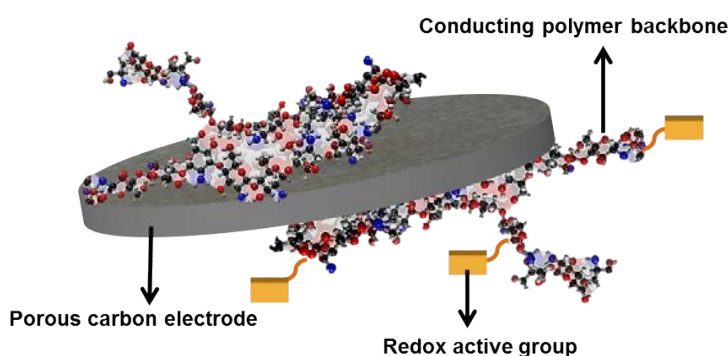


Figure 6.4. Schematic representation of a redox-hydrogel electrode.

6.4. REDOX HYDROGEL ELECTROCHEMICAL CHARACTERIZATION

Once the redox hydrogels were incorporated into the two types of electrodes, their electrochemical evaluation was carried out with the objective of identifying the electronic conduction system that will best adapt to the button cell design and generate more voltage and power output.

6.4.1. Effect of the hydrogel gelation in the open circuit voltage

So as to successfully evaluate the effect of the gelation process of the redox hydrogels, a study of the open circuit voltage obtained from the redox species couple in liquid solution and in gelation processes was carried out. To that end, the performance in three different stages was compared: liquid, hydrogel before incubation (*BI*) and hydrogel after incubation (*AI*).

PMMA setup used in the previous BioPEM chapter (Figure 6.5) with one compartment for the anolyte, another for the catholyte, these being separated by the electrolytic membrane was adapted for this particular study. Both, the SPE and Toray carbon electrodes were used during this evaluation. The CH:HPMC+gly BioPEM was selected as a polymer electrolyte separator between both compartments.

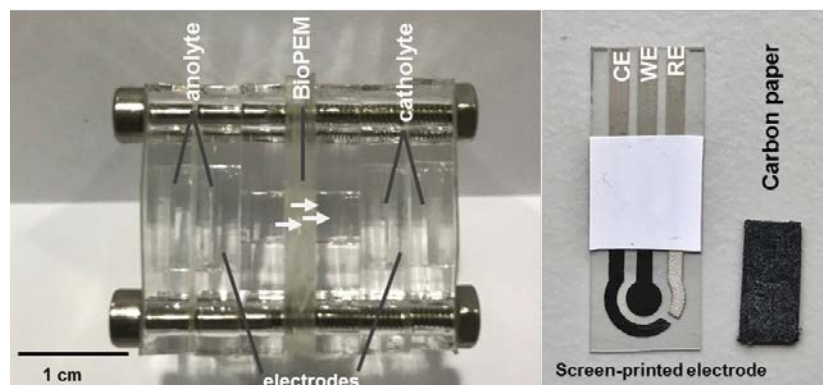


Figure 6.5. PMMA cell setup for open circuit voltage measurements (left). Screen printed electrodes and carbon paper electrodes (right).

Foremost, redox solutions were prepared at concentrations of 0.1 M AA in 1 M KOH and 0.2 M Fe^{3+} in 0.5 M $\text{C}_2\text{H}_2\text{O}_4$, as the solution regime, and were placed in the anode and cathode side of the cell, respectively. The second system evaluated in the same PMMA setup consisted of the redox-hydrogels *BI*. As the third and last condition redox-hydrogel *AI* were used. For this case, an amount of hydrogel *AI* was deposited in the surface of the working electrode ($\varnothing=3$ mm) of the SPE, leading to a hydrogel volume of 7 mm^3 . For this regime, infused Toray porous electrodes were also evaluated in order to observe what effect having a three-dimensional reaction area represented, where the hydrogel could be spreading through the porosities of the electrode and not just on its surface. The dimension of the Toray electrodes used for this particular test was 5 mm-wide x 10 mm-long, where the active area was $5 \times 5\text{-mm}$. The electrodes were placed in a Petri dish ($55 \times 12\text{-mm}$) in order to infusing their area with the redox-hydrogel mixture.

A cell configuration was achieved by stacking an AA redox-hydrogel-electrode as an anode, the biopolymeric membrane and a Fe^{3+} redox hydrogel-electrode as the cathode. This stack structure was the result of removing a large amount of solvent in the hydrogels (*AI*), which led to a significant reduction in the volume of the same.

The resulting cells were connected to a potentiostat (DropSens $\mu\text{Stat}400$ Bipotentiostat/Galvanostat and DropView 8400 Software (DropSens S.L., Asturias, Spain)) by short-circuiting its reference electrode with its counter electrode acting as the anode of the cell, and the working electrode being the cathode. After this, the open circuit voltage in these three models was measured and compared in order to know the effect of the gelation process in the voltage output of the batteries.

The first regime of the redox species in solution was labeled 0% gelation, the regime of the redox hydrogels *BI* was labeled 60% of gelation and the redox-hydrogels *AI* 90% of gelation, due to its absence of solvent.

The open circuit voltages of the different regimes were measured and are shown in Figure 6.6. The regime with the redox species in solutions has shown an OCP of $1.1 \pm$

0.05 V using SPE and Toray electrodes. The same chemical couple evaluation was presented in chapter 2 of this thesis and, as expected, the same voltage was obtained.

Despite both electrodes being coated with the same redox-hydrogel, the Toray electrode showed a higher OCP of 0.95 ± 0.3 V, while the open circuit voltage exhibited by the SPE was found to be slightly lower at approximately 0.62 ± 0.2 V due to internal losses inside the cell. A reasonable explanation for this is that part of the of the hydrogel that has permeated through the porous electrode, has remained in a semi-liquid state in their electrode pores, leading the redox species to behave as if in liquid state. It is well known that water in a hydrogel enhances the ionic conductivity, due to the fact that it frees segments of the redox polymer to move short, but finite, distances [6].

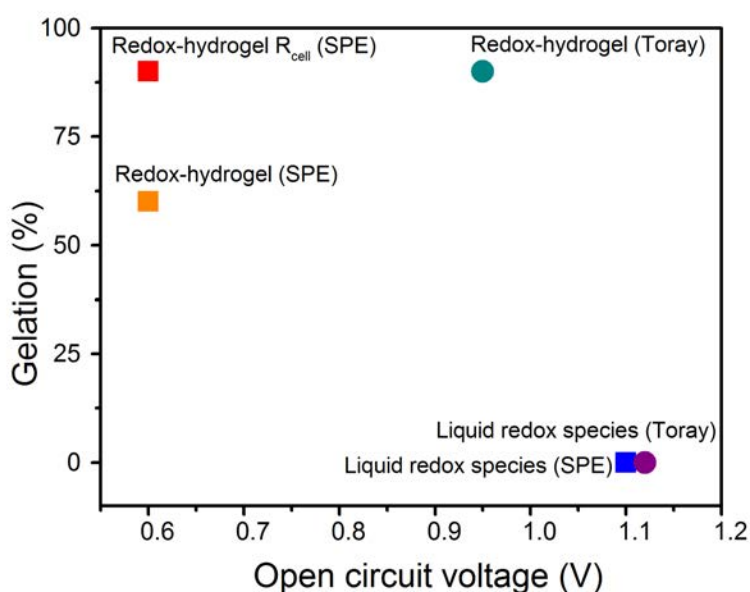


Figure 6.6. Open circuit voltage of the redox-hydrogels in different gelation stage.

6.4.2. Electrochemical performance of redox hydrogel electrodes

Once the open circuit voltage of the redox hydrogels was known using SPE and Toray porous electrodes, the electrochemical characterization of both systems was carried out, in order to know and evaluate the performance obtained with the two types of electrodes. A PMMA vertical setup was fabricated using PMMA pieces to hold both types of electrodes the Toray carbon electrodes (5 x 10 –mm), where only a 5x5 mm area was coated with the redox-hydrogel matrix, the same amount of redox-hydrogel (7 mm³) as in the previous section of this chapter was placed in the working electrode of the SPEs. During this evaluation, the electrodes were stacked one on top of the other, and the BioPEM was placed between in a sandwich arrangement, in order to separate the cathode and the anode. The design of both setups using SPE and 3D porous electrodes is shown in Figure 6.7.

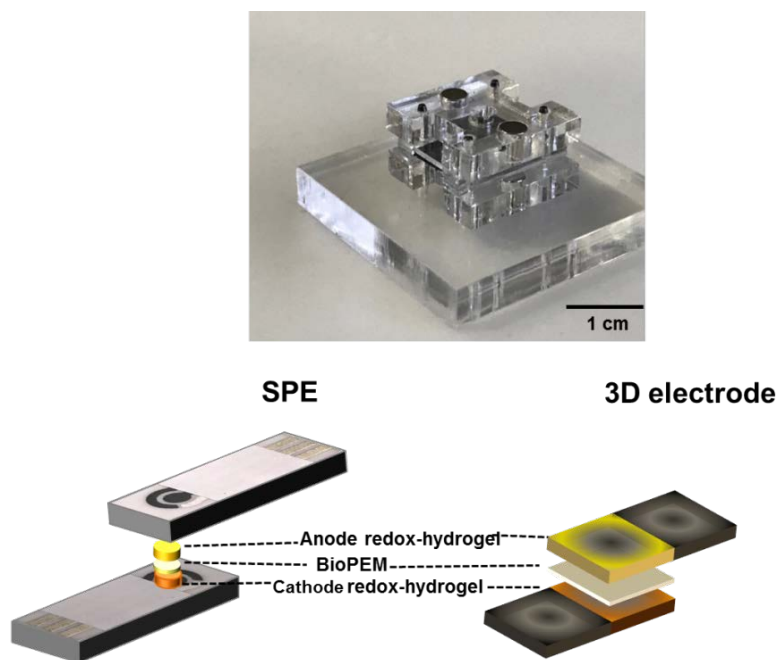


Figure 6.7. Vertical configuration setup for electrochemical characterization using SPE and 3D porous carbon electrodes.

The two configurations made possible to evaluate the performance of the redox-hydrogel cell and the results are shown in Figure 6.8. The current of the polarization curves was normalized to the projected active area to make a comparison between the two cells; due to the different reaction area of the electrodes involved. This comparison suggests that the stack configuration using toray porous electrodes overdoes the cell using SPE. The voltage output for the SPE cell was 0.66V as expected in relation to its level of gelation on the surface of the electrode, while the porous electrode generated a voltage of 0.95 V, due to the semi-liquid condition inside its porous structure as it was previously shown. Regarding current and power density outputs, the systems using 3D porous electrodes were also higher by providing values of $16 \text{ mA}\cdot\text{cm}^{-2}$ and $0.85 \text{ mW}\cdot\text{cm}^{-2}$ against the $6 \text{ mA}\cdot\text{cm}^{-2}$ and $0.7 \text{ mW}\cdot\text{cm}^{-2}$ obtained with SPE electrodes.

Although both battery configurations were able to produce an power output, it was clear that they suffer high activation losses and cell resistance. This internal cell resistance could be owed of the low ionic conductivity of the CH: HPMC+gly hydrogel matrix.

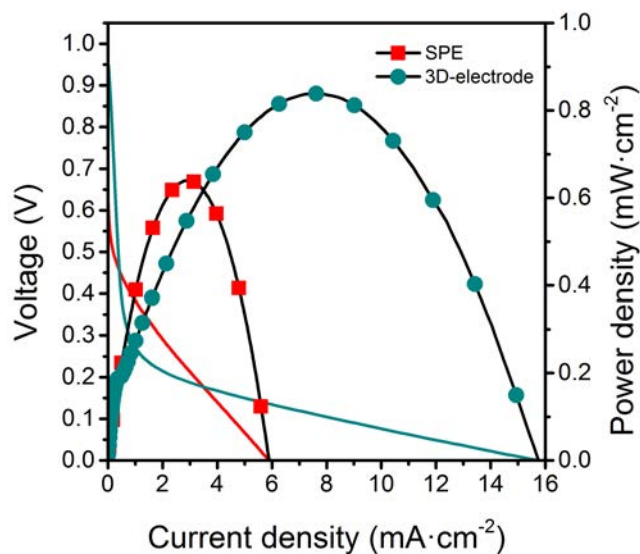


Figure 6.8. Polarization curves comparison of the redox-hydrogel cells using SPE and porous carbon electrodes.

6.4.3. Increasing ionic conductivity of redox hydrogels

Increasing the ionic conductivity of hydrogels can improve the charge transference in the backbone and provide good electrochemical stability[13]. To that end, the redox-hydrogels were doped with different known electrolyte compounds, such as: KOH, NH₄Cl and NaCl, chemical compounds with different properties such as pH, ionic conductivity, solubility and low toxicity. The aim was increasing the relatively low ionic conductivity of the redox-hydrogels for enhance the battery performance. It was sought to avoid changes in the hydrogels mechanical properties due to pH changes. The pH was set around 4-5 to avoid chitosan precipitation at alkaline pH, as it is well known that chitosan hydrogels have pH-dependent structural and mechanical property changes [14][15]. Therefore, AA and Fe³⁺ redox hydrogels were prepared and KOH (0.2% w/ v), NaCl (0.5% w/v) and NH₄Cl (0.5% w v) were added. Toray carbon electrodes of 5 x 10 mm with an active area of 5x5 mm were used, as well as the above section. All the redox-hydrogel electrode preparations were submitted to incubation for 48 h at 25 ° C so that the solvent could evaporate slowly and the excessive formation of bubbles or dryness in the electrode could be avoided. The batteries were assembled using the setup in Figure 6.7.

Polarization curves were performed using 3D porous electrodes to the effect exerted by the minimum addition of compounds with higher ionic conductivity to the hydrogels matrix. Based on Figure 6.9, it can be observed that the three dopings of KOH, NH₄Cl and NaCl hydrogels improved the performance of the cell significantly, starting from a bare hydrogel of 0.2 mW of power output at power values of 0.3, 0.4 and 0.6 mW for NaCl, NH₄Cl and KOH. The cell resistance was observed to have decreased considerably. The minimum addition of KOH (0.2%) did not represent any alteration to the mechanical or physical composition of the redox-hydrogels. However, it did



represent a substantial increase in the performance of the cell, showing that this strategy could be beneficial to the goals of this work.

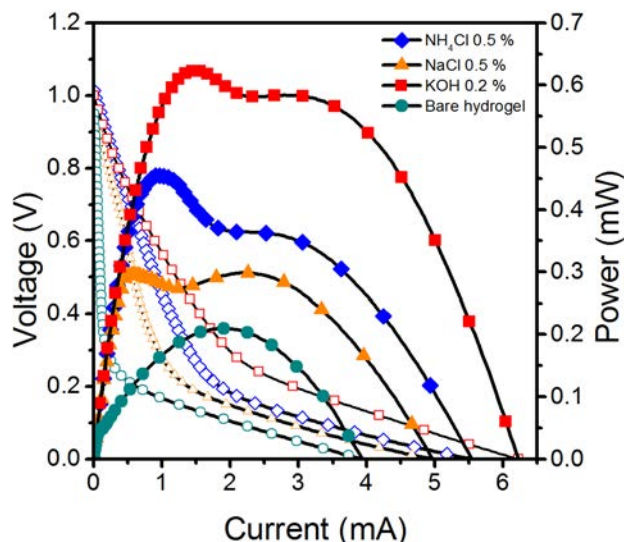


Figure 6.9. Polarization curves of the redox-hydrogel cells doped with KOH 0.2%, NH₄Cl 0.5% and NaCl 0.5%.

6.5. REDOX HYDROGEL-BASED BUTTON BATTERY

Once the ionic conductivity of the redox hydrogels was increased and the activation losses were reduced due to the addition of KOH to the matrices, the final device was fabricated to obtain the button primary battery designed for this work.

6.5.1. Battery design and fabrication

The goal of the research carried out in this thesis chapter has been the development of a biodegradable button battery in harmony with the environment and that followed the principles of circular economy. A schematic representation of the prototype of the button battery is shown in Figure 6.10. In the foreseen device the redox-hydrogels electrodes are placed in a sandwich configuration using a bio-polymeric membrane as separator. The connections would be made of carbon caps that allow the current collection. The casing of the battery would be made using 3D printing using a bioplastic such as PLA or another biopolymer that would allow the battery to be completely biodegradable. However, the gasket development section remains pending for future research in the line of study of this thesis. The challenge in this work was to emulate a button battery design, which has a shaped as a squat cylinder typically 5 to 25 mm (0.197 to 0.984 in) in diameter and 1 to 6 mm high. In this work, it has been sought to develop a prototype of 10 mm in diameter and 1.0 - 2.5 mm thick.

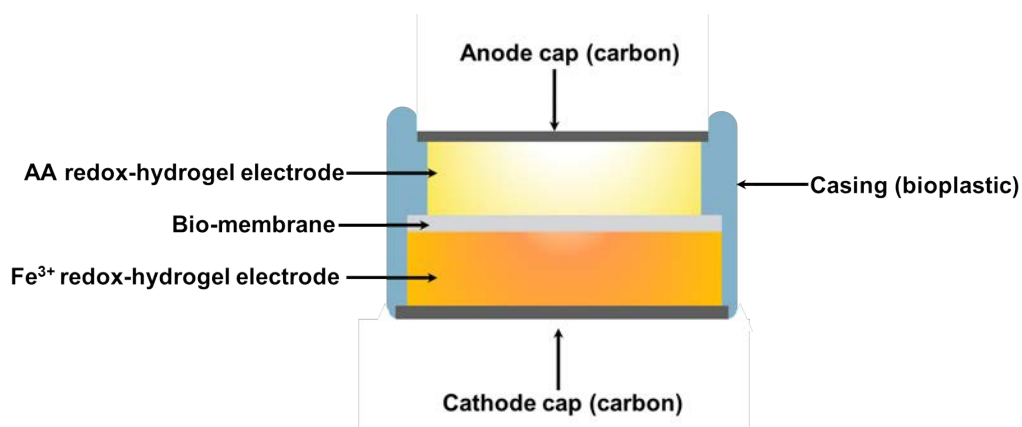


Figure 6.10. Schematic of biodegradable button cell battery prototype.

With the purpose of building the button cell battery, a new batch of redox-electrodes was obtained. For this new approach, the redox-hydrogel mixture was poured into a polymerization mold, which consisted of a piece of Poly(methyl methacrylate) (Plexiglas, Evonik Performance Materials GmbH, Darmstadt, Germany) -PMMA- with circular cavities to hold the porous electrodes (\varnothing 10 mm) as it can be seen in Figure 6.11. Hence, the surrounding amount of hydrogel could be controlled. The electrodes were incubated for 48 h at 25°C to evaporate the solvents. Once the solvent was evaporated and the hydrogels were formed surrounding the electrode perimeter, the button battery design was assembled for its further characterization. To accomplish the 3D electrode impregnation, all the porous carbon electrodes were annealed in a butane flame to confer it the hydrophilic behavior needed for the flow-through configuration [16].

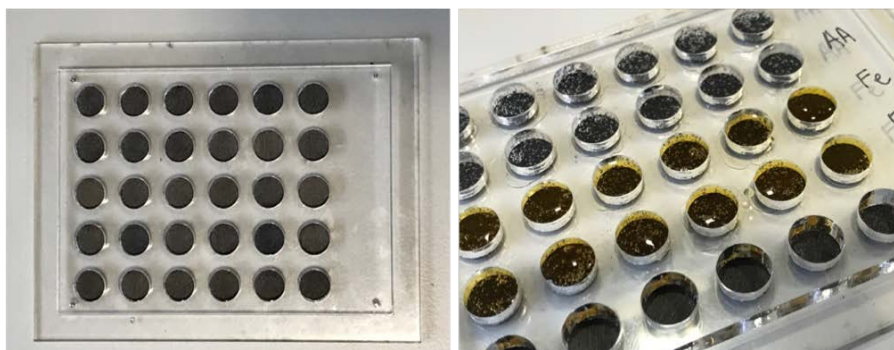


Figure 6.11. PMMA piece holder for the button cell electrodes.

The battery electrodes were fabricated with two different redox hydrogel thicknesses: one of them consisted in a scraped electrode (370 μm), so the only amount of hydrogel that remained would be the one that had been absorbed inside the electrode pores, the excess of hydrogel being scraped off completely. The second approach consisted of a Toray carbon electrode (370 μm thick) topped with a 1-mm thick redox-hydrogel mixture. (Figure 6.12).

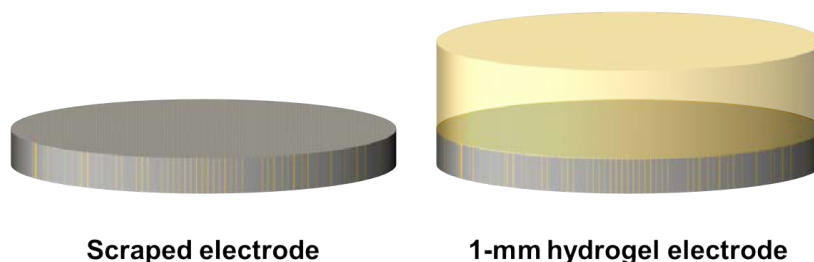


Figure 6.12. Tested electrodes with different hydrogel thickness.

PMMA (5 mm thick) were used to support the battery components. A layer of PMMA of different thicknesses (375 μm or 1 mm) with a 10 mm hole was used to hold the two different redox-hydrogel electrodes, previously synthesized, using a PMMA layer of 100 μm to align the BioPEM used to separate the anode and the cathode in the battery.

The two electrodes were put together in a sandwich configuration, separated by the BioPEM and making the electrical connections by means of two gold electrodes located on the top and bottom of the cell working as current connectors (Figure 6.13). Moreover, all the pieces were aligned with pins and held together thanks to the addition of magnets that allowed to keep all pieces together under the same pressure.

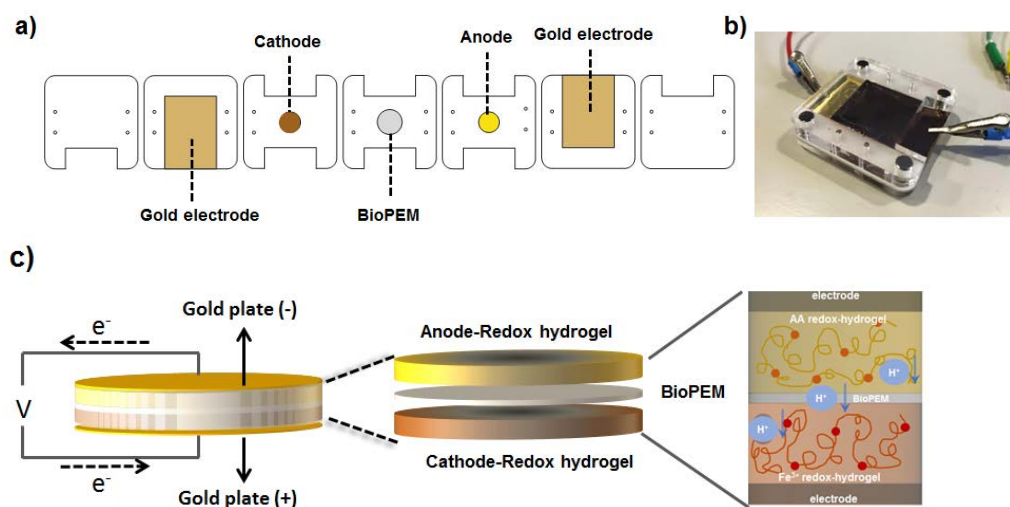


Figure 6.13. Diagram and setup of the button cell battery. a) PMMA pieces and holding parts. b) Button cell setup connected to potentiostat. c). Button cell battery scheme.

6.5.2. Button cell battery electrochemical characterization

The electrochemical characterization of this battery was made through polarization curves. The open circuit voltage and current output were recorded using a DropSens $\mu\text{Stat}400$ Bipotentiostat/Galvanostat and DropView 8400 Software (DropSens S.L., Asturias, Spain). The polarization and power curves were generated using linear sweep voltammetry, sweeping from the open circuit voltage (OCV) to 0 V at a scan rate

of 10 mV s^{-1} . The discharging curves were recorded under different external loads of Ω . All tests were performed at room temperature.

The polarization curves are presented in Figure 6.14. It is observed that higher power output was obtained with the 1-mm electrode cell (1.28 mW), compared to the scraped electrode (0.08 mW).

It can also be observed that the first polarization curves in both systems started at 0.95 V, however, over time, the voltage decreased to 0.75 V and higher current output was generated (dashed line), starting from currents of 6.8 mA to 8.8 mA and 9.3 mA to 10.4 mA, for scraped and 1-mm electrodes, respectively. We have seen that the redox species in gelation in the SPE had lower open circuit voltages than those obtained using porous electrodes. This proves that the state of the redox species within the 3D electrodes tends to be more liquid than the hydrogel that covers the electrode on the outside. That is why the first IV were observed with a liquid-like state, while over time, the behavior of the hydrogel proliferates and we see a decrease in voltage plus an increase in current due to the greater amount of redox species found in gel form than in liquid state.

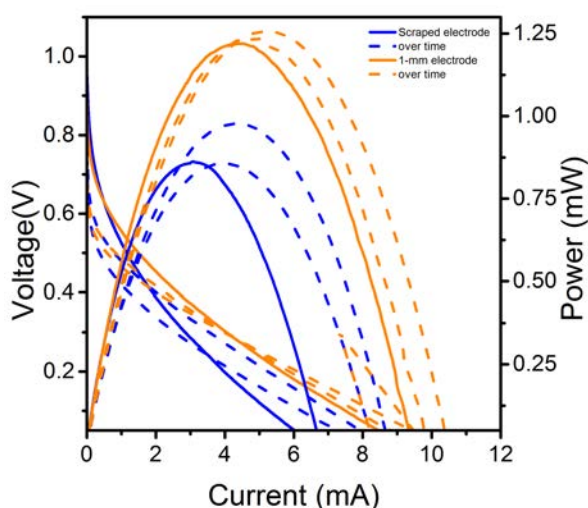


Figure 6.14. Polarization curves of the button cells using scraped and 1-mm electrode configurations.

The battery operation was characterized by measuring discharging curves for different external loads (60Ω and 100Ω) for the 1-mm and scraped regime, corresponding to their maximum power operating points. The curves obtained during the discharge process of the batteries at their maximum power values using a fixed load are shown in Figure 6.15. As expected, the battery with 1-mm electrodes generated higher power values (up to 1.2 mW) for longer operation time. The battery with scraped electrodes delivered power output for shortest service times. Controlling the hydrogel thickness on the redox electrodes becomes crucial when wanting to balance the power output generated and the battery operating time.



This is due the dynamic diffusion of reactants in the hydrogel matrix, spreading through the porous electrodes as a function of time. The close proximity of the redox-hydrogel electrodes allowed a gradual release of the species by a diffusive mass transport during battery discharge and improved the performance of the battery.

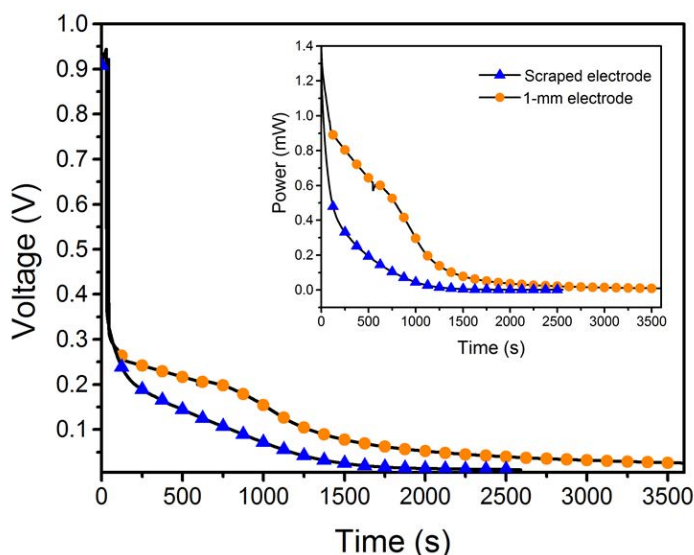


Figure 6.15. Discharge curves of the button cells using fixed loads for scraped ($100\ \Omega$) and 1-mm ($60\ \Omega$) electrodes.

The fuel utilization was calculated based on the coulombs (C) generated from the discharge curves of each of the batteries and the theoretical value obtained from the concentration of redox species. The values of the faradaic efficiency are shown in Table 6.1

Table 6.1. Faradaic efficiency comparison for the scraped and 1-mm electrode models.

Battery electrode	Faradaic efficiency
Scraped electrode	10.2 (%)
1-mm electrode	5.6 (%)

It can be seen that the system with scraped electrode provided higher faradaic efficiency, compared to the 1-mm electrode. As the hydrogel thickness increased in the system, the faradaic efficiency decreased, this can be explained because the hydrogel matrix opposes greater resistance to the transport of ions by diffusion. The closer the self-exchange between the redox hydrogel electrodes, the faster the rate of charge transfers to a redox hydrogel electrode, which also decreases the cell resistance.

6.5.3. In series connection of button-cell batteries

Many of the button cells miniature are zinc-air batteries that have a nominal voltage of 1.2 V [17]. In order to emulate the voltage of one of these button batteries and check the feasibility of making stacks of hydrogel cells, two single batteries were connected in series to scale the voltage. The 1-mm electrode cells were selected due to the higher

performance previously obtained. The voltage increase was carried out connecting the positive side of one of the cells to a bare carbon electrode, which worked as a connector between the two cells, to which the anode of the second cell was connected (Figure 6.16). The battery was assembled layer by layer with PMMA layers designed to hold the electrodes and membranes. The resulting battery had a size of 10 x 4.5-mm.

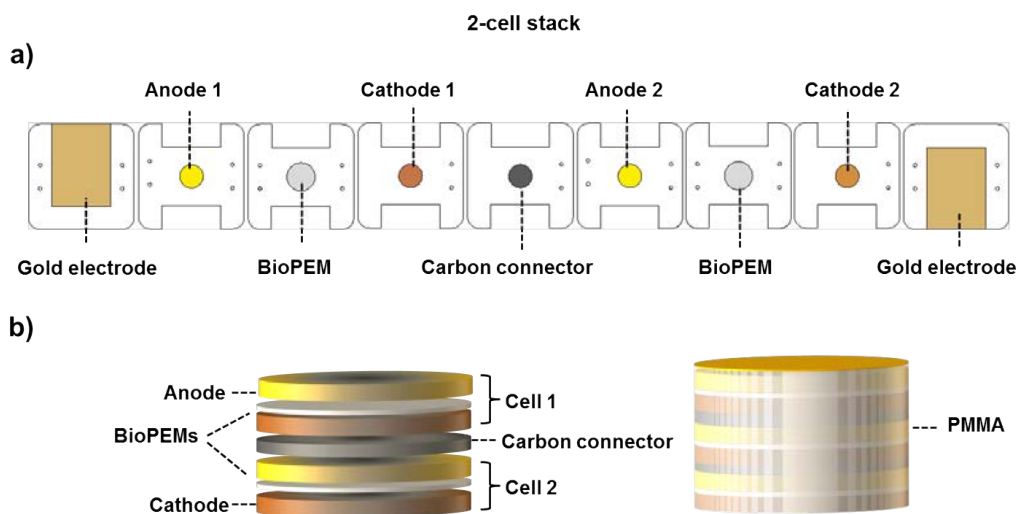


Figure 6.16. Schematic of 2 button cell stack in series. a) PMMA pieces to assembly the battery. b) Internal arrangement of the electrodes and membrane.

Figure 6.17 shows the polarization curve of the single battery and 2-cell stack. it is observed that the stack of button batteries reached a 1.6 ± 0.2 V open circuit voltage and delivered a maximum power output of 2.2 ± 0.2 mW, a very similar behavior to the one expected if the performance of a single cell had been doubled. This indicates that it is feasible to connect several button batteries in series to increase the output voltage according to the application.

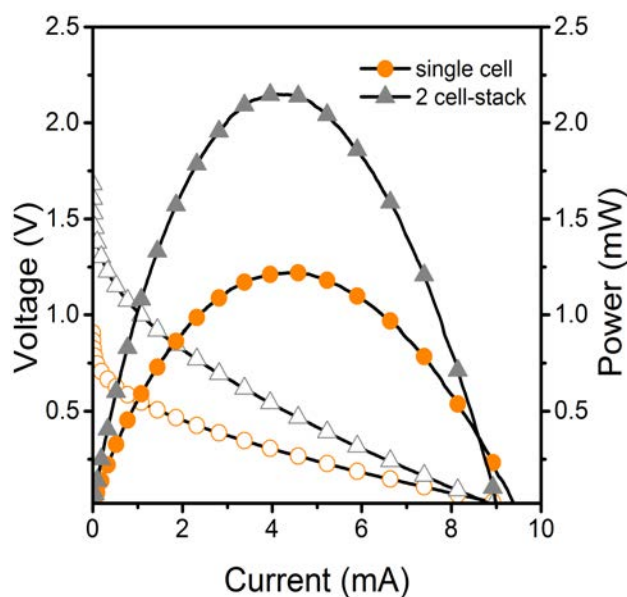


Figure 6.17. Polarization curves of the single cell and 2-cell stack button battery, using 1-mm redox hydrogel electrodes.

Based on the geometrical electrode area of 0.78 cm^2 , the stacked button battery yielded a maximum power density of $2.82 \pm 0.2 \text{ mW cm}^{-2}$ at a current density of 11.54 mA cm^{-2} , which is comparable to the powerPAD device shown in chapter 3 and at least an order of magnitude higher than some of the transient battery reported so far [18] [19].

6.6. CONCLUSIONS

This chapter described the synthesis and electrochemical characterization of redox-hydrogels incorporating ascorbic acid and iron nitrate to a chitosan and hydroxypropylmethyl cellulose backbone. It was a successful combination of conducting polymers and redox chemistry. In addition, the feasible incorporation of these materials to porous carbon electrodes to develop a button battery was demonstrated. The materials present mass transport anion-cation and proton transport during the redox reaction $\text{AA} - \text{Fe}^{3+}$. We conclude that redox-hydrogels in porous electrodes can provide a small, practical and disposable power source device.

In this work, a contribution has been made in the search for transient batteries based on natural redox polymers. For the first time, the combination of chitosan hydrogels with vitamin C as the anode has been tested and its redox operation validated, as well for the cathode made by an iron salt and the same polymeric backbone. Have been able to manufacture a button battery of small dimensions ($10 \text{ mm} \times 4.5 \text{ mm}$), from naturally abundant materials, with low toxicity and environmental impact. Furthermore, its manufacture was achieved using energy efficient instruments. The battery presented a good electrochemical performance under maximum power output with an operating time of 30 min. The battery showed capability and practicality to make

connections in series and the ability to adapt the device to the power needs required for the target application.

Future work will be focused on standardizing the system to increase the power density and operation time of the battery. This will be done by introducing changes in the system design and architecture and improving the quality of the packaging of the device. The casing of this device should be developed using biomaterials to fulfill the sustainability goals.

**References in Chapter 6.**

- [1] M. Winter, R.J. Brodd, What Are Batteries , Fuel Cells , and Supercapacitors ? What Are Batteries , Fuel Cells , and Supercapacitors ?, 104 (2004) 4245–4270. doi:10.1021/cr020730k.
- [2] C.P. Fonseca, D.S. Rosa, F. Gaboardi, S. Neves, Development of a biodegradable polymer electrolyte for rechargeable batteries, *J. Power Sources*. 155 (2006) 381–384. doi:10.1016/J.JPOWSOUR.2005.05.004.
- [3] A. Tsuzaki, H. Ando, M. Yao, T. Kiyobayashi, R. Kondo, H.T. Takeshita, A New Bio-based Battery Material: Effect of Rate of Anthraquinone Skeleton Incorporation into Polyglycidol on Battery Performance, *Energy Procedia*. 89 (2016) 207–212. doi:10.1016/J.EGYPRO.2016.05.027.
- [4] T. Suga, S. Sugita, H. Ohshiro, K. Oyaizu, H. Nishide, p- and n-Type Bipolar Redox-Active Radical Polymer: Toward Totally Organic Polymer-Based Rechargeable Devices with Variable Configuration, *Adv. Mater.* 23 (2011) 751–754. doi:10.1002/adma.201003525.
- [5] M. Sterby, R. Emanuelsson, X. Huang, A. Gogoll, M. Strømme, M. Sjödin, Characterization of PEDOT-Quinone Conducting Redox Polymers for Water Based Secondary Batteries, *Electrochim. Acta*. 235 (2017) 356–364. doi:10.1016/J.ELECTACTA.2017.03.068.
- [6] A. Heller, Electron-conducting redox hydrogels: design, characteristics and synthesis, *Curr. Opin. Chem. Biol.* 10 (2006) 664–672. doi:10.1016/J.CBPA.2006.09.018.
- [7] R. Gracia, D. Mecerreyes, Polymers with redox properties: materials for batteries, biosensors and more, *Polym. Chem.* 4 (2013) 2206. doi:10.1039/c3py21118e.
- [8] A. Heller, Implanted Electrochemical Glucose Sensors for the Management of Diabetes, *Annu. Rev. Biomed. Eng.* 1 (1999) 153–175. doi:10.1146/annurev.bioeng.1.1.153.
- [9] C. Karlsson, H. Huang, M. Stromme, A. Gogoll, M. Sjödin, Impact of linker in polypyrrole/quinone conducting redox polymers, *RSC Adv.* 5 (2015) 11309–11316. doi:10.1039/C4RA15708G.
- [10] K. Zhang, C. Guo, Q. Zhao, Z. Niu, J. Chen, High-Performance Organic Lithium Batteries with an Ether-Based Electrolyte and 9,10-Anthraquinone (AQ)/CMK-3 Cathode, *Adv. Sci.* 2 (2015) 1500018. doi:10.1002/advs.201500018.
- [11] Andrew P. Doherty, Margaret A. Stanley, Johannes G. Vos, Electrocatalytic oxidation of ascorbic acid at [osmium(2,2'-bipyridyl)2-(poly-4-vinylpyridine)10Cl]Cl modified electrodes; implications for the development of biosensors based on osmium-containing redox relays, *Analyst*. 120 (1995). http://books.google.com/books?hl=en&lr=&id=OAzUyTf0O9wC&oi=fnd&pg=PA1&dq=Redox+hydrogel-based+electrochemical+biosensors&ots=VL_8fDRJQd&sig=4_FiNspa pRxXUfkJqvRTRdetmkY.
- [12] L. del T. Román, M. Navarro, G. Hughes, J.P. Esquivel, R.D. Milton, S.D. Minter, N. Sabaté, Improved performance of a paper-based glucose fuel cell by capillary induced flow, *Electrochim. Acta*. (2018). doi:10.1016/j.electacta.2018.05.074.
- [13] Y. Tominaga, Ion-conductive polymer electrolytes based on poly(ethylene carbonate) and its derivatives, *Polym. J.* 49 (2016) 291. <http://dx.doi.org/10.1038/pj.2016.115>.
- [14] S.T. Koev, P.H. Dykstra, X. Luo, G.W. Rubloff, W.E. Bentley, G.F. Payne, R. Ghodssi, Chitosan: an integrative biomaterial for lab-on-a-chip devices, *Lab Chip*. 10 (2010) 3026. doi:10.1039/c0lc00047g.

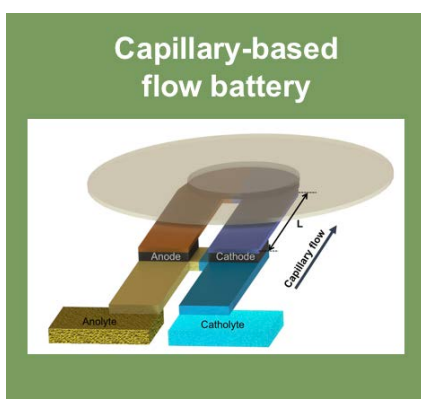
- [15] H. Xu, S. Matysiak, Effect of pH on chitosan hydrogel polymer network structure, *Chem. Commun.* 53 (2017) 7373–7376. doi:10.1039/C7CC01826F.
- [16] E. Kjeang, R. Michel, D.A. Harrington, N. Djilali, D. Sinton, A Microfluidic Fuel Cell with Flow-Through Porous Electrodes, *J. Am. Chem. Soc.* 130 (2008) 4000–4006. doi:10.1021/JA078248C.
- [17] K.-H. Choi, H.-W. Kim, S.-S. Lee, J. Yoo, D.-G. Lee, S.-Y. Lee, All-Hand-Drawn Zn-Air Batteries: Toward User-Customized On-the-Fly Power Sources, *Adv. Sustain. Syst.* 1700132 (2018) 1700132. doi:10.1002/adsu.201700132.
- [18] Y.J. Kim, S.-E. Chun, J. Whitacre, C.J. Bettinger, Self-deployable current sources fabricated from edible materials, *J. Mater. Chem. B.* 1 (2013) 3781–3788. doi:10.1039/C3TB20183J.
- [19] L. Yin, X. Huang, H. Xu, Y. Zhang, J. Lam, J. Cheng, J.A. Rogers, Materials, designs, and operational characteristics for fully biodegradable primary batteries, *Adv. Mater.* 26 (2014) 3879–3884. doi:10.1002/adma.201306304.

Conclusions

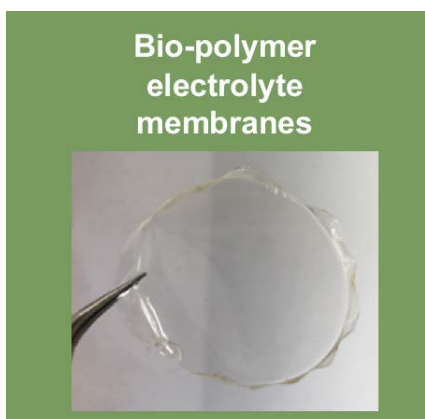
This thesis has presented the development of different biodegradable batteries as sustainable power sources for portable devices. The work includes the design, fabrication and characterization of the different approaches starting with the identification of redox species suitable for these devices. The redox species to be used in the development of these biodegradable batteries should meet requirements such as water solubility, storability in solid state, biodegradability, low toxicity. The overall most effective chemistry identified for disposable cells was based on either ascorbic acid or H_2BQS in KOH and pBQ and Fe^{3+} in oxalic acid at the negative and positive electrodes, respectively.



The first concept of biodegradable battery was achieved. The PowerPAD (Portable and disposable) power source was based on cellulose, organic redox species, porous carbon electrodes and beeswax. Connections in series of the single-cell batteries allowed to reach the voltage needed to power a portable water monitoring system. Moreover, powerPAD is a biodegradable device that can be disposed of in the soil or water bodies and the microorganisms will convert it to basic compounds with minimal environmental impact.



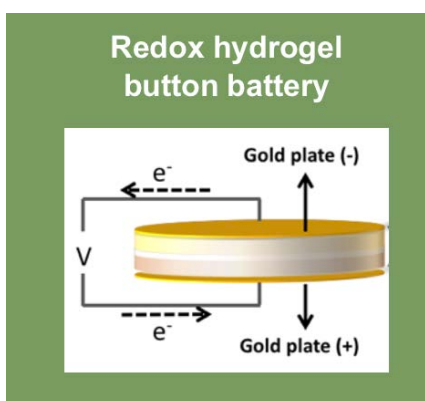
A paper-based battery with quasi-steady capillary flow was developed using paper channels, porous carbon electrodes and a circular absorbent pad. The redox species flowed by capillarity in three different quasi-steady flow rates due to the modifications in the geometry of the paper channels, generating different power outputs in each system. Moreover, the reaction zone in the flow battery was improved by increasing the length of the electrodes. This device demonstrated that the faradaic efficiency increased at low flow rates and increased electrode area, achieving an almost complete fuel utilization.



**Bio-polymer
electrolyte
membranes**

Naturally derived, non-toxic, low cost bio-polymer electrolyte membranes (BioPEMs) were developed for primary redox flow battery systems. These BioPEMs were synthesized from chitosan and cellulose and enhancers of ionic conductivity compounds as glycerol. The BioPEMs were evaluated based on their mechanical properties, ionic conductivity and resistance to crossover of redox species across their matrices. Then, their electrochemical performance was tested in primary redox batteries. The glycerol-BioPEM showed to be

a membrane with acceptable ionic conductivity and low crossover of the redox species evaluated.



**Redox hydrogel
button battery**

The development of a button battery based on redox hydrogels was carried out. The effective manufacture of the battery from hydrogels of chitosan, cellulose, vitamin C and an iron salt was achieved. This battery used the BioPEM previously synthesized to separate anode and cathode. The performance of the battery was above the values reported for transient batteries to date. The scalability of its voltage was demonstrated by successfully connecting single cells in series.

This work represents a significant advance in the development of biodegradable batteries for single use applications. The approaches reported here are expected to be a cornerstone in the search for more sustainable sources of energy that minimize the overload of conventional batteries in our planet.

Ongoing and future work

The work carried out during this thesis has started a research line in the area of portable biodegradable batteries that will lead to many different outcomes. The future work for the devices presented in this work can be framed in three main areas for optimization: the architecture of the devices, the evaluation and implementation of different redox species and the biodegradable packaging.

The capillary-based flow battery presented here will be turned into a compact device based on the optimized parameters and conditions found. This will include the development of an architecture that allows the portability of the device, as well as its manipulation, that will be oriented to specific target applications.

The redox chemistry involved for devices such as those presented in this paper presents a wide variety of candidates that could be evaluated. The use of organic redox species such as other quinones species, organic radical TEMPO (4-hydroxy-TEMPO) and viologen. As well as expanding the gathering to inorganic species, always having the firm objective of obtaining an eco-friendly product or even beneficial to the environment as compostable. The ideal would be to have redox couples that are better adapted to the intended application, in sectors such as agriculture, environmental monitoring, internet of things, among others.

In terms of the casing for biodegradable batteries, it is intended to identify the bio-materials that provide this harmony with the environment and also allow a scalable manufacturing of the devices. Biopolymers such as agar, chitosan, silk and bio-plastics such as PHA and PLA that could meet the desired characteristics are available and could be suitable candidates for this purpose.

Scientific contributions

Journal Articles

- Esquivel, J. P., Alday, P., Ibrahim, O. A., Fernández, B., Kjeang, E., & Sabaté, N. (2017). **A Metal-Free and Biotically Degradable Battery for Portable Single-Use Applications.** *Advanced Energy Materials*, 1700275. <https://doi.org/10.1002/aenm.201700275>
- Ibrahim, O. A., Alday, P., Sabaté, N., Esquivel, J. P., & Kjeang, E. (2017). **Evaluation of Redox Chemistries for Single-Use Biodegradable Capillary Flow Batteries.** *Journal of The Electrochemical Society*, 164(12), A2448–A2456. <https://doi.org/10.1149/2.0971712jes>
- Alday, P., García, D., Ibrahim, O., Kjean, E., Sabaté, N., Esquivel, J.P. **A paper-based capillary flow battery optimization with flow-through electrodes.** *In preparation.*
- Alday, P., Barros, S., Da Silva, M., Sabaté, N., Esquivel, J.P. **Bio-Polymeric Electrolyte Membranes (BioPEMs) for a primary redox battery.** *In preparation.*

Patent

- Esquivel, J. P., Sabaté N., Alday, P., Kjeang, E., Ibrahim, O. A. *ES Patent EP15200865*, 2015.

Workshops and conferences

- *Authors:* Esquivel, J. P., Alday, P., Ibrahim, O. A., Fernández, B., & Kjeang, E., Sabaté, N.
- *Title:* Powerpad: Non-Toxic Capillary-Based Flow Battery for Single Use Applications
- *Congress:* 229th ECS MEETING - ECS - The Electrochemical Society. San Diego, USA, 2016.
- *Type:* Poster

- *Authors:* Esquivel, J. P., Alday, P., Ibrahim, O. A., Fernández, B., & Kjeang, E., Sabaté, N.
- *Title:* Powerpad: Non-Toxic Capillary-Based Flow Battery for Single Use Applications
- *Congress:* 229th ECS MEETING - ECS - The Electrochemical Society. San Diego, USA, 2016.
- *Type:* Oral (invited)

- *Authors:* O. A., Alday, P., Sabaté, N., Esquivel, J. P., & Kjeang, E. (2017)
Title: Powerpad: Evaluation of Redox Chemistries for Disposable Power Sources
Congress: 229th ECS MEETING - ECS - The Electrochemical Society. San Diego, USA, 2016.
Type: Oral (invited)
- *Authors:* Alday, P., García, D., Ibrahim, O., Kjean, E., Sabaté, N., Esquivel, J.P.
Title: A paper-based capillary flow battery optimization with flow-through electrodes.
Congress: HYCELTEC VI Symposium on Hydrogen, Fuel cells and Advanced Batteries. Porto, Portugal, 2017.
Type: Oral
- *Congress:* Jornada d'Investigadors Predoctorals Interdisciplinària: JIPI. Barcelona, Spain, 2016.
Type: Attendance
- *Authors:* Alday, P., Sabaté, N., Esquivel, J.P.
Title: Biodegradable batteries for single-use applications
Congress: Thesis in 3 Minutes (3MT) Contest. Jornadas de Cooperación Conacyt-Catalunya 2018. Barcelona, Spain. 2018.
Type: Award (1st prize)
- *Authors:* Alday, P., Sabaté, N., Esquivel, J.P.
Title: A biotically degradable paper-based battery for single use application.
Congress: Jornadas de Cooperación Conacyt-Catalunya 2018. Barcelona, Spain. 2018.
Type: Oral

APPENDIX 1: Biodegradability assay

Detailed study of the biodegradability test carried out at the IRTA (Agrifood Research and Technology Institute) facilities.

Biodegradability study

The OECD-Test 311, for anaerobic biodegradability of organic compounds in digested sludge, is a guideline that included ISO 11734 (ISO, 1995) besides others, as the Shelton and Tiedje method (Shelton et al., 1984). This test has become the American standards (ASTM, 1992; US-EPA, 1998) for biodegradability, although problems related to the differing solubility of CO₂ and CH₄ in the test medium or to the calculation of the theoretical gas production of a test substance were not resolved. The ECETOC report (Birch et al., 1989) recommended the additional measurement of the dissolved inorganic carbon content of the supernatant liquid, which made the technique more widely applicable. After an international calibration exercise (or ring test), the ECETOC method became the ISO Standard ISO 11734 (ISO, 1995).

It is a screening method under a specific condition of an anaerobic digester, at a given time and range of concentration of microorganisms. The conditions of the test do not necessarily correspond to the conditions in all anaerobic digesters nor it is applicable for the assessment of anaerobic biodegradability under different environmental conditions, because (i) a diluted sludge is used with a relatively high concentration of test substance; and (ii) the duration of the test is typically longer than the retention time in anaerobic digesters. Nevertheless, this test provides the “inherent biodegradability” that refers to a classification of materials for which there is unequivocal evidence of biodegradation (primary or ultimate) in any test of biodegradability. Since inherent biodegradability is considered as a specific characteristic of a material, it is not necessary to define or limit the biodegradation rate. Biodegradation above 20% of theoretical (measured as %TC) may be regarded as evidence of primary biodegradability, whereas biodegradation above 70% of theoretical (measured as %TC) may be regarded as evidence of ultimate biodegradability. When results of other biodegradability tests, such as “ready biodegradation assays”, indicate that the pass level criterion is almost fulfilled (i.e. slightly below 60-70%), such results can be used to indicate inherent biodegradability.

Table 1. Characterization of batteries for biodegradability.

Material	Description	Total solids (gTS kg ⁻¹)	TCOD (gO ₂ kg ⁻¹)	TC (gC kg ⁻¹)
Battery	Battery with H ₂ BQS-KOH & pBQ-C ₂ H ₂ O ₄	965.6 ± 3.5	2204.0 ± 68.3	610.9 ± 9.7
Blank battery	Battery without reactants	974.1 ± 3.5	2112.9 ± 228.4	653.4 ± 0.6
Cellulose	Acetate flakes	980.5 ± 1.1	1278.9 ± 0.0	461.6 ± 2.5

Table 2. Initial test conditions for biodegradability study.

Material	Vessel		Material		Material		Inoculum	
	Liquid medium (mL)		TCOD (gO ₂ L ⁻¹)		Initial TC (mgC L ⁻¹)		Total solids (gTS L ⁻¹)	
Battery	50.10 ± 0.07	±	7.60 ± 4.17	±	2.19 ± 1.20		14.50 ± 0.01	±
Blank battery	50.05 ± 0.06	±	5.16 ± 0.01	±	1.57 ± 0.00		14.50 ± 0.01	±
Cellulose	50.03 ± 0.04	±	5.50 ± 0.18	±	1.98 ± 0.07		14.49 ± 0.01	±

Supplementary references:

- ISO 11734. Water Quality: Evaluation of the ultimate anaerobic biodegradation of organic compounds in digested sludge. Method by measurement of the biogas production. International Organization for Standardization.1995.
- Shelton D.R. and Tiedje, J.M. 1984. General method for determining anaerobic biodegradation potential. Appl. Environ. Microbiology, 47, 850-857.
- ASTM .1992. E1192-92 Standard Test Method for Determining the Anaerobic Biodegradation Potential of Organic Chemicals. ASTM, Philadelphia.
- US-EPA. 1998. Fate, Transport and Transformation Test Guidelines OPPTS 835.3400 Anaerobic Biodegradability of Organic Chemicals.
- Birch, R. R., Biver, C., Campagna, R., Gledhill, W.E., Pagga,U., Steber, J., Reust, H., Bontinck, 1989. W.J. Screening of chemicals for anaerobic biodegradation. Chemosphere 19, 1527-1550. (Also published as ECETOC Technical Report No. 28, June 1988).

APPENDIX 2: Bill of materials for powerPAD batteries

PowerPAD biodegradable battery - Bill of Materials

	Single cell		2-cell stack		4-cell stack	
	QUANTITY	COST (€)	QUANTITY	COST (€)	QUANTITY	COST (€)
CELLULOSE						
Cellulose 601 (Ahlstrom)	13.52 cm ²	0.033	13.52 cm ²	0.033	13.52 cm ²	0.033
Cellulose 222 (Ahlstrom)	4 cm ²	0.009	8 cm ²	0.018	16 cm ²	0.037
Cellulose 238 (Ahlstrom)	21.78 cm ²	0.027	23.28 cm ²	0.029	26.28 cm ²	0.033
Cellulose 320 (Ahlstrom)	13.52 cm ²	0.053	13.52 cm ²	0.053	13.52 cm ²	0.053
Cellulose 270 (Ahlstrom)	6.76 cm ²	0.026	6.76 cm ²	0.026	6.76 cm ²	0.026
CARBON ELECTRODES						
Carbon paper TGP-H-120	1 cm ²	0.115	2.35 cm ²	0.270	3.3 cm ²	0.380
WAX						
Beeswax sheets	2 g	0.052	2 g	0.052	2 g	0.052
CHEMICAL REAGENTS						
H ₂ BQS (H18402, Sigma Aldrich)	0.0089 g	0.004	0.0178 g	0.008	0.0356 g	0.015
pBQ (B10358, Sigma Aldrich)	0.0046 g	0.001	0.0092 g	0.002	0.0184 g	0.005
KOH (P1767, Sigma Aldrich)	0.023 g	0.001	0.046 g	0.003	0.092 g	0.005
C ₂ H ₂ O ₄ (247537, Sigma Aldrich)	0.026 g	0.007	0.052 g	0.015	0.104 g	0.029
TOTAL		0.33 €		0.51 €		0.67 €

Price references from:

- <https://us.vwr.com/store/product/12610321/thick-chromatography-paper-grade-222-ahlstrom>
- <http://fuelcellstore.com/toray-carbon-paper-120>
- <http://www.iberceras.es/>
- <http://www.sigmaaldrich.com/catalog/product/fluka/p1767>
- <http://www.sigmaaldrich.com/catalog/product/sial/247537>
- <http://www.sigmaaldrich.com/catalog/product/sial/b10358>
- <http://www.sigmaaldrich.com/catalog/product/aldrich/h18402>

Resumen

Esta tesis presenta el desarrollo de baterías biodegradables siguiendo una aproximación alineada con los principios de sostenibilidad de la economía circular. Estas fuentes de energía están enfocadas especialmente en reducir la exorbitante cantidad de desecho eléctrico y electrónico causado por el crecimiento acelerado de dispositivos electrónicos.

El presente trabajo se ha desarrollado en el Instituto de Microelectrónica de Barcelona, IMB-CNM (CSIC). Las baterías presentadas en esta tesis se han construido completamente a partir de materiales orgánicos y pueden fabricarse mediante métodos económicos con bajo consumo de energía. Esta tesis se compone de seis capítulos: el capítulo de introducción y cinco capítulos experimentales.

El capítulo 2 de este trabajo está dedicado a la exploración de diferentes especies redox apropiadas para el desarrollo de dispositivos ecológicos. En este capítulo, se llevó a cabo la caracterización electroquímica de diversas especies redox y de electrolitos que cumplieran los requerimientos para las baterías proyectadas. La selección de las especies redox se basó en su potencial de oxidación, solubilidad, almacenaje en estado sólido y su baja toxicidad.

En el capítulo 3 se presenta el concepto PowerPAD, el desarrollo de la primera batería biodegradable hecha de papel, electrodos de carbono, especies redox orgánicas y cera de abeja. La batería tiene una degradación biótica, es decir, los microorganismos presentes en suelos y aguas pueden degradar la batería a compuestos básicos con un mínimo impacto ambiental. Esta nueva clase de baterías de flujo redox portátiles y biodegradables es ideal para proporcionar energía a una nueva generación de dispositivos electrónicos ecológicos.

El capítulo 4 de esta tesis está dedicado a la fabricación de una batería de flujo capilar. Esta celda de flujo se ha diseñado como un esfuerzo para la optimización del dispositivo PowerPAD y ha utilizado los mismos materiales naturales. Sin embargo, se ha incorporado un absorbedor de celulosa al final del dispositivo que proporciona un flujo constante de las especies redox. Durante este trabajo, la evaluación electroquímica de la celda se realizó a diferentes velocidades de flujo capilar y áreas de reacción de los electrodos. De esta forma, se presenta una batería redox de flujo capilar con una optimización de su eficiencia farádica.

En el quinto capítulo, se presenta un nuevo enfoque para desarrollar baterías biodegradables. La síntesis y evaluación de membranas electrolíticas a base de biopolímeros (BioPEM). Estas BioPEMs han sido fabricadas a base de polímeros naturales y compuestos orgánicos, como quitosano, celulosa liofilizada y glicerol como plastificante. Durante este capítulo fue posible llevar a cabo la síntesis de dos membranas con baja toxicidad y bajo costo de fabricación que presentaron conductividad iónica adecuada y baja migración de especies redox, características adecuadas para su uso en baterías redox primarias.

El capítulo 6 de esta tesis presenta el desarrollo de una batería de botón primaria basada en hidrogeles de celulosa liofilizados, quitosano y especies redox. Este

dispositivo ha sido fabricado utilizando electrodos porosos de carbono, que han sido impregnados con hidrogel redox y utiliza una BioPEM para la separación del ánodo del cátodo. Como resultado se obtiene una batería de botón con notable potencia y en armonía con el medio ambiente.

Finalmente, se presentan las conclusiones generales de la tesis destacando los aspectos más remarcables de este trabajo y se definen líneas del trabajo futuro en esta prometedora investigación.

Nomenclature

Abbreviations

Ag/AgCl	Silver/silver chloride
BioFC	Bio-flow cell
BioPEM	Biopolymeric electrolyte membrane
CE	Counter electrode
CH	Chitosan
CPE	Conducting redox polymer
CV	Cyclic Voltammetry
FC	Flow cell
GC	Glassy Carbon
HPMC	Hydroxypropyl methyl cellulose
LVS	Linear sweep voltammetry
OCP	Open Circuit Potential
OCV	Open Circuit Voltage
PAFC	Phosphoric Acid Fuel Cell
PDMS	Polydimethylsiloxane
PMMA	Polymethyl Methacrylate
RE	Reference electrode
SCE	Saturated Calomel Electrode
SPE	Screen Printed Electrode
WE	Working electrode

Symbols

C_0	Initial specie concentration	mol
E_T	Theoretical voltage	V
ε_E	Energy efficiency	%
ε_F	Faradaic efficiency	%
η	Dynamic viscosity	Kg/ms
γ	Surface tension	J/mm ²
ϕ	Contact angle	
ΔA	Area difference	mm ²
Δt	Time difference	s
A	cross-sectional vector area	mm ²
C	absorbent capacity	$\mu\text{l}/\text{mm}^2$
E	Operating voltage	V
e^-	Electron	
F	Faraday constant	sA/mol
i	Current intensity	A
n	Number of electrons/mol	
Q	Flow rate	$\mu\text{l}/\text{s}$
V	Volume	L
v	Flow velocity	mm/s

